Phosphate Ester Hydrolysis Promoted By Lanthanide (III) and Transition Metal Complexes

Daniel M. Williams

A thesis submitted to the faculty of Graduate Studies and Research of McGill University in partial fulfillment of the requirements for the degree of Doctor of Philosophy.

July, 1999
Department of Chemistry
McGill University
Montréal, Québec, Canada

Abstract

Phosphate ester linkages are omnipresent in nature and are found in many biologically important molecules such as DNA, RNA and ATP. Many enzymes that hydrolyze phosphate esters are activated by metal ions. Since the structure of biological enzymes can be quite complicated, it is often useful to work with simpler artificial metalloenzymes to help elucidate the mechanisms by which phosphate ester hydrolysis is activated by metals.

In principle, simple dinuclear metal complexes could hydrolyze phosphate esters by double Lewis acid activation or by a combination of single Lewis acid activation and metal-hydroxide activation. These two mechanisms are kinetically indistinguishable. In this study, two different phosphate substrates are used to distinguish these mechanisms.

Lanthanide (iii) salts have proven extraordinarily effective in accelerating the rate of phosphate ester hydrolysis by several orders of magnitude. Consequently, there has been much effort in recent years to develop a ligand that would bind lanthanides so as to further improve their ability to hydrolyze phosphates. These efforts have met with limited success. Reported here is a dinuclear lanthanide (iii) complex which hydrolyzes BNPP (bis *p*-nitrophenyl phosphate) with unprecedented reactivity at pH 7.0 and 25°C.

A mononuclear copper (ii) 6,6'-diamino-2,2'-bipyridyl complex is synthesized which gives one of the fastest rate accelerations reported for hydrolyzing 2',3'-cAMP. A hydrogen bonding mechanism is proposed for the acceleration of the rate of hydrolysis of the cyclic phosphate.

Résumé

Les phosphates se trouvent partout dans la nature et surtout dans les molécules très intéressantes biologiquement comme ARN, ADN et ATP. Il y a plusieurs exemples des métaux qui demeurent au coeur des sites actifs de quelques phosphoesterases. Puisque la structure des enzymes peut être complexe, il est valable d'utiliser les métalloenzymes artificielles plus simples pour clarifier les mécanismes de l'hydrolyse des phosphates effectué par des métaux.

La double activation de l'acide de Lewis et l'activation de l'acide de Lewis coordonnée avec une attaque métal-nucléophile ne peuvent pas être distinguées par les lois de la cinétique. Dans cette étude, deux substrats sont utilisés pour distinguer ces deux mécanismes.

Des ions lanthanides (iii) ont demontré leur efficacité en accélerant le taux d'hydrolyse des phosphates. Par conséquent, il y a eu un grand effort récemment pour développer un ligand qui lierait les métaux lanthanides d'une manière efficace afin d'améliorer leur aptitude à hydrolyser les phosphoesters. Ces efforts ont eu une réussite limitée. On mentionne dans cette thèse un complexe dinucléaire de lanthanide (iii) qui hydrolyse le phosphate activé BNPP avec un taux sans précedent à pH 7,0 et 25°C.

Un complexe mononucléaire de cuivre (ii) 6,6'-diamino-2,2'-bipyridyl est préparé, et donne un des plus haut taux d'accélération pour l'hydrolyse de 2',3'-cAMP. Un mécanisme de liaison d'hydrogène est proposé pour expliquer l'accélération du taux d'hydrolyse du phosphate cyclique.

ACKNOWLEDGMENTS

I would like to express my heartfelt thanks to my research supervisor, Dr. Jik Chin, for his advice, guidance and patience.

Special thanks to Dr. Brent Stranix for initially synthesizing hbt and for your invaluable discussions vis-à-vis the lanthanides project.

I am grateful to all my coworkers in Room 230: Dr. Bryan Takasaki, Dr. Barry Linkletter, Dr. Daphne Wahnon, Dr. Mark Wall, Dr. Jin Seog Seo, Dr. Mary Jane Young, Dr. Philip Hurst, Dr. Nick Williams, James Connolly, William Cheung, Dr. Brent Stranix, Dr. Andrea Erxleben, Seongsoon Park and Assaad Ghoussoub for their help and friendship.

I would like to thank my collaborators in Korea, Young Seo Choi, Soon Jin Oh and Joon Won Park with regards to the work described in Chapter 3. I am thankful to Mr. Jungseok Heo for the X-ray crystallographic analysis.

I would like to thank the Natural Sciences and Engineering Research Council of Canada and the US Army for their financial support.

I would like to thank Evelyne Dietrich for her help with the French translation of my abstract.

Last but not least, I would like to thank all my good friends and family who were always supportive and made my time in Montréal some of the best years of my life.

Glossary of Symbols and Abbreviations

δ	chemical shift
ε	extinction coefficient
λ	wavelength
2′-AMP	adenosine 2′-monophosphate
3′-AMP	adenosine 3′-monophosphate
2′,3′-cAMP	adenosine 2′, 3′-cyclic monophosphate
3′,5′-cAMP	adenosine 3′, 5′-cyclic monophosphate
A	adenosine
Å	Angstrom
ApA	adenylyl(3′,5′)adenosine
ATP	adenosine triphosphate
BDNPP	bis(2,4-dinitrophenyl) phosphate
binp	2,2′-bi-1,8-naphthyridine
"bis-tris"	2,2-bis(hydroxymethyl)-2,2′,2"-nitrilotriethanol
BNPP	bis(4-nitrophenyl) phosphate
bp	2,2′-bipyridine
CHES	2-(cyclohexylamino)ethanesulfonic acid
conc.	concentrated
cyclen	1,4,7,10-tetraazacyclododecane
dabp	6,6′-diamino-2,2′-bipyridine
dap	2,9-diamino-1,10-phenanthroline
dmbp	6,6′-dimethyl-2,2′-bipyridine
DMP	dimethyl phosphate
DNA	deoxyribonucleic acid

DNase	deoxyribonuclease
EDTA	ethylenediaminetetraacetic acid
EPPS	4-(2-hydroxyethyl)-1-piperazinepropanesulfonic acid
h	hour(s)
hbd	2-hydroxypropyl-1,3-bis(diethanolamine)
hbt	2-hydroxypropyl-1,3-bis((trishydroxymethyl)methylamine)
HEPES	4-(2-hydroxyethyl)-1-piperazineethanesulfonic acid
HPLC	high pressure liquid chromatography
HP*m*NP	2-hydroxypropyl 3-nitrophenyl phosphate
HPNP	2-hydroxypropyl 4-nitrophenyl phosphate
Hz	Hertz
I	ionic strength
K	equilibrium constant
k	rate constant
Ka	acid dissociation constant
k_{obs}	observed rate constant
L	litres
M	molarity (moles/litre)
MeOH	methanol
MES	4-morpholineethanesulfonic acid
min	minute(s)
µL	microlitre
mL	millilitre
µM	micromolar
mM	millimolar
mol	mole(s)

MPNP	methyl 4-nitrophenyl phosphate
MW	molecular weight
N	normality
neo	neocuproine
pH	-log(proton concentration)
phen	1,10-phenanthroline
PIPES	1,4-piperazinebis(ethanesulfonic acid)
pK	-log(K)
ppm	parts per million
R	correlation coefficient
RNA	ribonucleic acid
RNase	ribonuclease
s	second(s)
T	temperature
t	time
TAPS	(3-((tris-hydroxymethyl)methyl))amino)-1-propanesulfonic acid
TBP	trigonal bipyramidal
tris	tris(hydroxymethyl)amino methane
UV-vis	ultraviolet-visible

Structures of Ligands and Substrates

bbmp

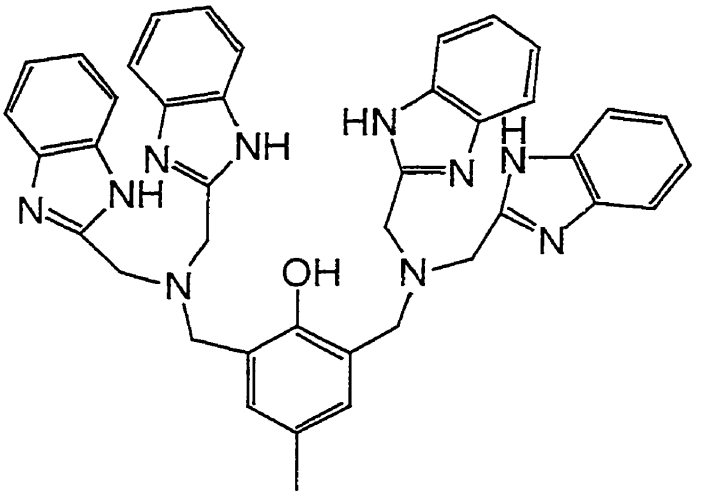

BDNPP

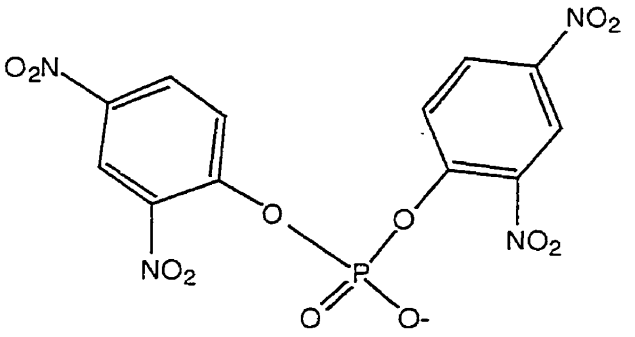

BNPP

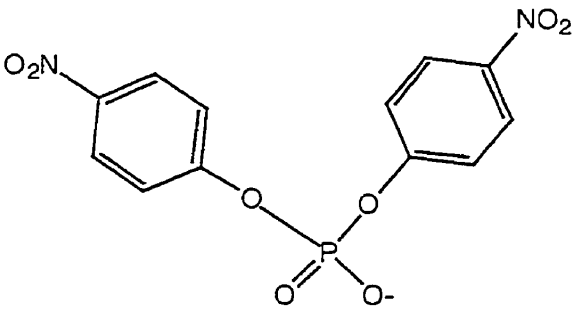

binp

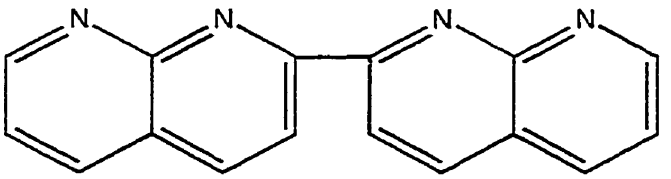

"bis-tris"

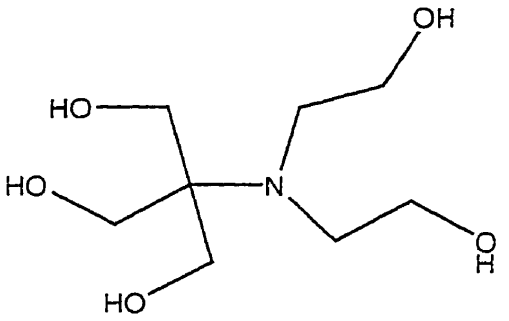

2',3'-cAMP

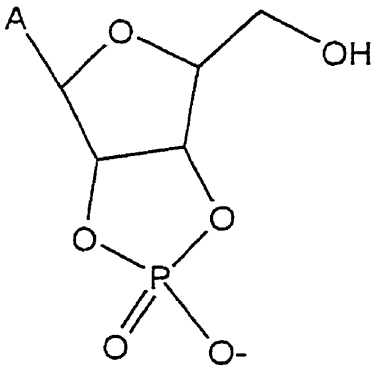

cyclen

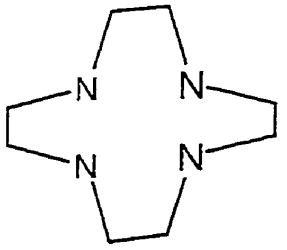

dabp

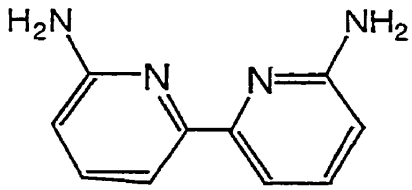

dap

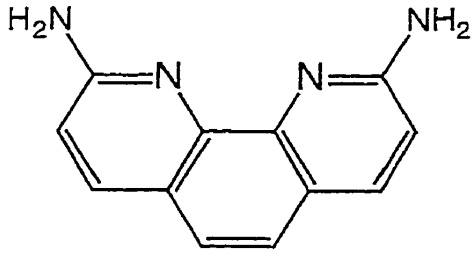

hbd

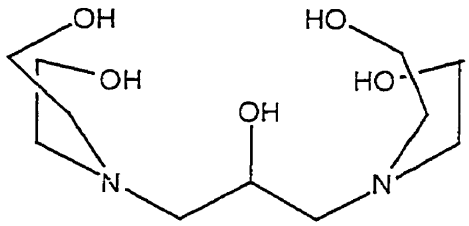

hbt

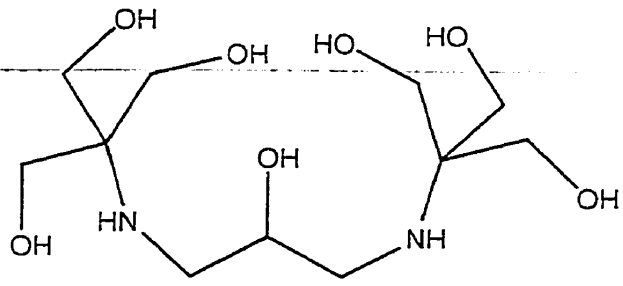

HPNP

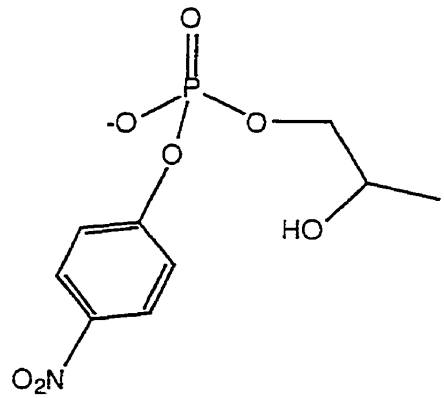

MPNP

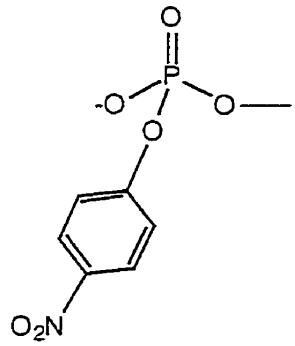

Table of Contents

Abstract i

Résumé ii

ACKNOWLEDGMENTS iii

Glossary of Symbols and Abbreviations iii

Structures of Ligands and Substrates vii

Chapter 1. Introduction 1
- 1.1. The Biological Importance of Phosphate Esters 1
- 1.2. Hydrolysis of Phosphate Esters An Introduction 6
  - 1.2.1. Enzyme-Catalyzed Phosphate Ester Hydrolysis 9
  - 1.2.2. Ribozyme-Mediated Phosphate Ester Hydrolysis 12
  - 1.2.3. Organic Compounds Which Hydrolyze Phosphate Esters 13
  - 1.2.4 Activation Modes for Metal-Promoted Hydrolysis of Phosphate Esters 14
  - 1.2.5 Cooperativity of Activation Modes for Metal-Promoted Phosphate Ester Hydrolysis 15
  - 1.2.6 Sequence-Specific Hydrolytic Cleavage of Nucleic Acids With Metal Complexes 19
- 1.3 Metal Complex-Promoted Oxidative Cleavage/Damage of Nucleic Acids 21
- 1.4 Plan of Study 25
- 1.5 Chapter 1 References 26

Chapter 2. Differentiation of Double Lewis Acid Activation From Other Modes of Activation for Phosphate Diester Cleavage 30
- 2.1 Introduction 30
- 2.2 Results 35
- 2.3 Experimental 42
  - 2.3.1 Instrumentation 42
  - 2.3.2. Kinetics 44
  - 2.3.3 Chemicals 45
- 2.4. Chapter 2 References 47
- Chapter 2 Appendix 48

Chapter 3. Lanthanide (iii) Complex-Promoted Hydrolysis of Phosphate Diesters 51
3.1 Introduction 51
3.2 Results and Discussion 55
3.2.1 Rationale for Development of Hbt as Ligand 55
3.2.2 Potentiometric Titrations 58
3.2.3 ^{1}H NMR and X-Ray Crystallographic Studies 66
3.2.4 Kinetics of BNPP Hydrolysis Using Ln_2hbt 74
3.2.5. Related Kinetics Studies 81
3.4 EXPERIMENTAL 86
3.5 Chapter 3 References 90
Appendix 3.1 92

Chapter 4. Copper (ii) 6,6'-Diamino-2,2'-Bipyridine Complex-Promoted Cleavage of Phosphate Diesters 93
4.1 Introduction 93
4.2 Results and Discussion 99
4.3 Experimental 111
4.3.1 Chemicals 111
4.3.2 Kinetics 112
4.3.3 Potentiometric Titrations 113
4.4 Chapter 4 References 114

Contributions to Knowledge 118

Publications Resulting from This Research 120

Appendix 5. Crystal Structure Data from Hbt Complexes 121

Chapter 1. Introduction

1.1. The Biological Importance of Phosphate Esters

In order to see the essential role that phosphate esters play in nature, one need only flip through an introductory biology textbook and notice the examples of phosphates that abound. There are the genetically important nucleic acids DNA and RNA, the phospholipids of the lipid bilayer of the cell membrane, the metabolically crucial energy conduit ATP and many, many others. Since so many biologically significant molecules are phosphates, it is logical that a further understanding of their chemistry will be extremely valuable in the fields of medicine and genetic engineering.

Nucleic acids are molecules that are divided into two subsets: RNA (ribonucleic acids) and DNA (deoxyribonucleic acids). These compounds are the major players in the transfer and storage of genetic information. DNA, the major component of chromatin, is found in the nucleus of eukaryotic cells. A messenger RNA (mRNA) molecule transcribes the information from the DNA molecule and leaves the nucleus to enter the cytoplasm of the cell. Subsequently a ribosomal assembly translates the code from the mRNA into an amino acid sequence to make valuable proteins.

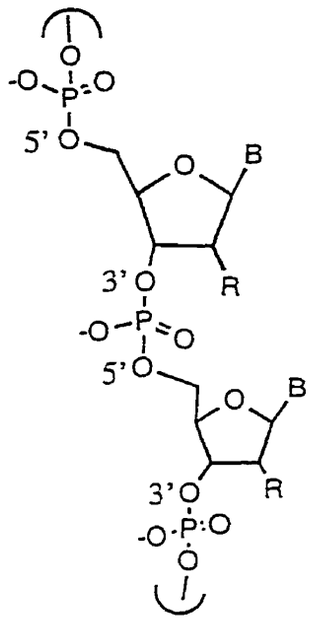

Figure 1.1 Structure of a dinucleotide portion of the phosphate diesters DNA and RNA, showing the 3′–>5′ linkage. B represents the nitrogenous base; in DNA, R=H and in RNA, R=OH. The difference in R group is important with respect to the difference in hydrolysis rates of the nucleic acids.

Nucleotides are phosphorylated pentoses which have a nitrogenous base at the 1′-position of the ribose. DNA and RNA are polymers of deoxyribonucleotides or ribonucleotides where the sugar moieties are linked by phosphate ester bonds which connect the 3′-hydroxyl group of one sugar residue to the 5′-hydroxyl group of another residue (Figure 1.1). In DNA, the four nitrogenous bases which are present in nature are the purines adenine (A) and guanine (G), and the pyrimidines cytosine (C) and thymine (T). In RNA, the nucleotide bases are composed of these same four bases with the exception that thymine is replaced by uracil (U). It is the sequence of these four base pairs in the nucleic acid that make up the genetic code and the hydrogen bonding interactions between complementary base pairs (Figure 1.2) of complementary

nucleic acid strands that allow for the formation of a double helix[1] and transfer of the genetic code.

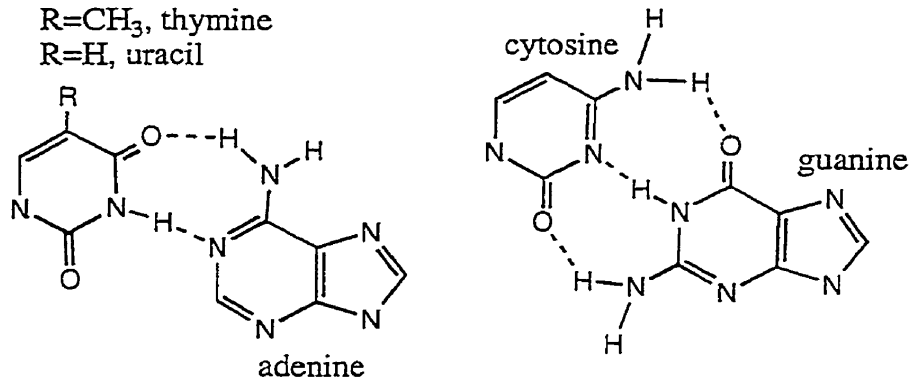

Figure 1.2 The Watson-Crick scheme of hydrogen bonding interactions between the complementary base pairs in nucleic acids. Note the presence of two H-bonds between A•T or A•U and three H-bonds between C•G.

Not surprisingly, the phosphate ester linkages of DNA are extremely stable. It is estimated that the half-life at neutral pH and 25°C for the hydrolysis of the phosphate bonds in DNA is 10-100 billion years!!![2] It is this stability that makes DNA a useful molecule for storing genetic information. By contrast, RNA, with its 2'-OH internal nucleophile that imparts a high effective molarity for transesterification, is an estimated nine orders of magnitude more susceptible to leaving group P-O bond cleavage.[3] This may account for the evolutionarily smaller size of RNA strands versus DNA strands and its resulting usefulness as a transporter of the genetic code.

3',5'-cAMP is another phosphate diester which is quite important in regulating biologically important processes. When hormones such as norepinephrine and epinephrine in the muscle (or glucagon in the liver) extracellularly stimulate the enzyme adenylate cyclase, 3',5'-cAMP is produced.

By inducing phosphorylation in key enzymes, the presence of 3′,5′-cAMP activates or deactivates various enzymes. For example, 3′,5′-cAMP stimulates the enzyme cascade which causes the breakdown of the storage polysaccharide glycogen to glucose for further metabolism while simultaneously inhibiting glycogen synthase which catalyzes the conversion of glucose to glycogen. Similarly, 3',5'-cAMP uses enzyme phosphorylation to regulate the opposing glycolytic/gluconeogenetic pathways (gluconeogenesis is favored by phosphorylation). This 3',5'-cAMP-stimulated phosphorylation also activates triacylglycerol lipase to yield fatty acids that activate the protein thermogenin. Thermogenin is a protein found in brown adipose tissue and is used to dissipate the electrochemical gradient generated from electron transport by generating heat through a proton pumping process.

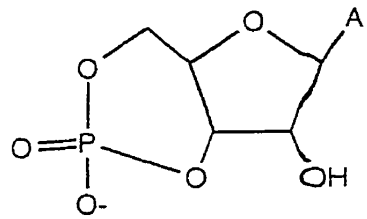

3'5'-cAMP

Figure 1.3 3',5'-cAMP: a biologically important second messenger

ATP (adenosine-5'-triphosphate) is an extremely important biological molecule (Figure 1.4) that is used to store energy from various sources for use in a number of important physiological processes. Photosynthesis, oxidative phosphorylation and the breakdown of monosaccharides via glycolysis are examples of metabolic pathways where ATP is made to harness energy for later use in various anabolic and catabolic processes. ATP is also used to actively transport ions and molecules across a membrane, such as in the Na^+-K^+-ATPase pump which prevents cell swelling and breakage. Additionally, ATP functions

to allosterically modulate protein activity. For example, ATP (along with 2,3-bisphosphoglycerate (BPG) and inositol hexaphosphate) binds the deoxygenated form of hemoglobin, thereby regulating oxygen uptake and release in a number of animal species.

Nicotine adenosine dinucleotide (NAD^+) (Figure 1.4) and flavine adenosine dinucleotide (FAD) are diphosphates which act as oxidizing agents during a number of processes including the oxidation of glucose to CO_2. These oxidizing agents may be recycled in aerobic sytems from O_2, NADH and $FADH_2$ while ATP is concomitantly produced in the metabolically important electron transport. In yeast, the reoxidation of NADH anaerobically allows the enzymatic reduction of pyruvate to ethanol and CO_2, a process that has important consequences in making certain alcoholic beverages and breads. $NADP^+$, which differs from NAD^+ only in that its 2'-OH is phosphorylated, is converted to NADPH by the pentose phosphate pathway. NADPH, which is not metabolically interchangeable with NADH, is a "currency" for endergonic reductive biosynthetic processes.

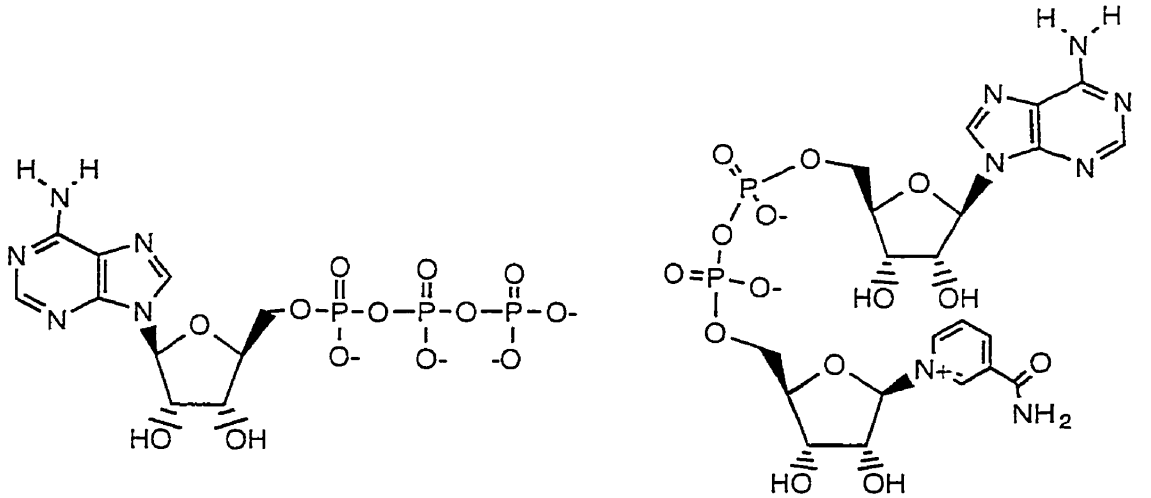

ATP NAD+

Figure 1.4 Chemical structures of ATP and NAD^+

Coenzyme A (CoA) is another biologically important phosphate (Figure 1.5) which covalently binds carbonyl groups at its sulfur position. Acetyl-CoA is an intermediate and regulator of the breakdown and biosynthesis of metabolic fuels such as amino acids, fatty acids and carbohydrates. Succinyl-CoA is the product of odd-chain fatty acid breakdown and amino acid degradation. Succinyl-CoA then enters the Krebs cycle, where it is broken down to CO_2 and energy in the form of ATP. Additionally, succinyl-coA is the starting material in the biosynthesis of porphyrins, which are integral structures of chlorophyll, the hemes in hemoglobin and the cytochromes of electron transport.

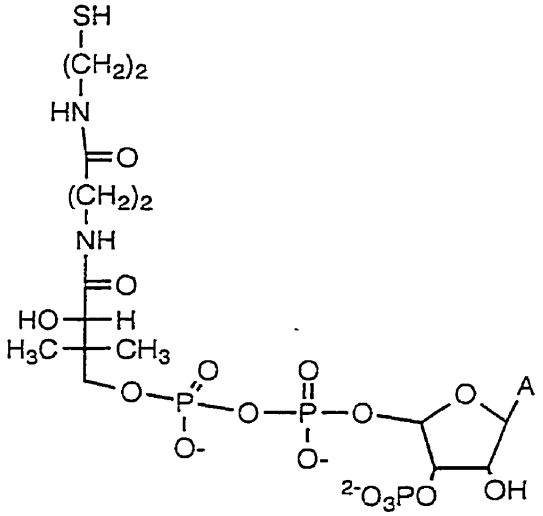

Figure 1.5 Chemical structure of Coenzyme A

1.2. Hydrolysis of Phosphate Esters: An Introduction

Given the biological importance of phosphates, it is not surprising that phosphate ester hydrolysis has been extensively studied. Phosphate esters may be cleaved by one of three mechanisms: dissociative, associative or concerted. In a dissociative mechanism, the leaving group departs to form a metaphosphate intermediate that is subsequently attacked by the nucleophile. In an associative mechanism, the nucleophile attacks the phosphorus centre to form a pentacoordinate phosphorus intermediate; leaving group departure follows. In a

concerted mechanism, nucleophile attack and leaving group departure occur with no intermediate formation.

A three dimensional energy plot is extremely useful in understanding the dynamics of phosphate diester hydrolysis, a reaction that typically occurs by a bimolecular, associative mechanism (Figure 1.6). The X-axis of this plot represents the percentage of cleavage of the phosphorus-leaving group bond and the Y-axis indicates the amount of formation of the nucleophile-phosphorus bond. Since phosphate diester hydrolysis occurs by an associative mechanism, the incoming nucleophile attacks the tetrahedral phosphorus centre to form a trigonal bipyramidal (TBP) intermediate with a pentavalent phosphorus centre. The pentacoordinate phosphorus intermediate contains three substituents in the equatorial position and two in the apical position (see Fig. 1.6). The leaving group is subsequently kicked out; the principle of microscopic reversibility governs that the leaving group is kicked out at the apical position since the nucleophile attacks in this position also.

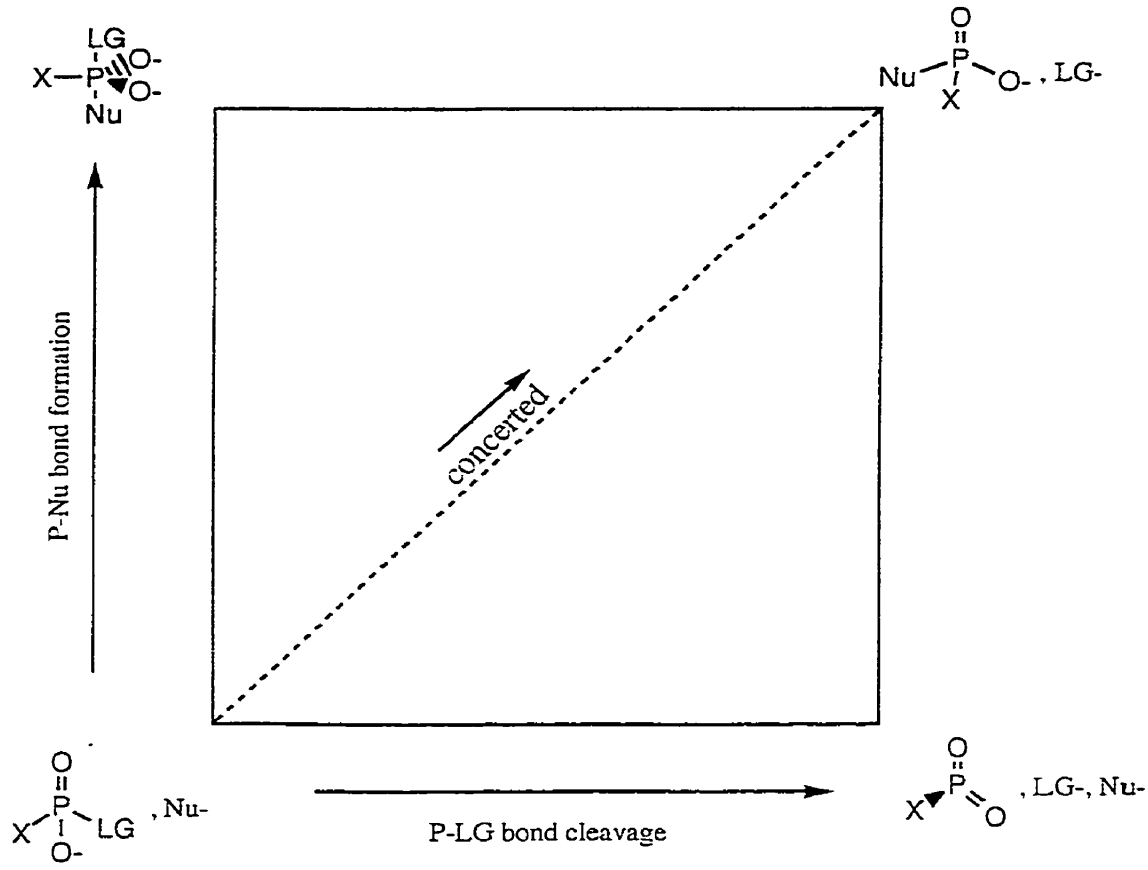

Figure 1.6 Three dimensional free-energy plot for phosphate ester hydrolysis. The free energy axis is orthogonal to the plane of the paper.

The trigonal bipyramidal intermediate may undergo pseudorotation (Figure 1.7) during which the bond angles deform so that two apical positions of the phosphorus are switched with two equatorial positions. Westheimer's rules dictate which substituents are favored in the equatorial position versus the axial position. For example, π-donor ligands and bulky substituents prefer to lie in the equatorial positions while electronegative atoms prefer to lie in the axial positions.[4-5]

Since singly-protonated phosphate diesters have a pKa of between one and two, under physiological conditions they exist in the deprotonated form. The phosphorus-oxygen bond of a phosphate diester is consequently quite

difficult to hydrolyze since the negative charge of an incoming nucleophile is repelled by the negative charge of the phosphate oxygens.

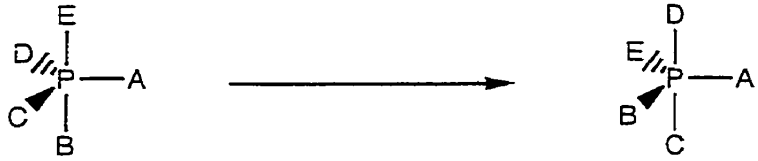

Figure 1.7 Pseudorotation of a pentavalent phosphorus

Phosphate monoesters have two pKas: one around 1 and another at ca. 6.5. As a consequence, at near neutral pHs, they exist in either the singly-deprotonated or doubly-deprotonated form. In general, phosphate monoesters are proposed to hydrolyze by a unimolecular dissociative mechanism. In the case of dissociative hydrolysis, the leaving group departs to form a proposed metaphosphate intermediate[6-7](see Figure 1.6) which is subsequently attacked by a nucleophile. Studies examining leaving group pKa versus rate of hydrolysis indicate that for phosphates with better leaving groups, the dianionic form of the monoester is more susceptible to hydrolysis.[8]

1.2.1. Enzyme-Catalyzed Phosphate Ester Hydrolysis

The highly negatively charged molecules DNA and RNA are very difficult substrates to hydrolyze. In the presence of enzymes called nucleases, however, DNA and RNA are rapidly cleaved in the enzyme's active site. For example, *Staphylococcal* nuclease is estimated to cleave DNA 10^{16} times faster than the background rate.[9-10] In addition to enzymes which are proteins with an amino acid backbone, RNA may act as a "ribozyme" in conjunction with metal ions to catalytically hydrolyze itself. Nucleases use a variety of mechanisms to effect phosphate cleavage, employing cofactors and side groups of amino acids placed

closely together by the protein folding to allow for tremendous rate acceleration of the nucleic acid hydrolysis.

Bovine pancreatic ribonuclease (RNase A) is one of the most widely studied[11-13] and best understood nucleases. X-ray crystallographic studies have shown that two histidine residues in the active site of the enzyme approach the RNA molecule.[14] It has been proposed that one of the histidine moieties (His-12) which lies in close proximity to the 2'-OH acts as a general base and deprotonates the hydroxyl group, which makes the latter a better nucleophile for transesterification. In concert with the general base action of His-12, the other histidine group (His-119) is believed to act a general acid, protonating the leaving group to facilitate its departure.[15] For the subsequent hydrolysis step, it is proposed that the roles of the histidines are interchanged with His-119 acting as a general base and His-12 acting as a general acid by protonating the leaving group. (Figure 1.8).

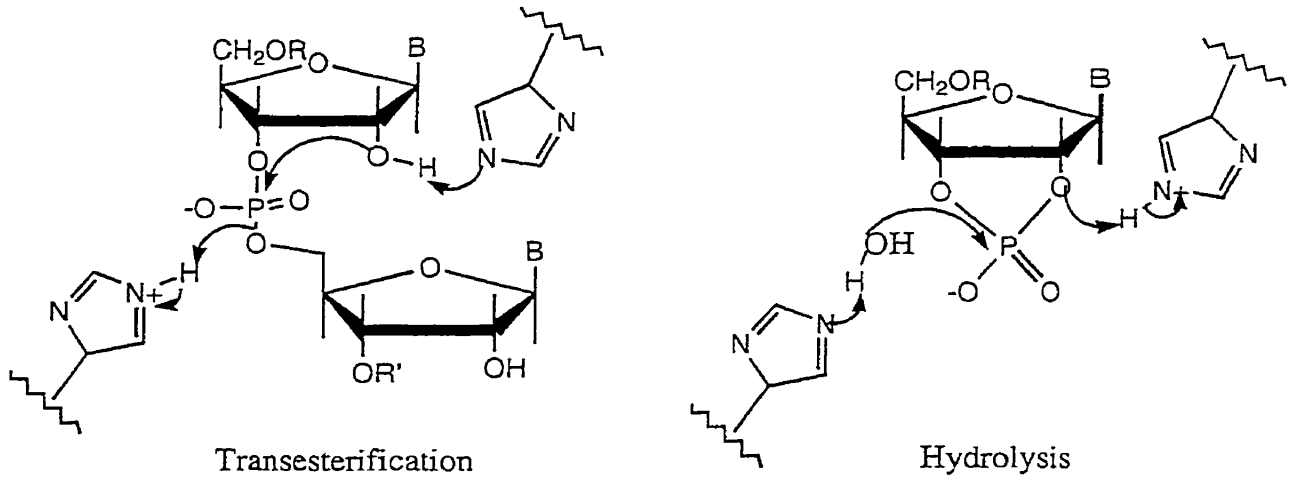

Figure 1.8 Mechanism of RNase A showing the activity of two histidine moieties as general acid and general base.

The 3′,5′-exonuclease fragment of DNA polymerase I is an example of a nuclease where metals play an important part.[16] In this system, the metals (which can either be Mg^{2+}, Mn^{2+} or Zn^{2+}) are believed to activate the hydrolysis of the phosphate in multiple ways (Figure 1.9)[17]. It is proposed that the M^{2+} ions act as Lewis acids, shielding the negative charge on the phosphate, making it more susceptible to hydrolysis. As a second mode of activation, one of the M^{2+} ions is in an ideal position to bind to the 3'-OH leaving group of DNA and is postulated to facilitate its departure upon nucleophile attack as a consequence. Lastly, one M^{2+} ion binds a hydroxyl group, which allows for an intramolecular metal-nucleophile attack of the phosphate. These motifs of metal activation are observed in other enzymes such as RNase H[18-19], alkaline phosphatase and phospholipase C[20] and serve as a framework for the design of novel metal complexes for hydrolyzing phosphate esters.

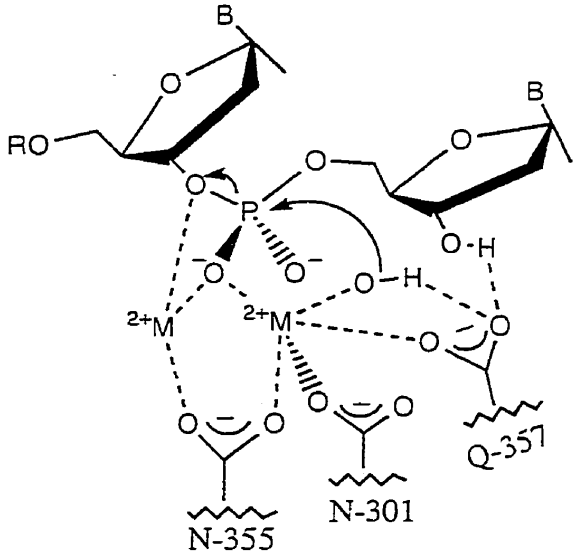

Figure 1.9 In the 3′,5′-exonuclease fragment of DNA Polymerase I, two metals interact cooperatively to hydrolyze DNA with multiple modes of activation.

1.2.2. Ribozyme-Mediated Phosphate Ester Hydrolysis

Cech and coworkers discovered that RNA could act as a "ribozyme" (a.k.a "catalytic RNA") to hydrolyze itself. In some landmark experiments using *Tetrahymena thermophila*, it was discovered[21] that in the absence of protein and when incubated with guanosine or guanine, that the protozoan's pre-rRNA undergoes a self-splicing process. This occurs when the 3'-OH of the guanosine attacks an RNA phosphate ester bond, causing the guanosine to attach to the 5'-end of the intron with concomitant release of the 3'-OH end of one exon. This 3'-OH subsequently attacks another phosphate ester linkage of the RNA, resulting in simultaneous intron removal and joining of exons.[22]

The ribozyme active site contains three Mg (ii) ions which were discovered to be necessary for its catalytic activity. In one experiment, the Mg(ii) ions were replaced with Ca(ii) ions or Sr(ii) ions.[23] Even though no change in protein folding properties occurred, all ribozymic activity was lost when the metal is exchanged. As additional proof of the importance of Mg(ii) in *Tetrahymena* ribozyme, an experiment was effected where the 3'-OH was replaced with a sulfur group. This replacement caused a thousand fold decrease in reactivity when Mg^{2+} ion is present. However, when Mg^{2+} is replaced by Mn^{2+} or Zn^{2+}, there is no loss in reactivity of the RNase when a 3'-S is used. Since Mg^{2+} binds sulfur much more weakly than its sister divalent ions, it was postulated that the Mg^{2+} is binding the 3'-O, acting as a Lewis acid to lower the pKa the leaving group.

In a recent paper, Cech and coworkers reported that a second metal ion may have a catalytic role in the group I *Tetrahymena* ribozyme. While one metal interacts with the leaving group, Cech showed that a second metal ion activates the 3'-hydroxyl group of guanosine to form an effective metal-nucleophile.[24]

1.2.3. Organic Compounds Which Hydrolyze Phosphate Esters

Using rigid, preorganized clefts, Anslyn *et al.* (Figure 1.10 **A**)[25] and Hamilton *et al.*(Figure 1.10 **B**)[26] working independently designed elegant receptors that bind phosphates and accelerate their cleavage by acting as hydrogen bond donors. The guanidinium groups involved in the hydrogen bonding resemble the arginine moieties in *Staphylococcus* nuclease. Anslyn and coworkers observed a 20-fold rate acceleration over imidazole-catalyzed ApA hydrolysis and Hamilton's group reported a 700-fold rate acceleration over uncatalyzed nitrophenyl phosphate ester hydrolysis.

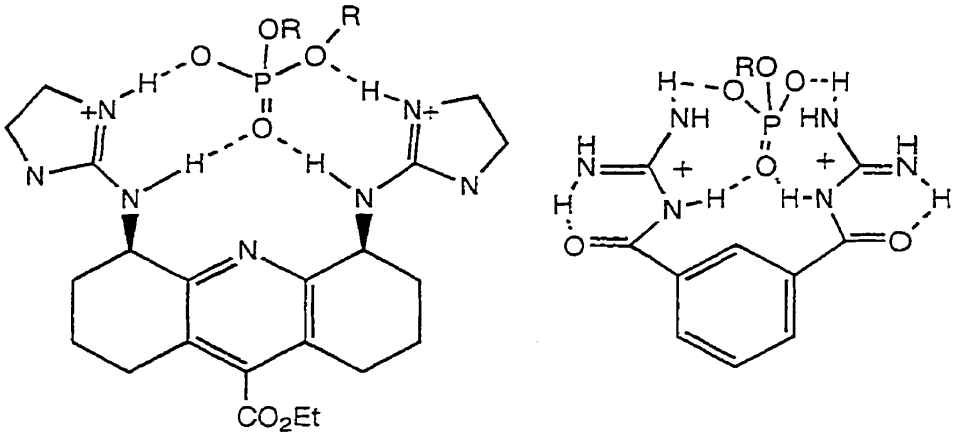

Figure 1.10 A (left), **1.10 B** (right) Receptors that bind phosphate esters in their cavities using hydrogen bonding.

Similarly, Lehn and coworkers[27] took advantage of the multiple hydrogen bonding of ammonium macrocycles to catalyze phosphate transfer reactions of ATP (Figure 1.11). While the rate enhancements are modest (k_{cat}= 0.064 min^{-1}) compared to enzymes (average k_{cat}= 1000 min^{-1}) and other reported artificial ATPases, this novel ligand brings invaluable insight into the design of artificial enzymes.

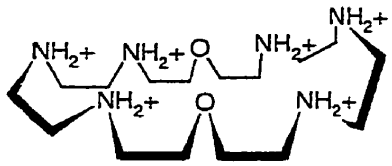

Figure 1.11 A supramolecular polyammonium macrocycle which binds ATP, thereby catalyzing phosphate transfer reactions.

1.2.4 Activation Modes for Metal-Promoted Hydrolysis of Phosphate Esters

There are numerous examples in nature of phosphoesterases that have metal ions in their active site. In recent years, there have been a number of papers discussing the mechanisms by which metal ions activate phosphate esters for hydrolysis. The modes of acceleration (Figure 1.12) include the single Lewis acid activation of the phosphate, the binding of the leaving group in order to facilitate its departure and the metal-nucleophile attack of the bound phosphate.

Single Lewis acid activation acts to accelerate the reaction by dispersing the electron density away from the phosphate. As a consequence, the electronegative nucleophile is no longer repelled by the negatively charged phosphate and is able to attack the phosphorus centre much more easily. Sargeson *et al.* have shown that single Lewis Acid activation gives 10^2-fold rate acceleration for phosphate ester hydrolysis.[28]

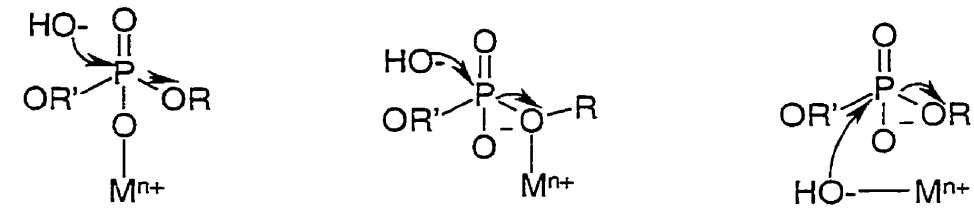

single Lewis acid activation | leaving group activation | metal-nucleophile attack

Figure 1.12 Modes by which phosphates are activated by metals

Metal-nucleophile attack can increase the rate of reaction also.[29] In the presence of a metal such as Cu^{2+} ion, the pKa of the metal-bound water is approximately 7.0. Therefore, at pH 8, for example, there is only a small amount of hydroxide in a metal-free solution, but in a solution with Cu^{2+} ion, a significant amount of hydroxo group bound to the metal ion is available to attack the phosphate.

Leaving group activation occurs when a metal binds to the leaving group of the phosphate thereby lowering the pKa of the leaving group. In a number of reported systems that use this mode of activation, often the leaving group phosphate oxygen is bound to the metal[30-31] but other positions on the leaving group may bind the metal also.[32] As a result of the binding, the activation energy for kicking out the leaving group is decreased and the rate of hydrolysis is accelerated.

1.2.5 Cooperativity of Activation Modes for Metal-Promoted Phosphate Ester Hydrolysis

In the past two decades, there has been a considerable amount of success in developing elegant metal catalysts that take advantage of a combination of single Lewis acid activation, metal-nucleophile attack and leaving group

activation to give remarkably fast rates of phosphate hydrolysis. Interestingly, when different modes of activation are working together, rates of acceleration that are observed are sometimes greater than the sum of the expected rates from each individual mode of activation.

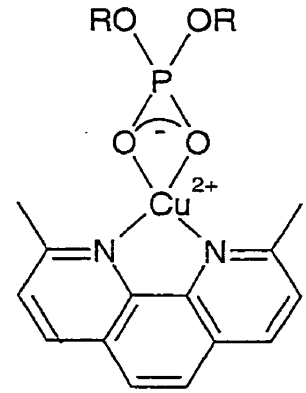

Figure 1.13 An example of a complex where phosphate diesters chelate the metal centre. $10^{6.6}$-fold rate acceleration is observed for ApA hydrolysis over the uncatalyzed reaction. Phosphates chelate Cu in Cu(neo) in a bidentate fashion[33]

Single metal ion complexes can chelate phosphate diesters in a bidentate fashion. In a chelated metal complex, the metal acts as a Lewis acid toward two phosphate oxygens to give a quasi-double Lewis acid activation (see chapter 4 and Fig. 1.13). Since both negative charges are quenched, larger rate accelerations are observed than when phosphates bind to the metal in a unidentate manner. Other single metal ions provide both the metal-nucleophile and the Lewis acid. The cooperativity between single Lewis acid activation and metal-hydroxide attack is quite impressive because the hydroxo group attacks the phosphate intramolecularly. Examples have shown that the effective molarity of the reaction is consequently increased considerably due to the greater entropic favorability.[3]

Two metals can also bind a ligand so that one metal binds the phosphate to provide single Lewis acid activation while the other metal provides the metal-nucleophile. Two metals can also provide double Lewis acid activation, a mechanism which has been estimated to give between 10^5 - 10^6-fold rate acceleration for phosphate diester hydrolysis (see Fig. 2.1).[34]

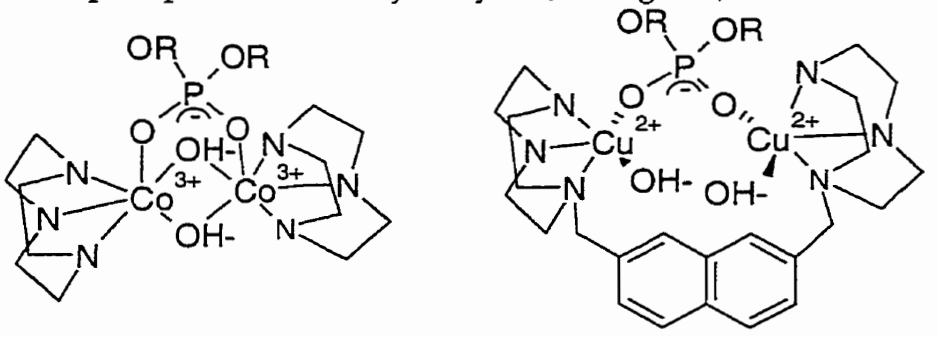

Figure 1.14 Two metal complexes that combine double Lewis acid activation and metal-nucleophile attack.

A few examples of two metal systems that use these modes of activation illustrate the importance of cooperativity in the design of artifical phosphoesterases. Wahnon *et al.* reported a $Co_2(tacn)_2$ complex that binds phosphates to both Co^{3+} ions so as to give double Lewis acid activation (Figure 1.14). Additionally, the two cobalt ions are proposed to be bridged by oxides that act as nucleophiles to hydrolyze phosphates. Indeed, the rate of hydrolysis for methyl *p*-nitrophenyl phosphate (MPNP) hydrolysis using this complex is an estimated 6×10^{11}-fold faster than the rate of background hydroxide-catalyzed MPNP hydrolysis, a rate acceleration that is significantly faster than the 10^5- to 10^6-fold acceleration expected from double Lewis acid activation alone.[35]

Young and Chin reported on a dinuclear copper ditriazacyclonane complex where the two tacn moieties of the ligand were separated by a naphthalene spacer (Figure 1.14). This complex also combines double Lewis acid activation and metal-hydroxide attack to cleave 2′,3′-cAMP and ApA (10^8- and

10^5-fold rate acceleration respectively) with extraordinary reactivity.[36] Additionally, Czarnik and coworkers reported that modest rate accelerations for *p*-nitrophenyl phosphate ester hydrolysis are observed when a similar dinuclear cobalt (iii) cyclen complex separated by an anthracene spacer is used as a catalyst.[37]

There are also examples in the literature of complexes that use leaving group activation in cooperativity with other forms of activation. Tsubouchi and Bruice reported a dinuclear lanthanide complex (Figure 1.15) which demonstrated 10^{13}-fold rate acceleration over the background rate for the hydrolysis of a novel phosphonate.[38] Leaving group activation combined with double Lewis acid activation and metal-hydroxide attack of the phosphate centre was proposed to explain the exceptional reactivity.

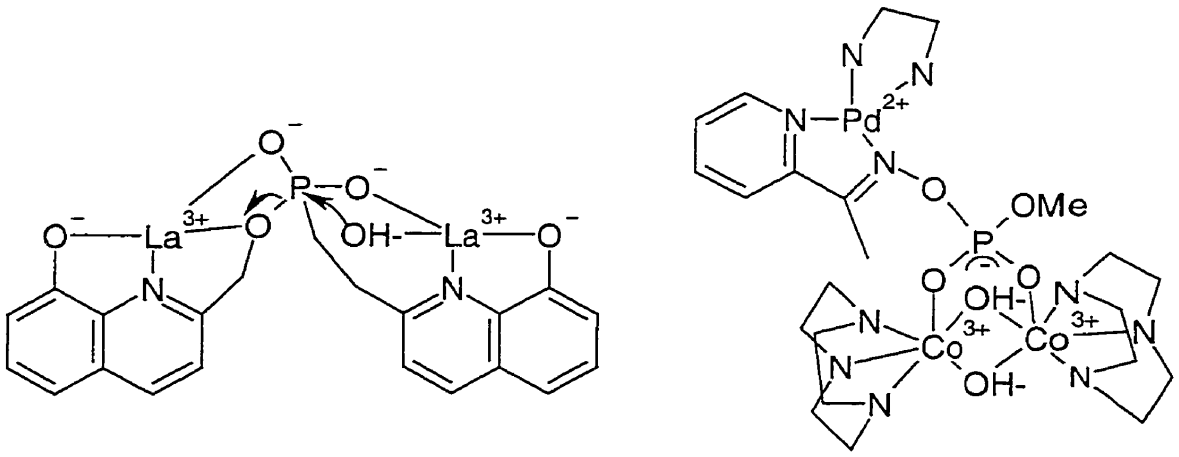

Figure 1.15 Metal complexes that use leaving group activation cooperatively with other modes of activation.

In 1997, Seo *et. al.* designed a novel phosphate diester with a poor leaving group. Seo showed that this phosphate binds to the dinuclear cobalt (iii) complex above (Figure 1.15). When the phosphate's leaving group is bound to a palladium (ii) ethylenediamine metal complex, it is hydrolyzed an estimated 10^{17} times faster than the background rate.[39] The presence of the third metal ion

bound to the leaving group is required for the hydrolysis of the phosphate diester to occur; in the absence of the metal, dissociation of the phosphate from the cobalt complex results instead. The remarkable reactivity of this metal complex illustrates the importance of leaving group activation when it is used in combination with double Lewis acid activation and metal-nucleophile attack.

1.2.6 Sequence-Specific Hydrolytic Cleavage of Nucleic Acids With Metal Complexes

In order to develop effective drugs, it is important to find catalysts that cleave phosphate diesters not only rapidly but also sequence-specifically. Developing sequence-specific artificial endonucleases is an important challenge as there is a limited range of sites of the DNA or RNA sequence that natural restriction enzymes or ribozymes can cleave. By increasing the number of prospective sites of cleavage on the nucleic acid strands by using artificial restriction enzymes, there might be life-saving consequences when a novel gene sequence is targeted that translates into proteins associated with various illnesses.

A number of groups have used antisense technology by attaching metallic complexes to an oligonucleotide moiety which binds an RNA molecule.[40] For example, the europium (iii) texaphyrin carboxylic acid oligonucleotide-directed RNA cleavage developed by Magda and coworkers (Figure 1.16) hydrolyzes an RNA 30-mer at nanomolar concentrations by up to 30% after 24h.[41] Recently, Magda showed that the texaphyrin complex has the advantage that it may be prepared on solid support.[42] Matsumura similarly observed significant RNA cleavage with a lanthanide iminodiacetate complex.[43]

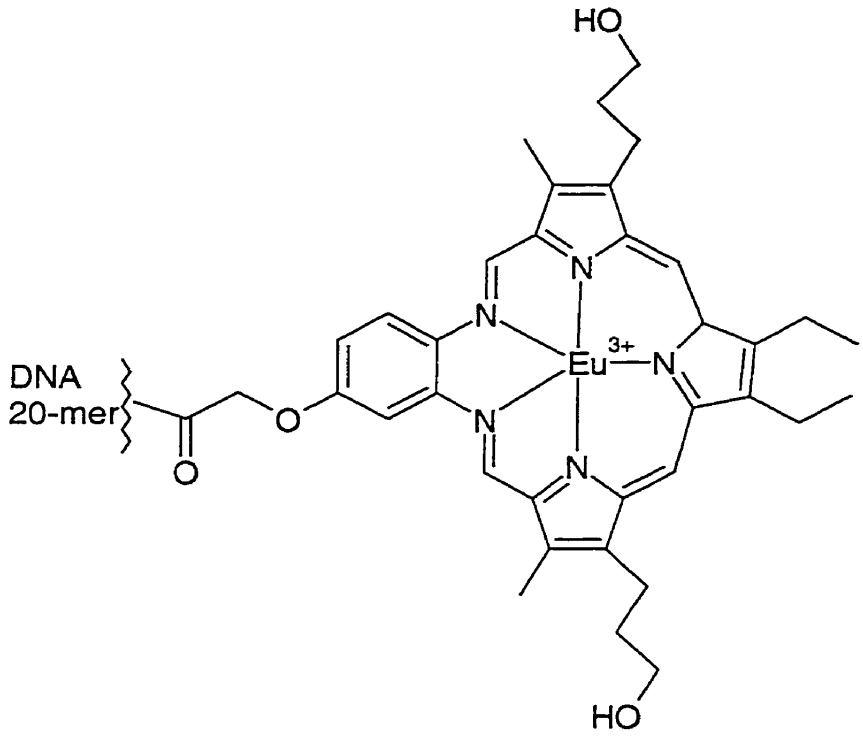

Figure 1.16 A europium (iii) texaphyrin complex that was used for site-directed RNA cleavage

A few examples of sequence-specific metal complex artificial endonucleases that cleave DNA have also been reported. Barton and coworkers worked on a rhodium DNA intercalator[44] covalently bound to a metallopeptide moiety that hydrolyzed DNA. Que *et al.* reported a dinuclear iron complex which in the presence of hydrogen peroxide was able to cleave a DNA plasmid with some specificity to give hydrolysis products.[45] These results are quite promising for the future of artificial restriction enzymes; however, in addition to sequence-specificity, other factors complicate the future of the artificial nucleases for drug development including drug delivery across the cell membrane, targeting to the correct region of the cell and the stability of the drug to enzyme nucleases/other degradation.[46]

1.3 Metal Complex-Promoted Oxidative Cleavage/Damage of Nucleic Acids

There are a number of metal complexes which can cleave DNA and RNA oxidatively under physiological conditions. Unlike in the case of hydrolytic nuclease cleavage, with most systems oxidative cleavage is destructive in that religation is not possible since both the 3′- and 5′-ends of the nucleic acids are converted to phosphates. As a consequence, so far the oxidative cleavage method has limited applicability in gene repair and manipulation. However, metal complexes that exhibit oxidative DNA cleavage have been been employed in the processes of DNA footprinting and affinity labelling—site- and sequence-specific techniques that help elucidate the secondary structure of nucleic acids and their interactions with other molecules.

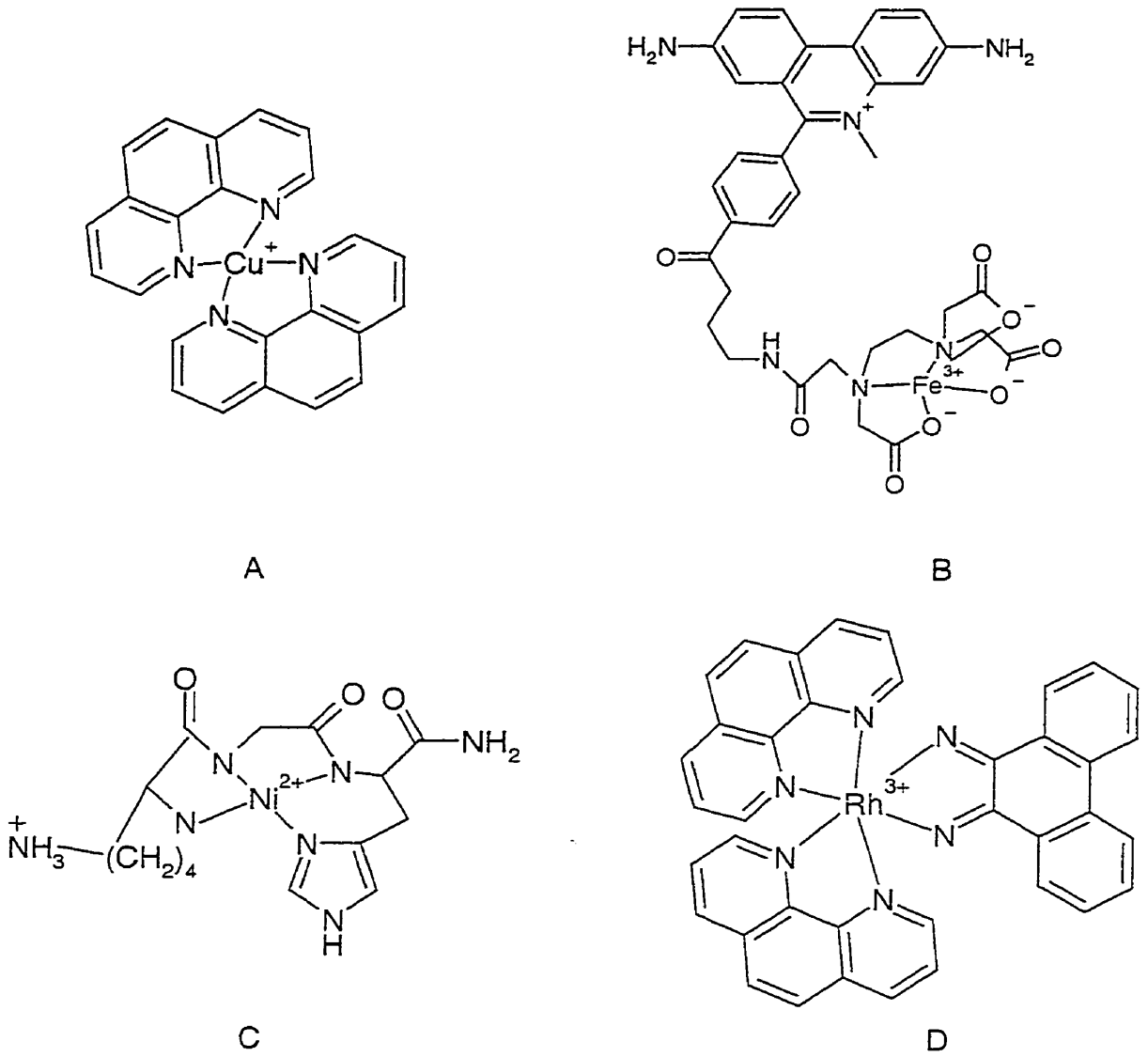

Figure 1.17 Some Metal Complexes That Oxidatively Cleave Nucleic Acids

A number of redox-active metal complexes (Figure 1.17) oxidize nucleic acids including copper (i) diphenanthroline ($Cu(phen)_2$), iron (ii) ethylenediaminetetraacetate (Fe(EDTA)), metalloporphyrins, metal-bound tripeptides and chiral octahedral rhodium and ruthenium complexes. These intercalating or groove-bound complexes use an oxidizing agent (such as hydrogen peroxide) which creates a hydroxy radical that acts to oxidize the ribose or deoxyribose sugar. A reducing agent such as ascorbate or dithiothreitol

is often present in order to recycle the reduced form of the metal complex. A number of mechanisms have been proposed to be involved in oxidative nucleic acid cleavage.

Copper (i) di-1,10-phenanthroline (Figure 1.17 **A**) in the presence of dioxygen and a reductant undergoes a Sigman-type oxidative cleavage. [47-49] Interestingly, the copper complex reversibly binds DNA's minor groove in such a fashion that only the deoxyribosyl group of DNA is attacked by the oxidant. For this cleavage mechanism, the orientation is such that a hydroxyl radical attacks the C-1 hydrogen of the sugar which leads to the formation of the 3′- and 5′-phosphate monoesters, free bases and 5-methylenefuranone (Figure 1.18).

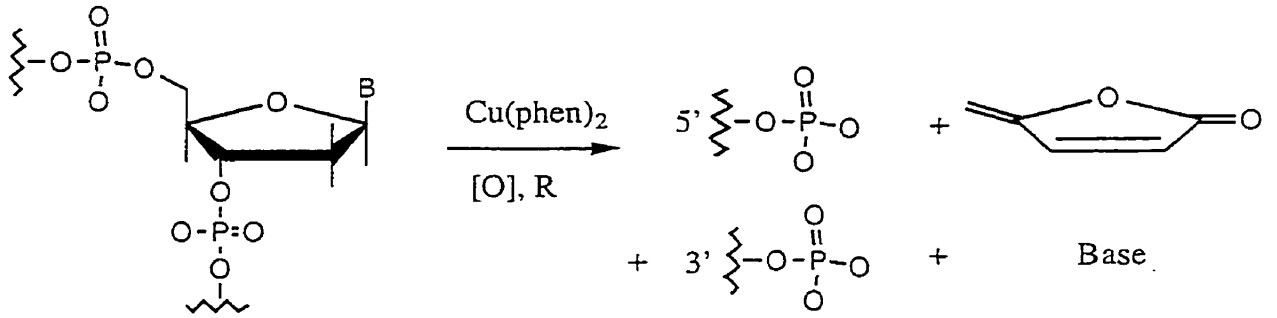

Figure 1.18 Sigman-fashion oxidative cleavage of DNA. [O] represents an oxidizing agent; R represents a reducing agent.

Iron (iii) EDTA (Figure 1.17 **B**) cannot attach to a DNA molecule directly. However, when the catalyst is bound to a methidium DNA intercalator[50] or alternatively is bound to oligonucleotides that Hoogsteen hydrogen bond to the major groove of DNA to form a triple helix (Figure 1.19)[51-52], oxidative double helix DNA cleavage is observed. When Fe(EDTA) is oxidized by hydrogen peroxide or oxygen, it has been proposed that a diffusable hydroxyl radical abstracts hydrogens from either the C-1 or C-4 positions of the sugar in Fenton-

type chemistry. The reaction conditions used greatly affected the ratio of attacked sugar to attacked nucleoside base for this catalyst.

Metallic tripeptides (e.g., Figure 1.17 **C**) have also been used to oxidatively cleave or damage DNA when they bind its minor groove.[53-56] In 1997, Burrows reports that sulfite from industrially-produced SO_2 may produce sulfate or monoperoxysulfate radicals; these radicals in conjunction with metallic tripeptides are able to damage DNA by forming a guanine radical cation intermediate.[57] Nickel (ii) Xaa-Xaa-His acts in the presence of oxone ($KHSO_5$), magnesium monoperoxyphthalate (MMPP) or hydrogen peroxide to cleave the sugar residue oxidatively.[58] Chiral rhodium and ruthenium complexes (e.g., Figure 1.17 **D**) which bind the major groove with high microstructural specificity due to their recognition of the specific shapes and asymmetries of DNA have also been used for oxidative cleavage.[59] The nickel, rhodium and ruthenium complexes above all give a wide array of oxidative products.

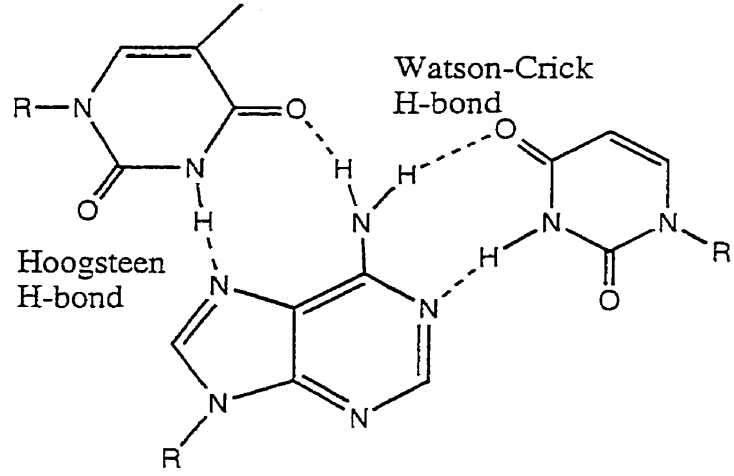

Figure 1.19 Iron (iii)EDTA may bind to oligonucleotides which form a Hoogsteen H-bond between the nucleotide and the double helix. This triple helix structure allows for sequence-specific oxidative cleavage by the iron EDTA.

1.4 Plan of Study

One of the main difficulties inherent in developing artificial restriction enzymes is that the phosphate diester bond is extremely resistant to hydrolytic cleavage. Over the past half century, many interesting mononuclear metal complexes that hydrolyze phosphate esters have been reported. More recently, dinuclear metal complexes that are significantly more reactive than the corresponding mononuclear complexes have been found.

A number of mechanisms have been proposed to explain the role of the two metals in a dinuclear metal complex-promoted phosphate diester hydrolysis. Here a study will be undertaken to distinguish three kinetically indistinguishable mechanisms: a) double Lewis acid activation b) joint single Lewis acid activation/metal-nucleophile attack and c) joint single Lewis acid activation/metal-leaving group activation (see Fig. 2.1).

It has been known for quite some time that trivalent lanthanide ions are highly effective at activating the phosphate diester bond to hydrolysis at moderately alkaline pHs. There have been many attempts to bind these lanthanides to various ligands in order to improve the ion's solubility and reactivity toward phosphate esters. In most reported cases, the ligand-bound Ln^{3+} ions hydrolyzed phosphates more slowly than the ligand-free Ln^{3+} ion. In this study, the data from previous work that showed that the buffer "bis-tris" bound the Ln^{3+} ion tightly is used to design a dinuclear Ln(iii) complex which will be characterized and tested for reactivity with phosphate diesters.

Developing mononuclear complexes that hydrolyze phosphates rapidly should provide valuable insights into developing novel artificial dinuclear phosphoesterases. Here, a novel mononuclear copper complex will be synthesized and tested for phosphate diester hydrolysis.

1.5 Chapter 1 References

1. Watson, J.D.; Crick, F.H.C. *Nature* **1953** 171,964-7.

2. Williams, N.; Takasaki, B.; Wall, M.; Chin, J. *Acc. Chem. Res.* **1999** 32, 485-93.

3. Kirby, A. Advances in Phys. Org. Chem. Eds. Gold, V. et al. Toronto: Academic Press, 17, 183-278.

4. Westheimer, F.H. *Acc. Chem. Res.* **1968** 1, 70-8.

5. Thatcher, G.; Kluger, R. *Adv. Phys. Org. Chem.* **1989** 25, 99-265.

6. Bunton, C.A. *Acc. Chem. Res.* **1970** 257.

7. Freeman, S.; Freeman, J.M.; Knowles, J.R. *J. Am. Chem. Soc.* **1988** 110, 1268.

8. Guthrie, J.P. *Acc. Chem. Res.* **1983** 16, 122.

9. Aqvist, J.; Warshel, A. *Biochem.* **1989** 28, 4680.

10. Weber, D.J.; Meeker, A.K.; Mildvan, A.S. *Biochem.* **1991** 30, 6103.

11. Anslyn, E.; Breslow, R. *J. Am. Chem. Soc.* **1989** 111. 4473-82.

12. Blackburn, P.: Moores, S. *The Enzymes* **1972** 15, 317.

13. Richards, R.M.; Wyckoff, H. *The Enzymes* **1961** 4, 648.

14. Fersht, A., Enzyme Structure and Mechanism (1985) 426-33, New York: W.H. Freeman.

15. Findlay, D.; Hemes, D.G.; Mathias, A.P.; Rabin, B.R.; Ross, C.A. *Nature* **1961** 190, 781.

16. Beese, L.S.; Steitz, T. A. *EMBO J.* **1991** 10, 25-33.

17. Steitz, T.; Steitz, J. *Proc. Natl. Acad. Sci USA* **1993** 90, 6498-6502.

18. Yang, W.; Hendrickson, W.A.; Crouch, R.J.: Satow, Y. *Science* **1990** 249, 1398-1405.

19. Hausen, P.; Stein, H. *Eur. J. Biochem* **1970** 14, 278-83.

20. Vallee, B.L.; Auld, D.S. *Biochem.* **1993** 32. 6493.

21. Cech, T.R.; Zaug, A.J.; Grabowski, P.J. *Cell* **1981** 27, 487-96.

22. Celander, D.; Cech, T. *Science* **1991** 251, 401-7.

23. Piccirilli, J.A.; Kyle, J.S.; Caruthers, M.H.; Cech, T.R. *Nature* **1993** 361, 85-88.

24. Weinstein, L.B.; Jones, B.C.N.M.; Cosstick, R.; Cech, T.R. *Nature* **1997** 388, 805-8.

25. Smith, J.; Ariga, K.; Anslyn, E. *J. Am. Chem. Soc.* **1993** 115, 362-4.

26. Jubian, V; Dixon, R.P.; Hamilton, A.D. *J. Am. Chem. Soc.* **1992** 114. 1120-1.

27. Hosseini, M.W.; Lehn, J.-M.; Jones, K.C.; Plute, K.; Mertes, M. *J. Am. Chem. Soc.* **1989** 111, 6330-5.

28. Hendry, P.; Sargeson, A.M. *Inorg. Chem.* **1990** 29, 92-7.

29. Hendry, P.; Sargeson, A.M. *Aust. J. Chem.* **1986** 39, 1177.

30. Benkovic, S.; Dunikoski, L. *J. Am.. Chem. Soc.* **1971** 93, 1526.

31. Murakami, Y.; Sunamoto, J. *Bull. Chem. Soc. Japan* **1971** 44, 1827.

32. Fife, T.; Pujari, M. *J. Am. Chem. Soc.* **1988** 110, 7790-7.

33. Linkletter, B.; Chin, J. *Angew. Chem.. Intl. Ed. Engl.* **1995** 34, 472-4.

34. Williams, N.H.; Chin, J. *J. Chem. Soc, Chem. Commun.* **1996** 131-2.

35. Wahnon, D.; Lebuis, A. *Angew. Chem. Intl. Ed. Engl.* **1995** 34, 2412-4.

36. Young, M.J.; Chin, J. *J. Am. Chem. Soc.* **1995** 117, 10577-8.

37. Vance, D.; Czarnik, A. *J. Am. Chem. Soc.* **1993** 113, 12165-6.

38. Tsubouchi, A.; Bruice, T. *J. Am. Chem. Soc.* **1994** 116, 11614-5.

39. PhD thesis, Jin Seog Seo, McGill University, 1997.

40. Bashkin, J.K.; Frolova, E.; Sampath, U. *J. Am. Chem. Soc.* **1994** 116, 5981-2.

41. Magda, D.; Miller, R. A.; Sessler, J.L.; Iverson, B. *J. Am. Chem. Soc.* **1994** 116, 7439-40.

42. Magda, D.; Crofts, S.; Lin, A.; Miles, D.; Wright, M.; Sessler, J. *J. Am. Chem. Soc.* **1997**119, 2293-4.

43. Matsumura, K.; Endo, M.; Komiyama, M. *J. Chem. Soc., Chem. Commun.* **1994**, 2019-20.

44. Fitzsimons, M.; Barton, J. *J. Am. Chem. Soc.* **1997** 199, 3379-80.

45. Schnaith, L.; Hanson, R.; Que, L. *Proc. Natl. Acad. Sci. USA* **1998** 91, 569-73.

46. Trawick, B.; Daniher, A.; Bashkin, J. *Chem. Rev.* **1998** 98, 939-60.

47. Zelenko, O.; Gallagher, J.; Xu, Y.; Sigman, D. *Inorg. Chem.* **1998** 37, 2198-2204.

48. Sigman, D.S.; Mazumder, A.; Perrin, D.M. *Chem. Rev.* **1993** 93, 2295-2316.

49. Sigman, D.S. *Biochem.* **1990** 29, 9097.

50. Hertzberg, R.; Dervan, P. *J. Am. Chem. Soc.* **1982** 104, 313-5.

51. Beal, P.; Dervan, P. *J. Am. Chem. Soc* **1992** 114, 4976-82.

52. Luebke, K.; Dervan, P. *J. Am. Chem. Soc.* **1991** 113, 7447-8.

53. Shullenberger, D.; Eason, P.; Long, E.C. *J. Am. Chem. Soc.* **1993** 115, 11038-9.

54. Mack, D.; Dervan, P. *J. Am. Chem. Soc.* **1990** 112, 4604-6.

55. Chen, X.; Rokita, S.; Burrows, C. *J. Am. Chem. Soc.* **1991** 113, 5884-6.

56. Cheng, C.; Rokita, S.; Burrows, C. *Angew. Chem. Intl. Ed. Engl.* **1993** 32, 277-8.

57. Muller, J.G.; Hickerson, R.; Perez, R.; Burrows, C *J. Am. Chem. Soc.* **1997** 119, 1501-6.

58. Liang, Q.; Ananias, D.; Long, E. *J. Am. Chem. Soc.* **1998** 120, 248-57.

59. Silani, A.; Long, E.; Pyle, A.; Barton, J. *J. Am. Chem. Soc.* **1992** 114, 2303-12.

Chapter 2. Differentiation of Double Lewis Acid Activation From Other Modes of Activation for Phosphate Diester Cleavage

2.1 Introduction

In their active site, quite a number of enzyme phosphoesterases contain two metal ions separated by 3-5 Å (Table 2.1). Consequently, there has been a fair amount of speculation about the role of these metals in enzyme-promoted phosphate ester hydrolysis.[1-3] Since enzymes are proteins which have complicated tertiary and quaternary structure, a number of research teams have developed simpler non-natural dinuclear metal complexes that bind and hydrolyze phosphates in order to elucidate the function of the two metals in nucleases.[4-8]

Enzyme	Intermetal Distance (Å)
alkaline phosphatase	4.1 Zn—Zn
phospholipase C	3.2 Zn—Zn
kidney bean purple acid phosphatase	3.1 Fe—Zn
RNase H	4.0 Mn—Mn
3′,5′-exonuclease of DNA polymerase I	3.9 Zn—Mg

Table 2.1 A sample of intermetal distances in enzyme phosphoesterases with two metals in the active site.

Double Lewis acid activation has been proposed as the mode of activation involved for a number of dinuclear metal complexes that hydrolyze phosphate diesters (Fig. 2.1). Although Sargeson estimated that single Lewis acid activation gives at most 2-3 orders of magnitude rate acceleration for phosphate diester hydrolysis[9-10], the estimated rate acceleration resulting from double Lewis acid activation has been postulated to be as high as between 5 and 6 orders of magnitude.[11] How might one explain the significantly greater reactivity from double Lewis acid activation? As stated previously, single Lewis acid activation acts to disperse the negative charge from the bound phosphate oxygen, allowing the incoming hydroxide to attack the phosphorus. However, as the hydroxide attacks the phosphorus centre, a negative charge develops on another phosphate oxygen. If a second metal is present, the developing negative charge will be quenched by that metal. As a consequence, double Lewis acid activation allows for greater rate accelerations for phosphate diester hydrolysis to be observed than in the case of single Lewis acid activation.

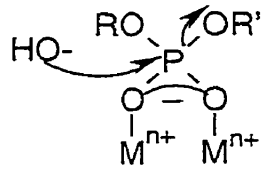

Double Lewis Acid Activation

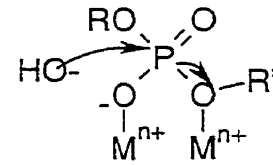

Joint Single Lewis Acid Activation/ Leaving Group Activation

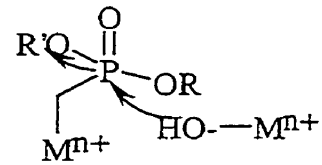

Joint Single Lewis Acid Activation/ Metal-Nucleophile Attack

Figure 2.1 Three kinetically indistinguishable mechanisms for two metal ion-promoted phosphate diester hydrolysis

Two metals can cooperate to hydrolyze phosphate diesters in other ways also. One metal may act to bind the leaving group while the other acts as a Lewis acid (joint single Lewis acid activation/metal-leaving group activation) (Fig. 2.1). Alternatively, a hydroxide group bound to one metal may provide a nucleophile while the other metal provides a Lewis acid. Joint single Lewis acid activation/metal-hydroxide attack and joint single Lewis acid activation/leaving group attack are kinetically indistinguishable from double Lewis acid activation (see derivation in Appendix 2.2). When mechanisms are referred to as kinetically indistinguishable this means that all three mechanisms have the same molecularity and are expected to show identical pH rate profiles and concentration rate profiles.

Two kinetically indistinguishable mechanisms may be distinguished using a number of techniques. The method of isotopic labelling is often invoked precisely for this purpose. For example, Wahnon *et al.* distinguished metal-oxide catalyzed phosphate diester hydrolysis from an external hydroxide-assisted hydrolysis for a $Co_2(tacn)_2(OH)_2$ complex (see Fig. 1.14) using isotopic labelling. In order to distinguish the two mechanisms, the products from a $Co_2(tacn)_2(OH)_2$-promoted MPNP hydrolysis reaction in O^{18}-labelled solvent were compared to the products from a solution where the bridging hydroxide of the dinuclear cobalt complex is O^{18}-labelled. Since O^{18} was incorporated into the methyl phosphate product only when the dinuclear complex was O^{18}-labelled, external nucleophile-promoted hydrolysis was ruled out and the metal-oxide-promoted reaction was instead proposed.

p-Nitrophenyl phosphate esters such as HPNP are often used as nucleic acid models because the hydrolysis product *p*-nitrophenolate has a large molar

absorptivity coefficient (ε= 18,700 $M^{-1}cm^{-1}$) at λ=400 nm. The reaction may therefore be monitored readily by UV/Vis spectrometry.

p-Nitrophenol is a good leaving group with a pKa of 7.2. As a consequence, the hydrolysis of the *p*-nitrophenyl phosphate esters may be observed on a laboratory time scale even using catalysts that only exhibit a few orders of magnitude rate acceleration. DNA, on the other hand, has a poor leaving group. Even if a catalyst were developed which could hydrolyze a DNA phosphate ester bond under ambient conditions with an impressive billion-fold rate acceleration, the half-life for the hydrolysis would still be at least 10 years!!![12] Although a number of voices refer to working with *p*-nitrophenyl phosphate esters disparagingly as the "*p*-nitrophenyl ester syndrome"[13], the author believes that since metals or protons can bind to DNA or RNA to make them better leaving groups, working with the model activated *p*-nitrophenyl phosphate esters may still be useful in the development of artificial endonucleases.

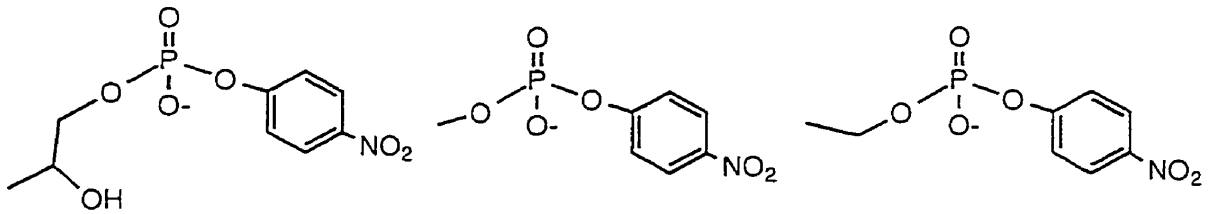

Figure 2.2 The internal nucleophile of HPNP provides several tens of thousands fold rate acceleration over the two alkyl analogues for hydroxide-promoted phosphate bond cleavage.

Like RNA, HPNP contains an OH group which can act as an internal nucleophile. A comparison of the hydroxide-catalyzed cleavage of HPNP to the hydrolysis of methyl *p*-nitrophenyl phosphate (MPNP)[14] reveals that HPNP[15] is cleaved tens of thousands of times more rapidly (Table 2.2). One would expect

that the rate of hydrolysis of ethyl (EPNP) or 1-propyl *p*-nitrophenyl phosphate would not be significantly different from that observed for MPNP (Figure 2.2) since a small change in the alkyl group should not interfere considerably with hydroxide attack of the phosphorus. And indeed, Hendry and Sargeson have reported a second-order rate constant of 3.3×10^{-7} $M^{-1}s^{-1}$ at 25°C for the hydrolysis of EPNP[16]. It is apparent from these rates that the OH group of HPNP provides a significant entropy advantage for phosphate cleavage over HPNP's alkyl aryl phosphate analogues.

	k ($M^{-1}s^{-1}$)	relative rate
HPNP	0.168 (25°C)	8.8×10^4
MPNP	1.9×10^{-6} (45°C)	1

Table 2.2 Second-order rate constants for the hydroxide-catalyzed cleavage of HPNP and MPNP.[15]

In this chapter, $Cu_2(bbmp)Cl_2$ (Figure 2.2) is used as a catalyst to distinguish mechanisms for two metal-promoted phosphate hydrolysis. In the case of $Co_2(tacn)_2(OH)_2$-promoted hydrolysis, isotopic labelling was used to distinguish between mechanisms. However, Co^{3+} ion is substitutionally inert while Cu^{2+} is substitutionally labile. Since the Cu^{2+} ion is substitutionally labile, isotopic labelling cannot be used to distinguish double Lewis acid activation from the other two metal ion-promoted hydrolysis mechanisms in the case of Cu_2bbmp.

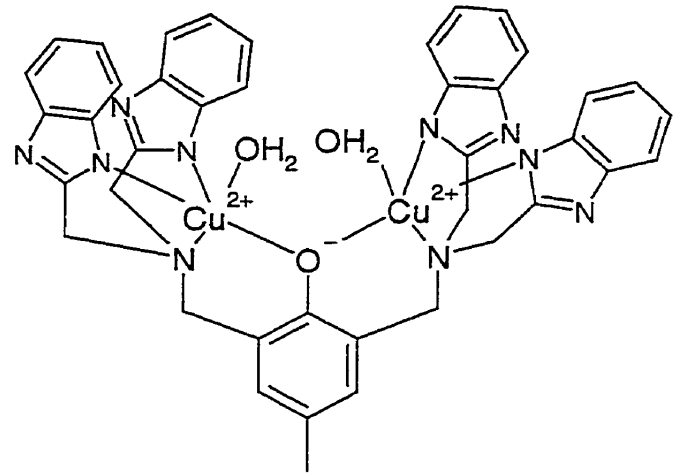

Figure 2.3 Dinuclear complex $Cu_2(bbmp)Cl_2$[17]

2.2 Results

To examine the feasibility of joint metal-nucleophile attack/single Lewis acid activation as the mechanism by which Cu_2bbmp cleaves HPNP, the cleavage rate of HPNP is compared to a phosphate substrate without an internal nucleophile, MPNP. By means of comparison, the hydrolyses of these two substrates are also tested using *cis*-diaquo cobalt (iii) cyclen complex (Table 2.3) as catalyst. *Cis*-diaquo cobalt (iii) cyclen is one of the fastest known metal catalysts for hydrolyzing certain phosphate esters.[18]

50μM phosphate	5 mM Co^{3+}(cyclen), pH 7.0, 50°C	1 mM Cu_2(bbmp) pH 7.0, 25°C
HPNP	$(1.3\pm0.2) \times 10^{-3}$ s^{-1}	$(2.1 \pm 0.2) \times 10^{-3}$ s^{-1}
MPNP	$(1.1\pm0.2) \times 10^{-3}$ s^{-1}	$(1.5 \pm 0.2) \times 10^{-5}$ s^{-1}

Table 2.3 The pseudo-first-order rate constants for HPNP and MPNP cleavage using Co^{3+}(cyclen) or Cu_2(bbmp) as catalyst.

Let us first consider the Co(cyclen)-promoted hydrolysis of the *p*-nitrophenyl phosphate esters. As discussed previously, in the case of hydroxide-promoted hydrolysis of HPNP and MPNP, the alcohol OH moiety of HPNP attacks the phosphorus centre to give a rate of transesterification which is tens of thousands of times faster than the MPNP hydrolysis rate. However, from the results in Table 2.3, in the case of Co(cyclen)-promoted hydrolysis, the rates of nitrophenol production are quite close. Evidently, the hydroxy internal nucleophile of HPNP is irrelevant to the reaction rate. One can therefore reasonably rule out a chelation/quasi-double Lewis acid activation as the mechanism involved. If chelation were indeed occurring, the transesterification of HPNP would be expected to be considerably faster than the hydrolysis of MPNP since an internal nucleophile would be much more effective than an external nucleophile. Instead, it is logical to propose that the Co(cyclen)-mediated reaction is taking place by joint metal-hydroxide/single Lewis acid activation (Figure 2.4).

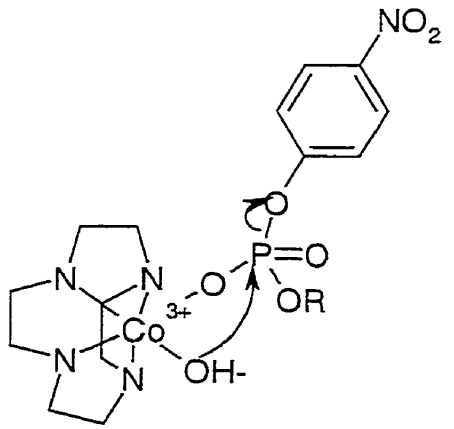

Figure 2.4 Proposed mechanism for Co^{3+}(cyclen)-mediated HPNP and MPNP hydrolysis

In the case of Cu_2(bbmp)-promoted cleavage of the *p*-nitrophenyl phosphate esters, HPNP cleavage is over a hundred-fold faster than MPNP

hydrolysis. Since one would expect that a joint single Lewis acid activation/metal-hydroxide attack mechanism would result in a similar rate for HPNP and MPNP hydrolysis as in the case of Co(cyclen)-promoted cleavage, this mode of activation may reasonably be dismissed (Figure 2.5).

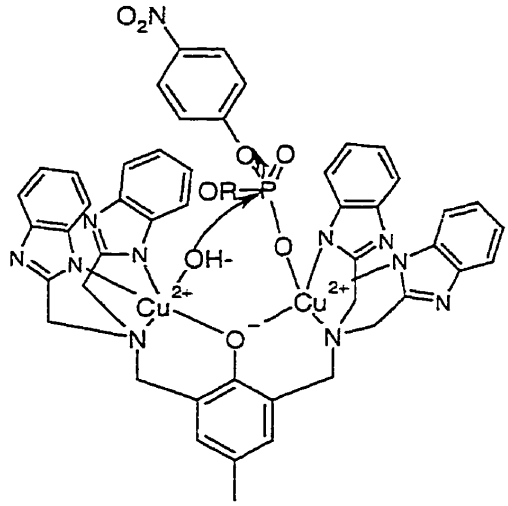

Figure 2.5 Joint single Lewis acid activation/ metal-hydroxide attack is RULED OUT for Cu2(bbmp)-promoted HPNP and MPNP cleavage. (See Figure 2.8 for possible mechanisms)

Joint single Lewis acid activation/metal-nucleophile attack has similarly been ruled out for another substitutionally labile metal complex. In this laboratory, Wahnon undertook a similar study to that shown here for a dinuclear copper (ii) tetrakis(benzimidazolyl)-2-hydroxy-1,3-diaminopropane complex- (Figure 2.6) promoted cleavage using HPNP and MPNP substrates.[19] This dinuclear Cu (ii) complex cleaved HPNP 355 times faster than MPNP at pH 7.0 and 25°C.

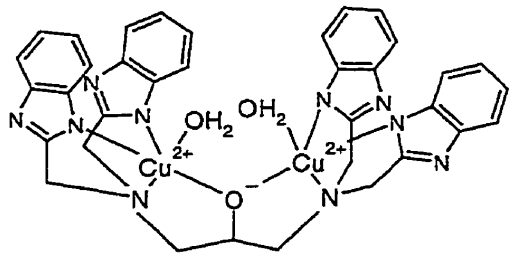

Figure 2.6 Wahnon's dinuclear copper (ii) complex

One might also propose joint single Lewis acid activation/leaving group activation as the mechanism for Cu2bbmp-mediated HPNP cleavage. To test this hypothesis, the cleavage reactions of HPNP and HP*m*NP (Figure 2.7) using Cu2bbmp are compared. These two substrates differ only in that the leaving group nitrophenol contains the nitro group in the para position in HPNP while the nitro group is in the meta position in HP*m*NP. The reported pKa of *p*-nitrophenol is 7.2 while the pKa for *m*-nitrophenol is 8.0. The greater stability of the *p*-nitrophenoxide anion over the *m*-nitrophenoxide anion can be ascribed to the greater number of resonance-stabilized forms of the *p*-nitrophenoxide ion.

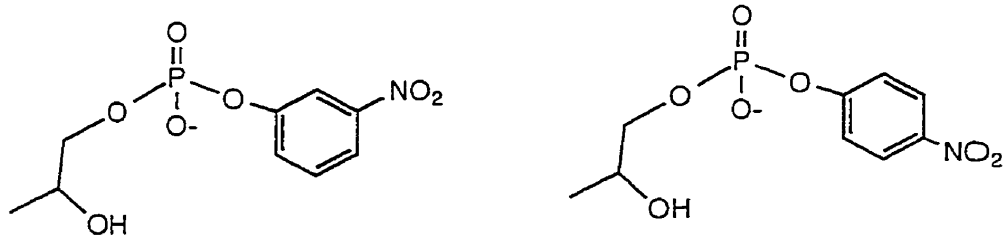

HP*m*NP HPNP

Figure 2.6 2-hydroxypropyl nitrophenyl phosphate esters examined to test joint leaving group activation/single Lewis acid activation hypothesis.

The relationship of the pKa of the leaving group to the rate constant for the hydrolysis of phosphate esters may be expressed in a plot known as a linear free energy relationship (LFER) profile. Recently, Williams *et al.* neatly demonstrated how methyl aryl phosphate hydrolysis and hydroxypropyl aryl

phosphate transesterification by a dinuclear cobalt (iii) complex would be affected by double Lewis acid activation.[11] Unlike the Cu^{2+} ion, the Co^{3+} ion is substitutionally inert which allowed phosphates which bind both Co^{3+} ions of the complex to be synthesized. In the case of the substitutionally inert Co^{3+} complex, there is no ambiguity therefore that double Lewis activation is indeed occurring. The LFER for this reaction is shown in the plot below (Figure 2.7) .

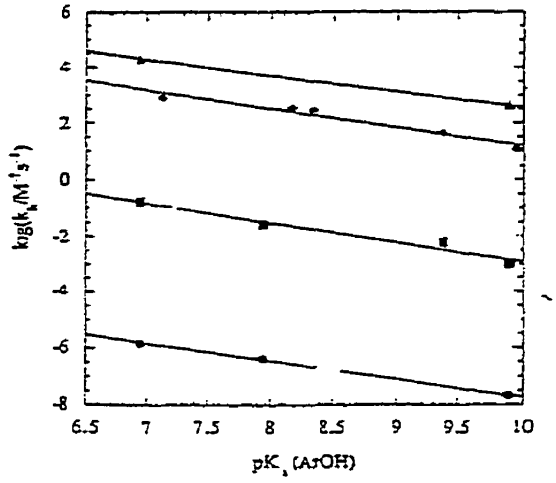

Linear free energy relationships between leaving group pK_a and second-order rate constants for hydrolysis or transesterification catalyzed by hydroxide for methyl aryl diesters (●), 2-hydroxypropyl aryl esters (■)

Figure 2.7 Linear free energy relationship plot for the hydrolysis and transesterification of phosphate diesters using $Co^{3+}_2(tacn)_2(OH_2)_2$ (photocopied with permission). [11]

Since *m*-nitrophenoxide ion is a better Lewis base than the *p*-nitrophenoxide ion, the phenolic oxygen for *m*-nitrophenol is expected to bind more tightly to a Lewis acid metal (Cu^{2+} in the case of Cu_2bbmp) than the phenolic oxygen of *p*-nitrophenol. If joint single Lewis acid activation/leaving group activation were indeed the mode of activation, one would expect that the slope of the linear free energy relationship profile for hydroxypropyl aryl phosphate ester cleavage would be more shallow (or positive) than that observed when double Lewis acid activation occurs (Fig. 2.7). This would occur since the *m*-nitrophenol leaving group of HP*m*NP would bind one metal of the dinuclear metal complex more tightly than the *p*-nitrophenol of HPNP and therefore be cleaved more rapidly than if double Lewis acid activation were the mechanism.

As it turns out, HP*m*NP transesterification using Cu_2bbmp is 34-fold slower than HPNP transesterification (Table 2.3).

1 mM Cu_2bbmp, pH 7.0, 25°C, 50μM S	kobs (s^{-1})
S= HPNP	$(2.1 \pm 0.2) \times 10^{-3}$
S=HP*m*NP	$(6.1 \pm 0.6) \times 10^{-5}$

Table 2.3 Comparison of rates of HPNP vs. HP*m*NP transesterification reactions using Cu_2bbmp complex.

Surprisingly, the observed rate for HP*m*NP hydrolysis is approximately 5-fold slower than what one would expect from the linear free energy relationship for hydroxypropyl aryl phosphate ester transesterification utilizing a double Lewis acid activation mechanism (see Figure 2.7). This slower than expected rate may result from differences in steric interactions between the bulky benzimidazole moieties and the *p*-nitrophenol versus *m*-nitrophenol group. A possible better future choice of substrate to test for joint single Lewis acid activation/leaving group activation would be two 2-hydroxypropyl aryl phosphate esters with similar steric properties. For example, 2-hydroxy *p*-chlorophenyl phosphate versus the *p*-nitrophenyl analogue or 2-hydroxypropyl phenyl phosphate versus fluorinated phenyl analogues might be good substrate choices.

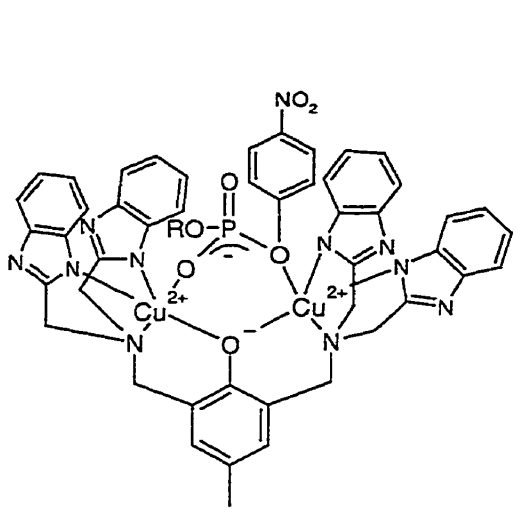

single Lewis acid activation/ leaving group activation could not be distinguished from double Lewis acid activation using HPNP and HP*m*NP substrates

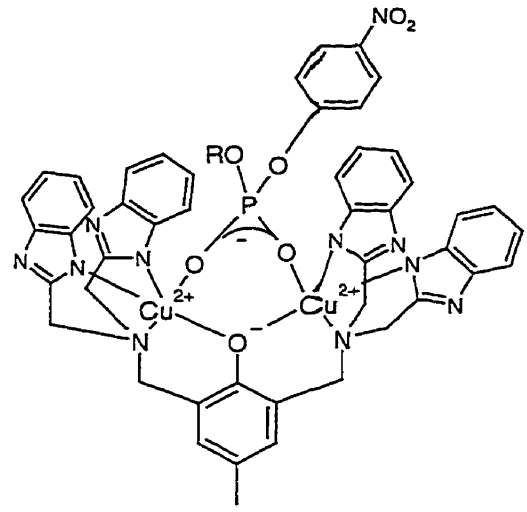

double Lewis acid activation is one proposed mechanism for Cu_2bbmp-promoted phosphate diester hydrolysis

Figure 2.8 Two possible mechanisms for Cu2bbmp-promoted hydroxypropyl aryl phosphate cleavage

2.3 Experimental

GENERAL INFORMATION

2.3.1 Instrumentation

^1H and ^{13}C NMR were recorded on Varian XL-200 MHz and Gemini 200 MHz NMR instruments. ^{31}P NMR were recorded on a Varian XL-300 MHz NMR instrument. The chemical shifts are reported in parts per million (ppm) and were referenced with respect to the solvent in the case of ^1H NMR (in $CDCl_3$ 7.26 ppm; CD_3OD 3.34 ppm; d6-acetone 2.14 ppm; DMSO-d_6 2.49 ppm; H_2O 4.76 ppm). ^{13}C NMR were referenced either with respect to solvent (such as $CDCl_3$ 77.0 ppm) or with an internal standard such as dioxane (67.7 ppm) when

the NMR spectra was collected in D_2O. ^{31}P NMR were referenced with respect to a trimethyl phosphate external reference standard (0 ppm).

UV-Visible kinetics and general scanning experiments were performed on a Hewlett Packard 8452-A silicone diode array spectrophotometer instrument equipped with a deuterium lamp and an RMS Lauda thermostatted water bath.

High performance liquid chromatography (HPLC) experiments were carried out a Hewlett Packard 1090M instrument equipped with a deuterium lamp, autosampler, programmable micro-oven and a silicon diode array detector.

Data points collected from HPLC and UV/Vis data were fit to lines or curves using the least-squares method with the Kaleidagraph 3.0.1 spreadsheet program issued by Abelbeck Software.

Elemental analyses were performed at Robertson Microlit Laboratories, Inc. in Madison, NJ.

A Radiometer Copenhagen RTS822 automatic titrator equipped with a PHM63 pH meter was used for the potentiometric titrations of ligands and metal complexes. A Radiometer K-4040 calomel reference elctrode and a G-2040-C glass electrode was used for pH measurements for titrations. Otherwise, pHs were measured using an Accumet pH meter and an Orion 8103 Ross Combination Electrode. The electrodes were calibrated using buffer solutions at pHs 4, 7 and 10 prior to use.

2.3.2. Kinetics

All solutions were degassed and prepared volumetrically. Aliquots of solutions were dispensed using Eppendorf pipettes which had been calibrated against the weight of degassed, Milli Q water. For HPNP and MPNP cleavage, 4-nitrophenoxide ion increase was monitored at λ=400 nm on the UV-Vis spectrophotometer. Pseudo-first-order rate constants for exponential increases were obtained by iteratively fitting reactions that were carried out to three half-lives or more to the equation: $[X]_t = [A]_0(1-e^{-kt})$. Pseudo-first-order rate constants for exponential decreases were obtained by fitting data to the equation $[X]t = [A]_0\ e^{-kt}$. Some rates were determined using the method of initial rates. For most accurate results, the metal complex solution prepared for HPNP transesterification was also used for MPNP hydrolysis and phosphate cleavage reactions were monitored simultaneously on the UV-Vis spectrophotometer. Kinetics runs were done in triplicate with a maximum error of 5%.

HP*m*NP cleavage was measured by following the decrease of HP*m*NP monitored by HPLC (Figure 2.9) using the same solution that was simultaneously tested by the UV-Vis method shown above for HPNP cleavage. HPNP hydrolysis was tested after six hours to check for any decomposition; the rate had not fallen below 10% error. Integrations for HP*m*NP were compared to an internal *p*-nitrobenzenesulfonic acid standard (Figure 2.9). Only *m*-nitrophenol was observed as a product under the HPLC conditions used.

HPLC CONDITIONS

Separation of HP*m*NP transesterification substrates and products were done on a 2.1 x 100 mm 5µM ODS Hypersil C-18 Reverse Phase column at 40°C. Five minutes of 0.2 M ammonium phosphate buffer (pH 5.5) is eluted initially followed by a linear gradient of 0 to 100% 3:2 methanol:water over a period of 15

minutes. Authentic samples tested immediately prior to Cu_2bbmp-catalyzed HP*m*NP transesterification showed the following retention times: *p*-nitrobenzenesulfonic acid 4.5 min; HP*m*NP 11.8 min.; *m*-nitrophenol 12.6 min.

2.3.3 Chemicals

The barium salts of HPNP and HP*m*NP were synthesized according to the method of Brown and Usher courtesy of Mary Jane Young and Nick Williams respectively.[15] Co(cyclen) was provided by Jin Seog Seo who used the standard literature procedures for making the aza macrocycle metal complex.[20] BBMP was synthesized according to the method of Stephan and Berends and checked by ^{1}H NMR and melting point determination before use. Cu_2bbmpCl_2 was synthesized as reported.[21-22] *m*-Nitrophenol, *p*-nitrophenol and *p*-nitrobenzenesulfonic acid were all purchased from Aldrich.

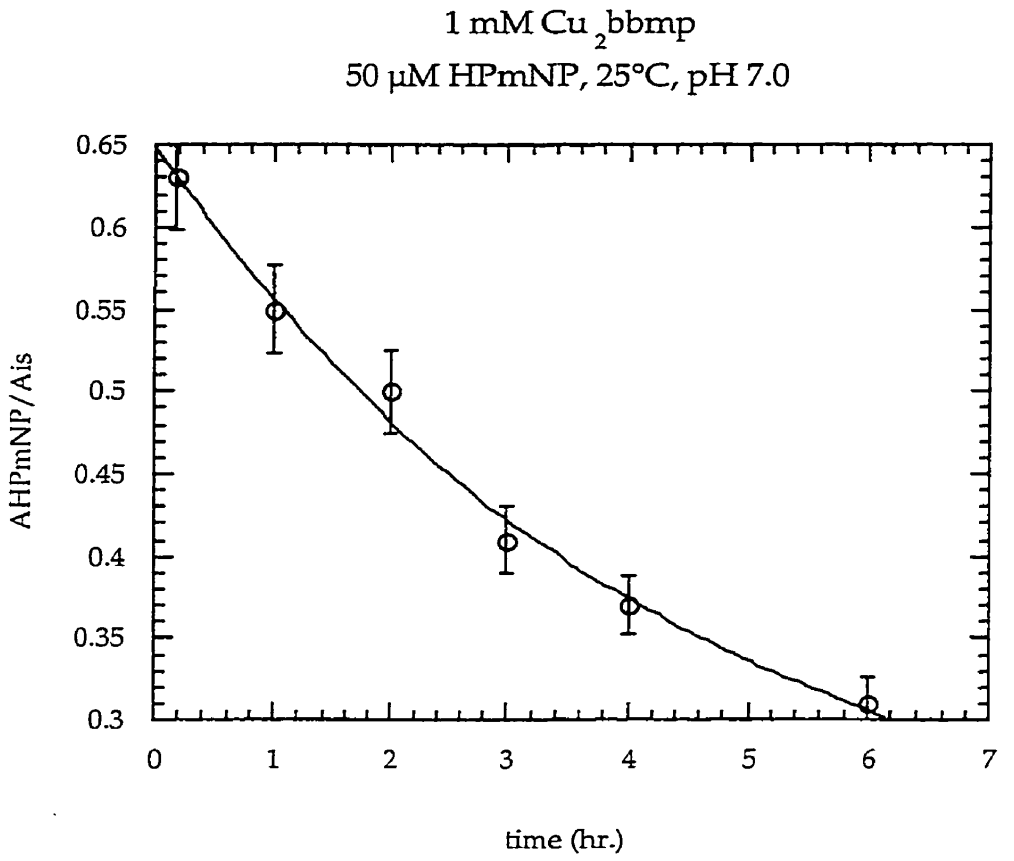

Figure 2.9 Sample run of HP*m*NP hydrolysis. Absorbance of HP*m*NP over *p*-nitrobenzenesulfonic acid internal standard absorbance vs. time. Additional points after 6 hours were not included due to decomposition of metal complex.

2.4. Chapter 2 References

1. Karlin, K *Science* **1993** 261, 701-8.

2. Sträter, N.; Lipscomb, W.; Klabunde, T.; Krebs, B. *Angew. Chem. Intl. Ed. Engl.* **1996** 35, 2024-55.

3. Wilcox, D.E. *Chem. Rev.* **1996** 96, 2435.

4. Young, M.J.; Chin, J. *J. Am. Chem. Soc.***1995** 117, 10577.

5. Ragunathan, K.G.; Schneider, H-J. *Angew. Chem. Intl. Ed. Engl.* **1996** 35,1219.

6. Molenveld, P.; Kapsabelis, S.; Engbersen, J.F.J.; Reinhoudt, D. *J. Am. Chem. Soc.* **1997** 119, 2948.

7. Yashiro, M.; Ishikubo, A.; Komiyama, M. *J. Chem. Soc. Chem. Commun.* **1995**, 1793.

8. Göbel, M.W. *Angew. Chem. Intl. Ed. Engl.* **1994** 33, 1141.

9. Hendry, P.; Sargeson, A.M. *Prog. in Inorg. Chem: Bioinorg. Chem* **1992** 38, 201-58.

10. Hendry, P; Sargeson, A.M. *Inorg. Chem.* **1990** 29, 92-7.

11. Williams, N.H.; Cheung, W.; Chin, J. *J. Am. Chem. Soc.* **1998** 120, 8079-87.

12. Williams, N.; Takasaki, B.; Wall, M.; Chin, J. *Acc. Chem. Res.* **1999** 32, 485-93.

13. Menger, F.M.; Ladika, M. *J. Am. Chem. Soc.* **1987** 109, 3145-6.

14. Hengge, A.C.; Cleland, W.W. *J. Org. Chem.* **1991** 56, 1972-4.

15. Brown, D.M.; Usher, D.A. *J. Chem. Soc.* **1965** 6558-64.

16. Hendry, P.; Sargeson, A. *Inorg. Chem.* **1990** 29, 97-104.

17. Wall, M.; Hynes, R.C.; Chin, J. *Angew. Chem. Intl. Ed. Engl.* **1993** 32, 1633.

18. Kim, J.H.; Chin, J. *J. Am. Chem. Soc.* **1992** 114, 9792-5.

19. Wahnon, D., Ph.D. thesis, McGill University, 1989.

20. Richiman, J.E.; Atkins, T.J. *J. Am. Chem. Soc* **1974** 96, 2268.

21. Berends, H.P.; Stephan, D.W. *Inorg. Chim. Acta* **1985** 99, L53-L56.

22. Berends, H.P.; Stephan, D.W. *Inorg. Chem.* **1987** 26, 749-54.

23. Wall, M., Ph. D. thesis, McGill University, 1997.

Chapter 2 Appendix

Appendix 2.1 X-ray crystal structure for Cu_2bbmp (photocopied with permission)[23]

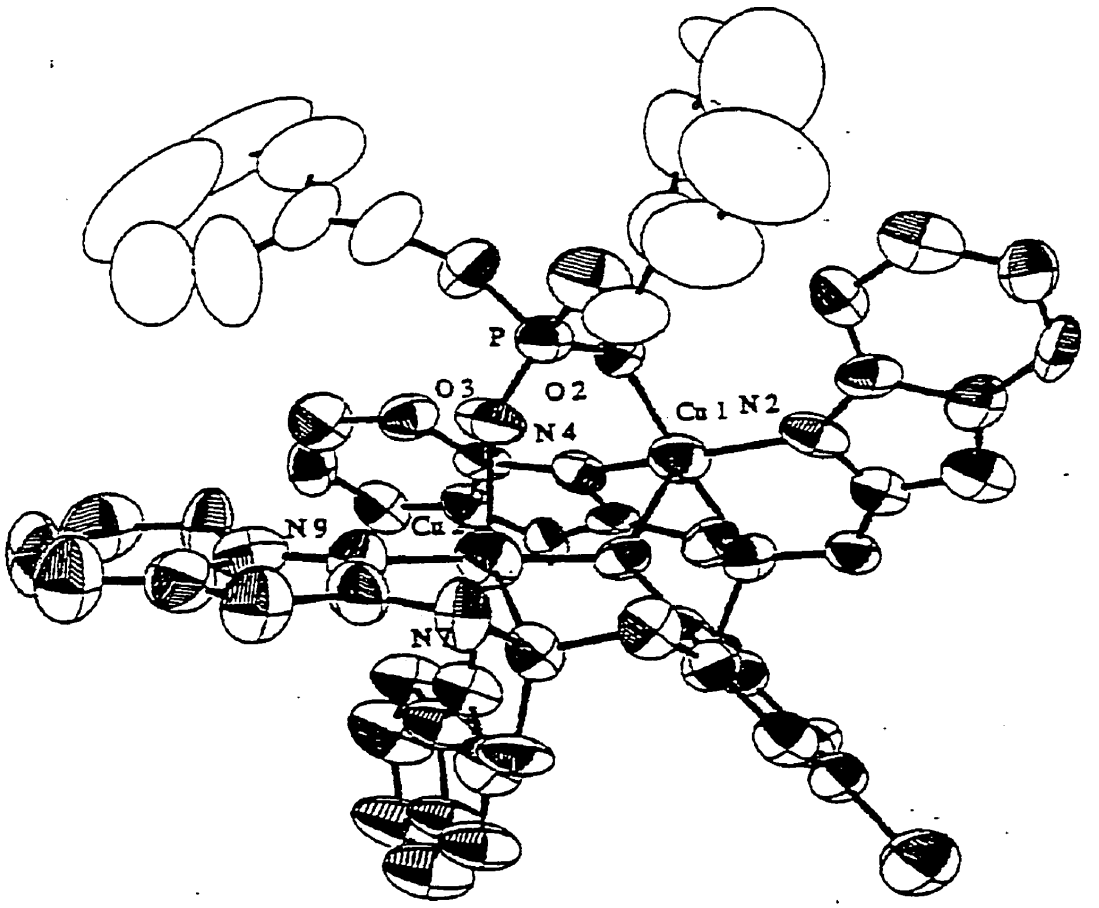

Appendix 2.2 Derivation of Rate Equations for Three Kinetically Indistinguishable Mechanisms for Two Metal-Promoted Phosphate Diester Hydrolysis

Appendix 2.2.1 Double Lewis Acid Activation

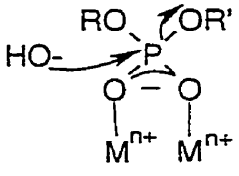

A

Double Lewis Acid Activation

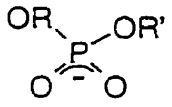

B

+

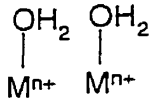

C

A + H_2O

Equation 1 $dP/dt = k[A][OH^-]$ where k is the rate constant for the two-metal-promoted phosphate diester hydrolysis by a double Lewis acid activation mechanism.

Equation 2 $[A] = K[B][C]$

Plug equation 1 into equation 2.

Equation 3 $dP/dt = kK[B][C][OH^-]$

Appendix 2.2.2 Joint Single Lewis Acid Activation/ Leaving Group Activation

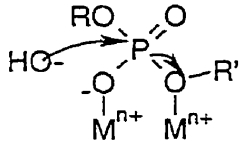

D

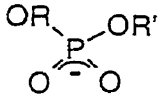

B

+

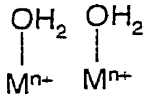

C

D + H_2O

Joint Single Lewis Acid Activation/ Leaving Group Activation

Equation 4 $dP/dt = k'[D][OH^-]$ where k' is the rate constant for the two-metal-promoted phosphate diester hydrolysis reaction by a joint single Lewis acid activation/leaving group activation mechanism.

Equation 5 [A] = K'[B][C]

Equation 6 dP/dt= k'K'[B][C][OH-] is obtained by plugging Eq. 5 into Eq. 4.

Appendix 2.2.3 Joint Single Lewis Acid Activation/ Metal-Hydroxide Attack

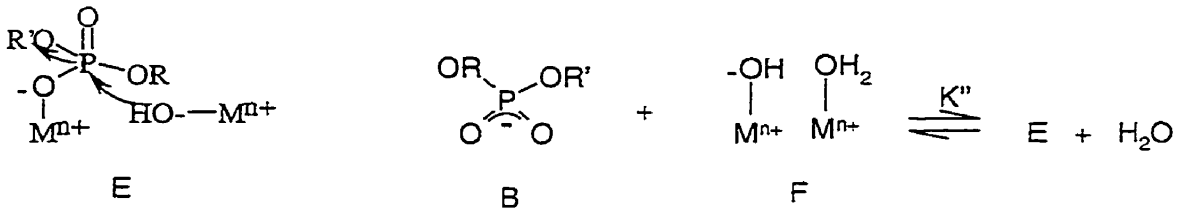

E B F

Joint Single Lewis Acid Activation/
Metal-Nucleophile Attack

Equation 7. dP/dt= k''[E] where k'' is the rate constant for two-metal-promoted phosphate diester hydrolysis by a joint single Lewis acid activation/metal-nucleophile attack mechanism. (Remember that the two metals are both contained in a single molecule.)

Equation 8. [E]= K''[B][F]

Equation 9. dP/dt= k''K''[B][F]

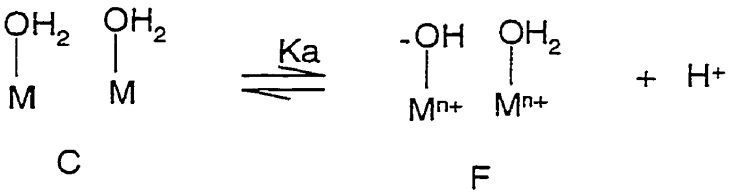

C F

Equation 10 Ka= [F][H+]/[C]

Equation 11. Kw= [H+][OH-]

Plug equation 11 into 10 and then plug 10 into 9 to arrive at the equation below.

Equaton 12. dP/dt= (k"K" Ka/Kw) [B][C][OH-]

Chapter 3. Lanthanide (iii) Complex Promoted Hydrolysis of Phosphate Diesters

3.1 Introduction

Over the past few decades, much of the work done in the area of phosphate diester hydrolysis has involved lanthanide ions, transition metal complexes and most recently actinide ions. In the case of transition metal complexes, extraordinary rates of acceleration for phosphate diester hydrolysis are observed over the free transition metal ion-promoted reaction when an appropriate ligand is used.[1-2] Using a ligand can be beneficial since it may prevent dimerization and create favorable bond angles for phosphate chelation. Although it has been known since the 1950s and 1960s that lanthanide ions are quite effective in accelerating phosphate diester hydrolysis, most attempts to develop a lanthanide-binding ligand which would accelerate the rate of hydrolysis versus the free lanthanide rate have been unsuccessful.

The recorded history of lanthanide-promoted phosphate ester hydrolysis begins in the mid-1950s, when Westheimer showed that phosphate monoesters are hydrolyzed by lanthanum hydroxide gels to give modest rate accelerations.[3] Eichhorn and coworkers showed that transfer RNA is cleaved by lanthanide (iii) ions in 1965.[4] Rutherford *et al.* reported in 1972 that TppT, a dinucleoside pyrophophate, is also cleaved by lanthanide (iii) ions.[5]

The 1990s have seen a large resurgence in the area of lanthanide ion-assisted phosphate diester hydrolysis. In 1993, Takasaki showed that the La^{3+} ion acts synergistically with ten-fold excess hydrogen peroxide to give 34,000 fold rate enhancement over peroxide-free La^{3+} ion-promoted BNPP hydrolysis at pH 7.0 and 25°C (Figure 3.1).[6] A similar synergism between lanthanides and

hydrogen peroxide is also observed by Komiyama and coworkers in 1998 for the hydrolysis of dinucleotides ApA and CpC.[7]

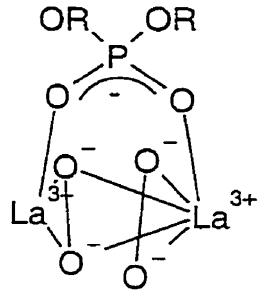

Figure 3.1 Lanthanum ion acts cooperatively with peroxide to hydrolyze phosphates with several orders of magnitude rate acceleration.

In a breakthrough discovery reported in 1994, Takasaki showed that Ce^{3+} ion in the presence of oxygen hydrolyzes dimethyl phosphate (DMP) twelve orders of magnitude faster than uncatalyzed DMP hydrolysis.[8] This unprecedented result was quite remarkable as a vast majority of artificial metal phosphoesterases are unable to hydrolyze phosphate esters with poor leaving groups (such as DNA). Consequently, Ce^{3+}/dioxygen-promoted dideoxynucleotide (dApdA) hydrolysis was also examined and was observed to be between 10^{10}-fold and 10^{11}-fold faster than the hydroxide-catalyzed reaction. Cerium was of particular interest since it is the only lanthanide ion which may readily convert to the +4 oxidation state. The mechanism for $Ce^{3+}\bullet O_2$-promoted phosphate cleavage hydrolysis is believed to involve autooxidation to Ce^{4+} but the exact mode of cleavage is still disputed. It is clear however that hydrolysis rather than oxidative cleavage is occurring from product analysis.

Moss and coworkers have also shown that Ce^{4+} ions may be used to cleave bis-*p*-nitrophenyl phosphate (BNPP) 2.4 billion times faster than the background rate in the presence of nonionic Brij-35 or other micelles.[9] In a

related study, Moss *et al.* also discovered that similar rate accelerations are observed when a tetravalent actinide ion (Th^{4+}) in the presence of Brij micelle is used to hydrolyze the *p*-nitrophenyl phosphate BNPP (2.82×10^{-2} s^{-1} at 37°C). [10]

In 1997, Hurst *et al.* showed that at moderately alkaline pHs, La^{3+} ions form dimers or higher order aggregates that hydrolyze ApA 4 orders of magnitude faster than the equivalent rate of lanthanum (iii) ion monomer-promoted hydrolysis.[11] Elegant kinetic studies indicate that the active form of the La^{3+} ion for phosphate hydrolysis contains five hydroxyl groups for every two La^{3+} ions (Figure 3.2).

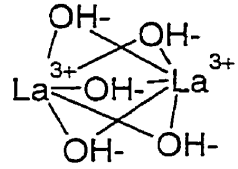

Figure 3.2 Proposed lanthanide dimer which hydrolyzes ApA with enormous rate acceleration.

Considering the remarkable rate accelerations observed using lanthanide ion-promoted phosphate hydrolysis, a number of groups sought to develop ligands which would further improve the reactivity of lanthanides toward phosphates. At moderately basic pH values, Ln^{3+} ions precipitate out to form lanthanide-hydroxide gels at concentrations above 2 mM in water; therefore, a suitable ligand has the potential of improving the solubility of lanthanide ions in aqueous solutions. Also, since lanthanide ions are relatively toxic, the discovery of a ligand that would bind the ions tightly could have important ramifications on their usage in medicine.

Morrow and coworkers have developed cyclen ligands with pendant alcohol (or amide) groups that cleave BNPP in a transesterification reaction

where approximately seven orders of magnitude rate acceleration over the hydroxide-catalyzed hydrolysis is observed (Figure 3.3).[12-14] However, these lanthanide complexes with a metal-alkoxide nucleophile only demonstrate a modest acceleration over the free Ln^{3+} ion-promoted reaction. Nevertheless, these complexes do have potential application as artificial restriction enzymes. Additionally, the europium complex in Fig. 3.3 also provides several orders of magnitude rate acceleration over the hydroxide-catalyzed reaction for the cleavage of the messenger RNA (mRNA) cap, m^7GpppG.[15-16]

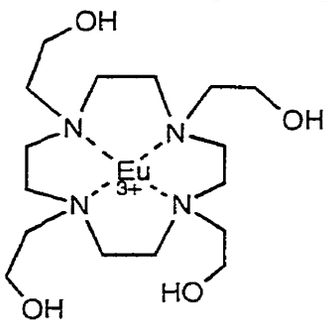

Figure 3.3 Europium complex that cleaves BNPP and m^7GpppG

Schneider and coworkers have done thorough studies on the effects of ligands on the rates lanthanide ion-promoted phosphate ester hydrolysis.[17-18] Their work has shown that carboxylic acids significantly decrease the rate of phosphate ester hydrolysis. For other ligands tested, ranging from amines to azacrown ether macrocycles to polyols, the rate of phosphate hydrolysis decreased slightly relative to the free lanthanide ion-promoted hydrolysis.

To the author's knowledge, only two ligands have been reported to date which increase the rate of reactivity relative to that of the unbound Ln^{3+} ion-promoted reaction. In 1996, Schneider *et al.*[19] reported that a dinucleating aza crown ether macrocycle ligand (Figure 3.4 **A**) in the presence of two equivalents of Pr^{3+} hydrolyzes BNPP 72-fold faster than the free Pr^{3+} ion under the same conditions. That same year, Komiyama *et al.* reported that a second dinucleating

ligand in the presence of 2 equivalents of La^{3+} hydrolyzes ApA 80-fold faster than that of the free La^{3+} ion-promoted reaction (Figure 3.4 **B**).[20]

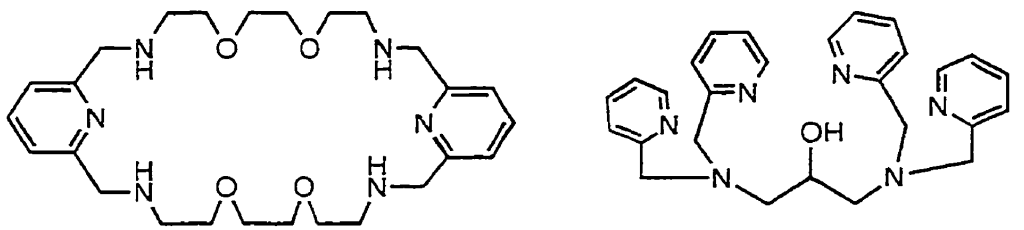

A **B**

Figure 3.4 Two reported ligands which purportedly bind two lanthanide ions. The lanthanide complexes give almost two orders of magnitude rate accelerations over the free lanthanide ion for phosphate diester hydrolysis reactions.

3.2 Results and Discussion

3.2.1 Rationale for Development of Hbt as Ligand

In order to develop a Ln^{3+} ion-binding ligand which will improve the rate of hydrolysis versus the free Ln^{3+} ion, it is important to find a ligand which will bind the Ln^{3+} ion tightly. It is true that negatively charged ligands (carboxylic acids, etc...) often bind Ln^{3+} ions tightly but experimentally they decrease the reactivity of the Lewis acidic metal toward phosphate ester hydrolysis. On the other hand, neutral ligands such as imines and aminocrown ethers have been shown to deligate from the Ln^{3+} ion quite easily.[17-18]

In 1998, Yatsimirsky *et al.* reported that lanthanide (iii) ions in the presence of a minimum of 5-fold excess of bistrispropane buffer are solubilized throughout the entire pH range of 7 through 10. Lanthanide ions in the presence of 5-fold excess bistrispropane are reportedly quite reactive toward the

hydrolysis of BNPP (La^{3+}/BTP, 25°C, pH 9.0: 2.2×10^{-3} s^{-1}).[21] The authors speculate on the possiblity of BTP acting as a ligand toward the lanthanide ion but do not show any direct evidence of this. The Yatsimirsky study showed the possible effectiveness of diaminopolyalcohols as ligands for binding lanthanide ions without a decrease in phosphate diester hydrolysis rates.

Recently, Park *et al.* reported that the La^{3+} ion binds the aminopolyalcohol buffer "bis-tris" tightly ($K_f = 5 \times 10^4$ M^{-1}).[22] Binding constants of other buffers such as tris and bistrispropane are apparently not nearly so high; for example, a binding constant of $K_f = 2.75 \times 10^2$ for tris to La^{3+} ion is reported by Pfefferlé and Bünzli.[23] Interestingly, it may be seen from the crystal structure that the La^{3+} ion only binds the nitrogen and four of the hydroxyl groups of the ligand (attempting to make the molecular model with all five hydroxy groups binding will convince the reader of the spatial impossibility of the binding of the fifth hydroxy group). The authors report that the 1:1 La^{3+}: "bis-tris" complex is negligibly slower than the free La^{3+} ion for hydrolyzing BNPP under identical conditions.

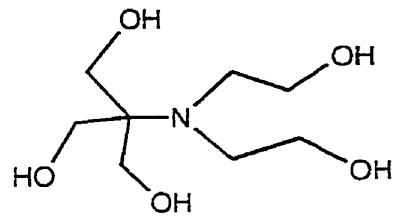

"bis-tris"

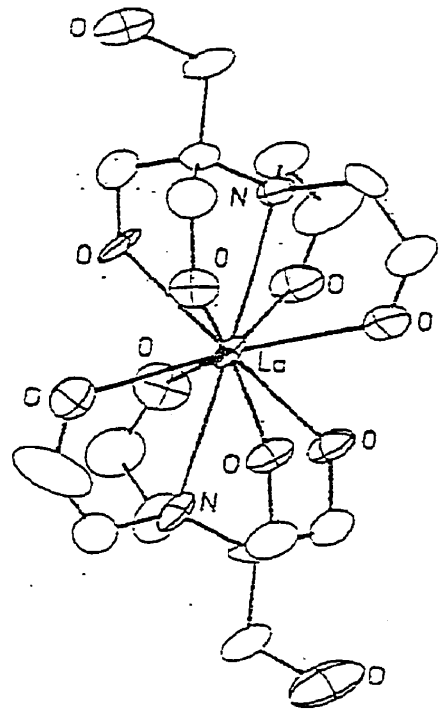

Figure 3.6 X-ray crystal structure of 1:2 La^{3+}:"bis-tris" complex reported previously by Park. (photocopied with permission)[23]

As was discussed in greater depth in the previous chapters, it has been documented that double Lewis acid activation can give between 10^5- and 10^6-fold rate acceleration over the uncatalyzed reaction for phosphate diester hydrolysis. Given the effective binding of "bis-tris" to lanthanides, it was surmised that the ligand hbt (2-hydroxypropyl-1,3-bis(tris(hydroxymethyl)methylamine) (Figure 3.7) with its two "bis-tris"-like subsections would bind two lanthanide ions tightly so as to give a dinuclear

lanthanide complex. Also, the similarity in hbt to other previously reported dinucleating ligands indicated that the metal-metal distance might be similar to those observed in enzyme and artificial phosphoesterases.

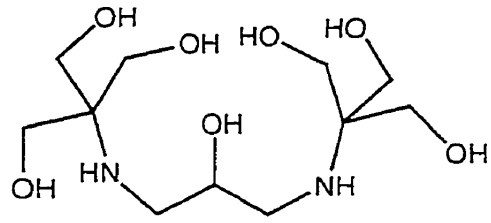

Figure 3.7 Ligand "hbt" with two "bis-tris"-like subsections that could bind two lanthanide ions.

3.2.2 Potentiometric Titrations

Hurst and coworkers have reported that when a 2 mM solution of $LaCl_3$ is titrated potentiometrically, 2.5 equivalents of hydroxide are consumed with a plateau reached at approximately pH 9.0.[11] The steepness of this titration curve is a good indication that a dimer or a higher order aggregate is formed. The number of equivalents of hydroxide consumed indicates that five hydroxy groups bridge two lanthanide ions at the high pH end of the titration curve (see Figure 3.2). The pH rate profile of ApA hydrolysis with 2 mM $LaCl_3$ shows that the rate sharply increases with pH until it plateaus at approximately pH 9.0 (Figure 3.8). The titration in combination with the pH rate profile indicates that the $La_2(OH)_5$ dimer or higher order aggregate is the maximally reactive ligand-free La^{3+} ion species for hydrolyzing phosphates. The $La_2(OH)_5$ species is several orders of magnitude more reactive than the La^{3+} ion monomer for hydrolyzing ApA. La^{3+} ion-promoted hydrolysis of other phosphate diesters such as BNPP and 3′,5′-cAMP also show a similar pH rate profile (to that of ApA) with a plateau observed around pH 9.[11]

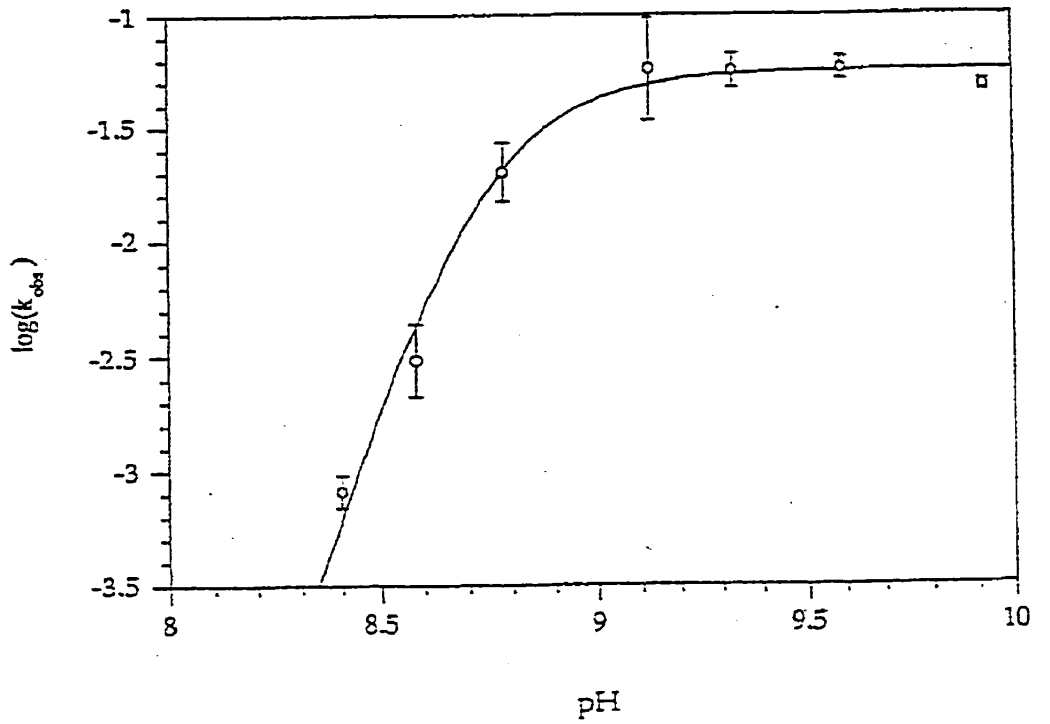

Figure 3.8 pH rate profile of $LaCl_3$ (2 mM)-promoted transesterification of ApA (25 μM) in sulfonate buffer (20 mM) at 25°C. k_{obs} is in units of reciprocal seconds. (photocopied with permission)[11]

As in the case of $LaCl_3$, most of the other lanthanide (iii) chlorides exhibit similar titration curves with five equivalents of hydroxide consumed for every two Ln^{3+} ions (Figure 3.9). (In the presence of oxygen, Ce^{3+} is a notable exception to this rule as it may autooxidize.) Observation of differences of the titration curves across the lanthanide series reveals a general trend that the steep increase around the pKa is observed at progressively lower pHs as one traverses the lanthanide series from left to right. Interestingly, the $La_2(OH)_5$ dimer or higher order aggregate is the most reactive of the lanthanides for hydrolyzing ApA in the plateau region of the pH rate profile.

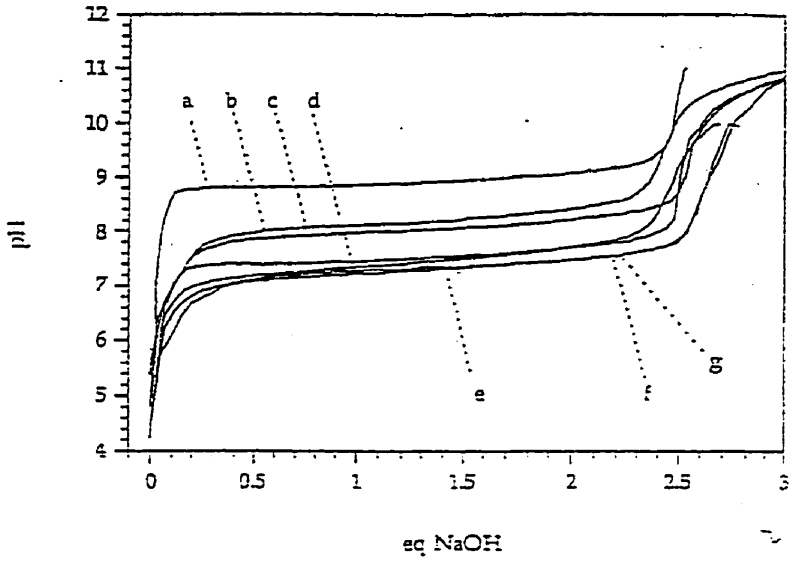

Figure 3.9 Potentiometric titration curves with sodium hydroxide: traversing the lanthanide series. The lanthanide (iii) chlorides used were as follows: (a) Lanthanum, (b) praseodymium, (c) neodymium, (d) europium, (e) holmium, (f) thulium and (g) lutetium. (photocopied with permission)[11]

Hbt ligand was synthesized according to literature procedure and purified in the form of the dihydrochloride salt.[34] The titration of hbt•2HCl (1 mM) with standardized NaOH reveals two pKas, one at pH 6.4 and the second at pH 8.5. One equivalent of hydroxide is consumed around each pKa. It is expected that these two pKas correspond to the deprotonation of each of the two nitrogens of hbt.

A solution of hbt•2HCl (2 mM) in the presence of two equivalents of $EuCl_3$ is prepared in situ. (The stock solutions of the lanthanide chloride are standardized by titration with a previously standardized NaOH solution.) When this solution is titrated with NaOH (Figure 3.10), two equivalents of hydroxide per equivalent of hbt (one equivalent of hydroxide per metal) are consumed initially around a pKa of 5.5. This first pKa corresponds to the initial binding of the europium to hbt ligand to likely form a 2:2 Eu^{3+}:hbt complex in solution, as will be explained by the ^1H NMR spectra and X-ray crystal structure on the

subsequent pages. A second pKa of 7.4 around which 5 equivalents of hydroxide per hbt are consumed is observed as more hydroxide is added. Note that the number of equivalents of hydroxide consumed around pKa_2 is the same as that consumed in the case of the free Eu^{3+} ion titration (2.5 equivalents hydroxide per europium). As in the case of free Ln^{3+} ions, the plateau region above the second pKa for the 2:1 Ln^{3+}:hbt solution corresponds to the region of maximal reactivity for phosphate diester hydrolysis, as will be detailed in the kinetics section of this chapter.

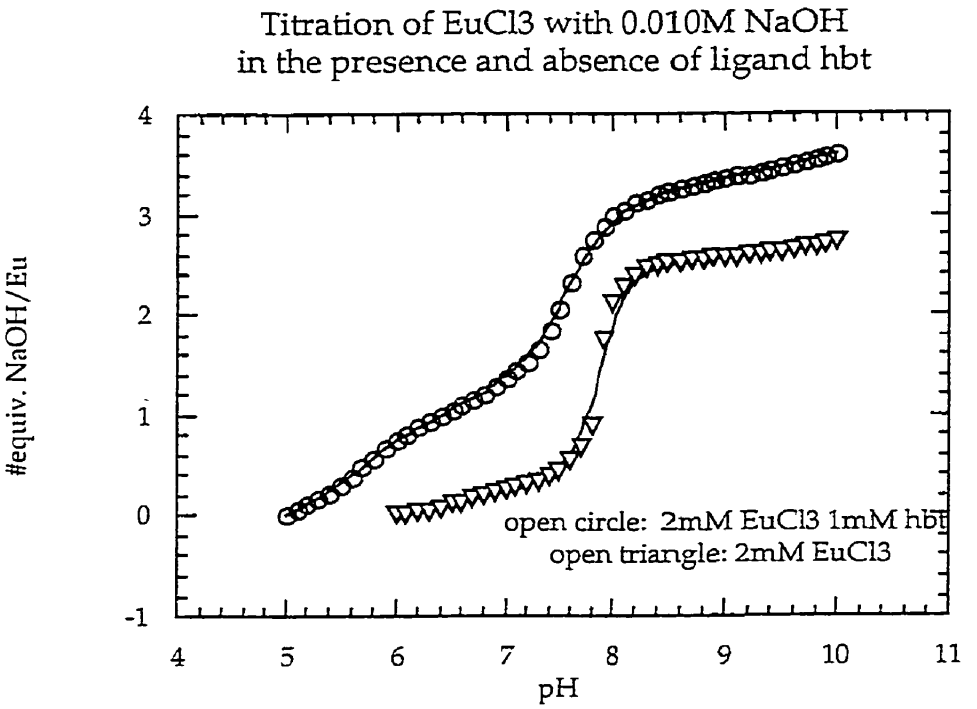

Figure 3.10 Titration of 2 mM $EuCl_3$ 1 mM hbt versus that of 2 mM $EuCl_3$ in H_2O with 0.010M NaOH at 25°C.

A survey of the effect of different lanthanides on the titration curves was done by titrating 2:1 Ln^{3+}:hbt solutions using Ln^{3+} ions from the left to the right end of the lanthanide row of the periodic table. Interestingly, a pattern emerges as is illustrated from the titrations of the 2:1 Pr^{3+}, Ho^{3+}, Lu^{3+}:hbt (Figure 3.11) solutions. As one crosses from left to right (Pr^{3+}-->Ho^{3+}-->Lu^{3+}) on the

periodic table, the pKa2 value shifts to progressively lower and lower pH values. Since it is at the plateau region above pKa2 that maximal reactivity for hydrolyzing phosphate diesters is reached, the choice of a Ln^{3+} ion toward the right end of the lanthanide series on the periodic table allows for maximal reactivity to be observed at a lower pH value than if a Ln^{3+} ion were chosen from the left end of the periodic table.

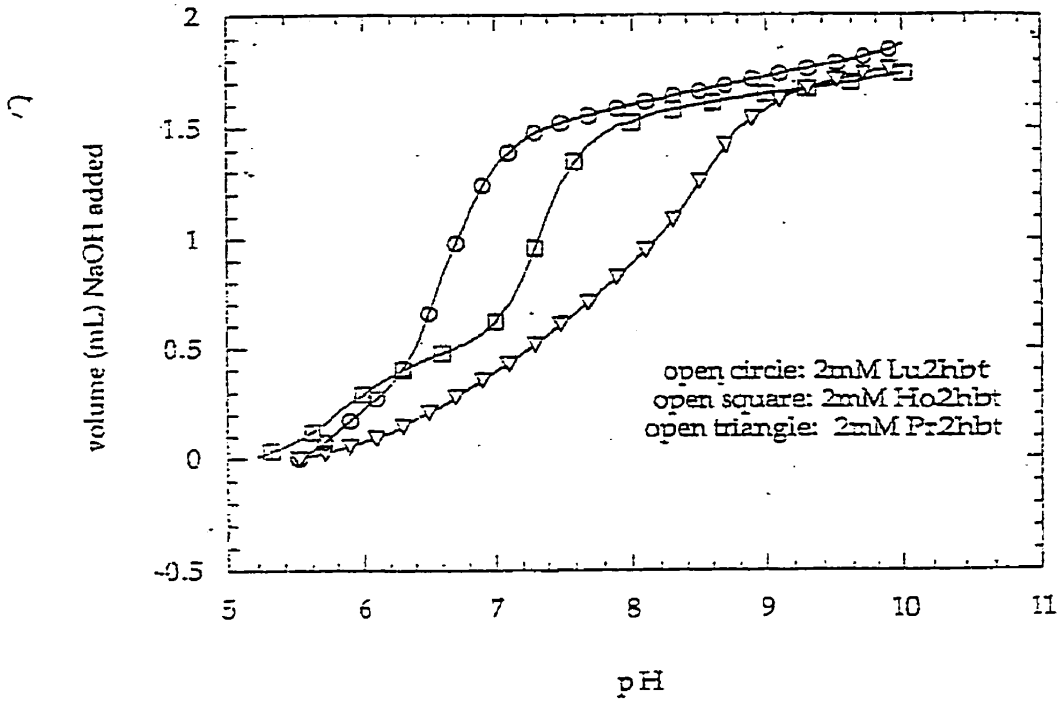

Figure 3.11 Titration of in situ 2 mM $LnCl_3$ 1 mM hbt solutions in H_2O with 0.01 M NaOH at 25°C; 0.5 mL NaOH corresponds to one equivalent of NaOH/$LnCl_3$.

A comparison of the titration of 2 mM $YbCl_3$ in the presence and absence of half an equivalent of hbt illustrates the advantage of choosing a lanthanide on the rightmost end of the periodic table. In the case of 2 mM $EuCl_3$ in the presence of 1 mM hbt, the plateau region above pKa2 (Figure 3.10) occurs at approximately the same pH value at which the plateau region above the pKa for ligand-free $EuCl_3$ occurs. However, in the case of a 2 mM $YbCl_3$ 1 mM hbt solution, the plateau region above its pKa2 occurs at a full 0.8 pKa units lower

than the plateau region above the pKa for the ligand-free $YbCl_3$ solution in the absence of hbt (Figure 3.12). In fact, the plateau region above the pKa_2 for hbt-bound Yb^{3+} is reached at a pH value of approximately 7, at which point the ligand-free Yb^{3+} ion is still mostly in monomer form with only a small percentage of free Yb^{3+} ion in dimeric or higher order aggregate form.

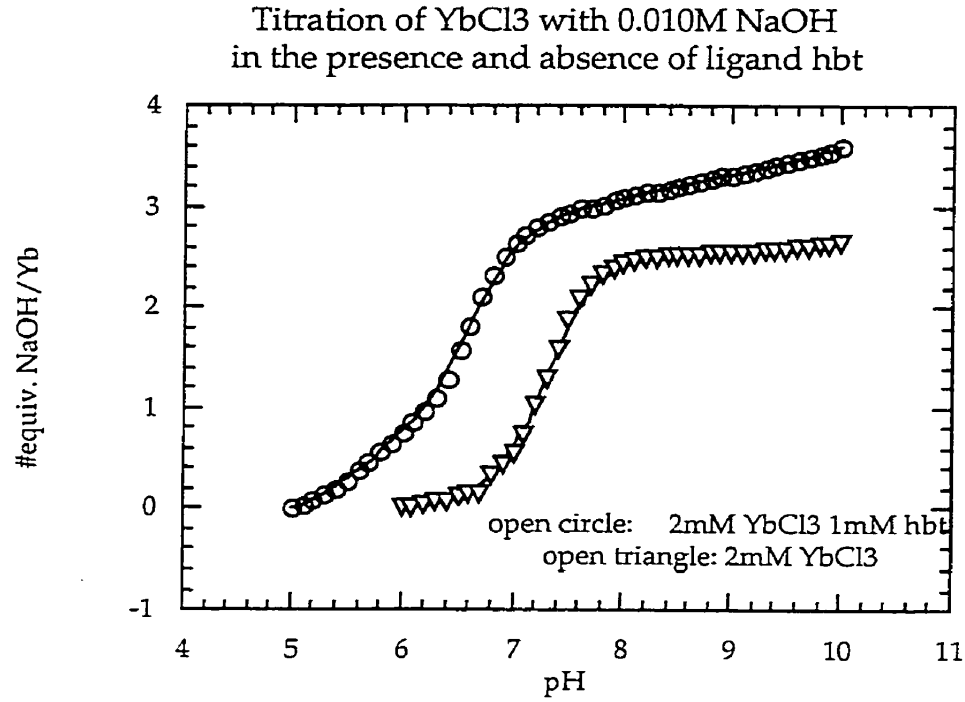

Figure 3.12 Titration of 2 mM $YbCl_3$ (aq.) in the presence and absence of half an equivalent of hbt at 25°C.

How might this shift in pH of the pKa_2 for 2:1 Ln^{3+}:hbt solutions across the lanthanide series be explained? The phenomenon of La^{3+} ion contraction going from left to right across the lanthanide series is well documented.[24] It is possible that the 2:1 Ln^{3+}:hbt complex (see ^1H NMR, X-ray crystal structure and kinetic evidence) is more likely to form in the case of a smaller lanthanide ion than in the case of a larger one. Another possiblity is that the differences in Lewis acidities across the lanthanide series come into play.[25]

As mentioned earlier, "bis-tris" (fig 3.6) binds Ln^{3+} ions quite tightly. In the curves shown below, 2 mM $YbCl_3$ or 2mM $EuCl_3$ (Fig. 3.13) aqueous solutions in the presence of one equivalent of "bis-tris" are titrated with 0.1 M NaOH. As is the case with 2:1 Ln^{3+}:hbt titration curves, a total of 3.5 equivalents of hydroxide per metal are consumed: likely one for the binding of "bis-tris" to the lanthanide and 2.5 for the formation of dimer. Interestingly, the plateau above the pKa_2 for the 1:1 Ln^{3+}:"bis-tris" solution occurs at a lower pH value in the case of $YbCl_3$ than in the case of $EuCl_3$, a similar shift as that observed for the 2:1 Ln^{3+}:hbt solution. Curiously, two equivalents are consumed around the pKa_1 of the 2 mM $YbCl_3$ solution in the presence of one equivalent of "bis-tris" while only one equivalent is consumed around the pKa_1 for the 2 mM $EuCl_3$ solution in the presence of one equivalent "bis-tris". This difference between the titration curves hopefully will be elucidated in further studies on Ln^{3+}: "bis-tris". For now, however, the titrations serve as a useful reference for the kinetics comparison between 2:1 Ln^{3+}:hbt and 1:1 Ln^{3+}: "bis-tris" solutions in the upcoming kinetics section of this chapter.

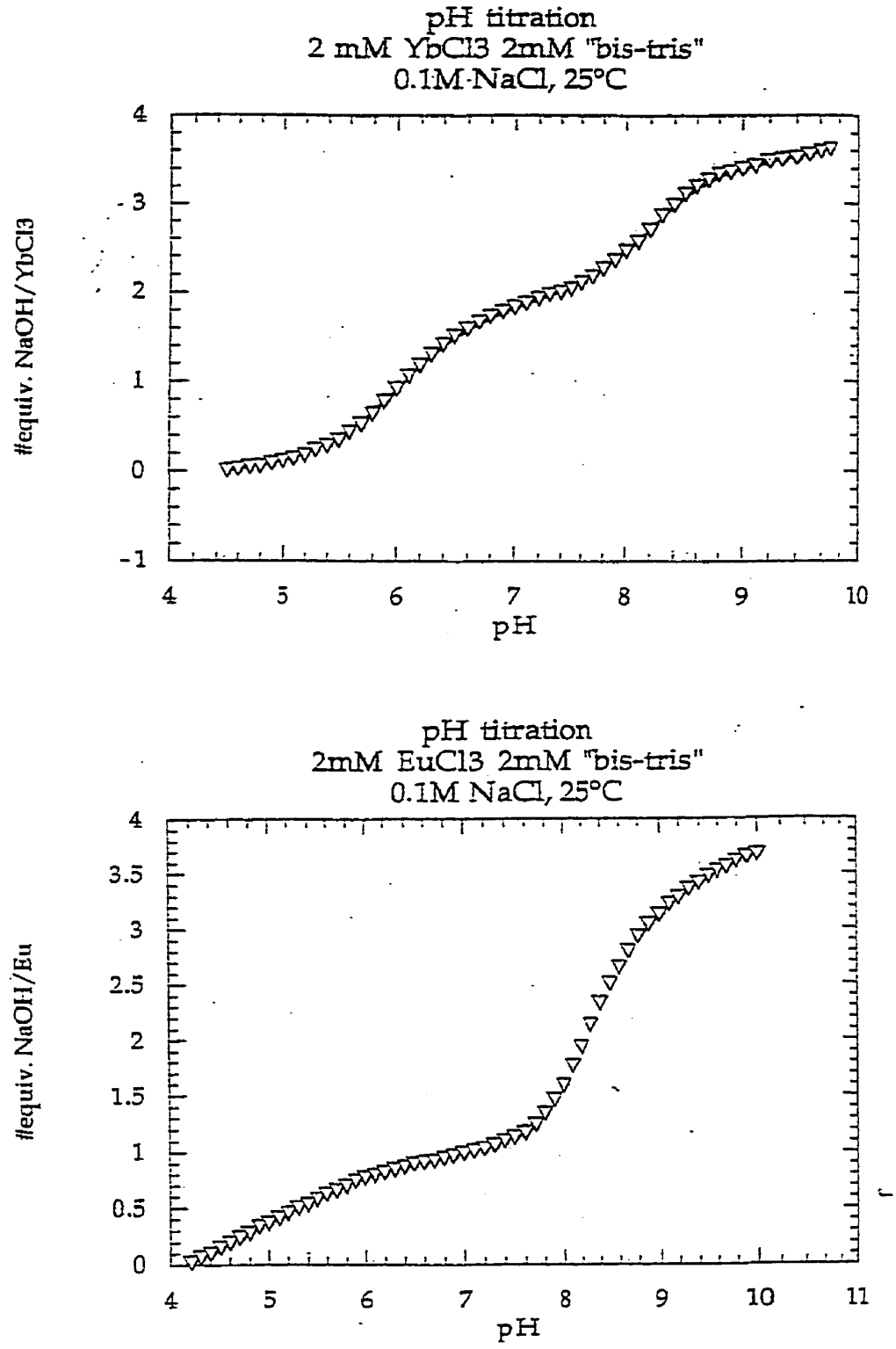

Figure 3.13 Titration curves of $YbCl_3$ and $EuCl_3$ (2 mM) in the presence of one equivalent of "bis-tris" in H_2O by 0.01 M NaOH at 25°C.

3.2.3 ^{1}H NMR and X-Ray Crystallographic Studies

The potentiometric titration of 2:1 Ln^{3+}: hbt leaves a number of questions unanswered about the nature of the species occurring on the titration curve. For example: if a lanthanide complex forms above pKa_1 (after one equivalent of hydroxide is consumed per metal ion), what is the ratio of Ln^{3+} to hbt of that complex in solution? What is the ratio of Ln^{3+} to hbt in the plateau region above pKa_2 where maximal reactivity toward phosphates is observed? What might these complexes look like in solution? In order to learn more about the structural details of the potentiometric titration of hbt in the presence of two equivalents of lanthanides, ^{1}H NMR and X-ray crystallographic studies were performed.

With the exception of La^{3+} and Lu^{3+}, Ln^{3+} ions are paramagnetic. Since a paramagnetic ion has electrons outside of closed valence shell, a nonzero net spin is observed that will cause NMR relaxation times to be extremely rapid. As a result, the ^{1}H NMR spectra of any ligand bound to a paramagnetic Ln^{3+} ion will be broadened.

The broadening effect of paramagnetic ions often proves to be a nuisance for chemists who wish to determine the structure of metal complexes. However, since unbound ligands are not broadened by the presence of the paramagnetic Ln^{3+} ion in solution, in the ^{1}H NMR spectra shown below the broadening phenomenon is actually beneficial in gleaning structural information about the interactions of paramagnetic Ln^{3+} ion with hbt.

On the subsequent pages, three spectra are shown that contain an equimolar mixture of hbt•2HCl, $EuCl_3$ and *t*-butanol (10 mM each) in D_2O (Fig. 3.14). The first spectra shows the mixture with 0 mM NaOD added to the solution (Fig. 3.14 **A**). The ratio of the integration of the singlet methylene peak of the doubly-protonated hbt (δ=3.78 ppm) to the integration of the singlet *t*-

BuOH peak (δ= 1.2 ppm) seen under these conditions is 4:3. This is exactly the ratio one would expect from an equimolar mixture of hbt•2HCl and *t*-BuOH with no metal binding to the ligand since there are 12 methylene protons for hbt and 9 methyl protons for *t*-BuOH. Since deuteroxide has not displaced the protons bound to the nitrogens of hbt, it is not suprising that no binding of hbt by the Eu^{3+} ion is observed by ^1H NMR.

When the equimolar hbt, $EuCl_3$ and *t*-butanol solution is titrated with 10 mM NaOD, all the ^1H NMR peaks for hbt completely disappear (Fig. 3.14 **B**). This indicates that the paramagnetic Eu^{3+} ion has bound hbt ligand to form a complex where the ratio of hbt:Eu^{3+} is at least 1:1. Although solid state structures are not necessarily indicative of solution state structures, the 2:2 Eu^{3+}:hbt X-ray crystal structure shown in the next few pages (Figure 3.16) indicates that a 2:2 complex may form after the consumption of one equivalent of OH- per equivalent of metal or hbt.

For the final ^1H NMR spectra of the series, the equimolar $EuCl_3$, hbt and *t*-butanol solution is titrated with 4.5 equivalents NaOD (Fig. 3.14 **C**). The pH of the titrated solution is 10.0—a pH value in the plateau region above the pKa_2 for the potentiometric titration curve shown previously for the 2:1 $EuCl_3$:hbt mixture (Fig. 3.10). In this solution, the ratio of the methylene peak of the free base form of hbt (δ= 3.52 ppm) to the *t*-BuOH peak is approximately 2:3. This ratio indicates that the disappeared half of the methylene peaks (5 mM) belong to the hbt ligand which is bound to Eu^{3+} ion while the other, visible methylene peaks belong to hbt ligand (5 mM) which is not bound to metal. Therefore, in the plateau region above the pKa_2 in solution, a 2:1 Eu^{3+}:hbt complex is evidently formed. Since 7 equivalents of NaOD per hbt ligand are required to titrate a 2:1 $EuCl_3$:hbt (5 mM in hbt) mixture up to the plateau region above pKa_2 (Fig. 3.10) and 2 equivalents of NaOD are required to titrate unbound hbt•2HCl (5 mM) to

the free base form, the choice of adding 45 mM NaOD to reach the plateau region becomes evident.

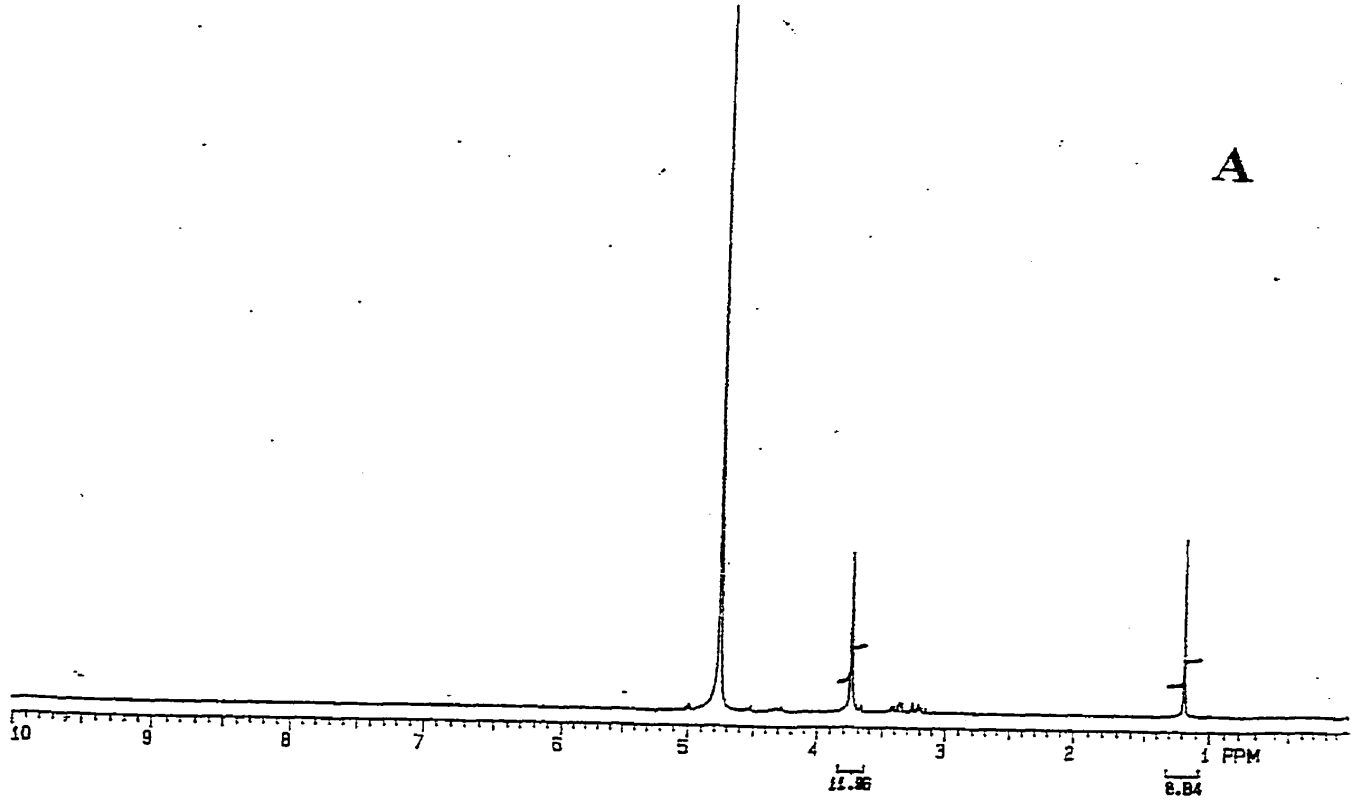

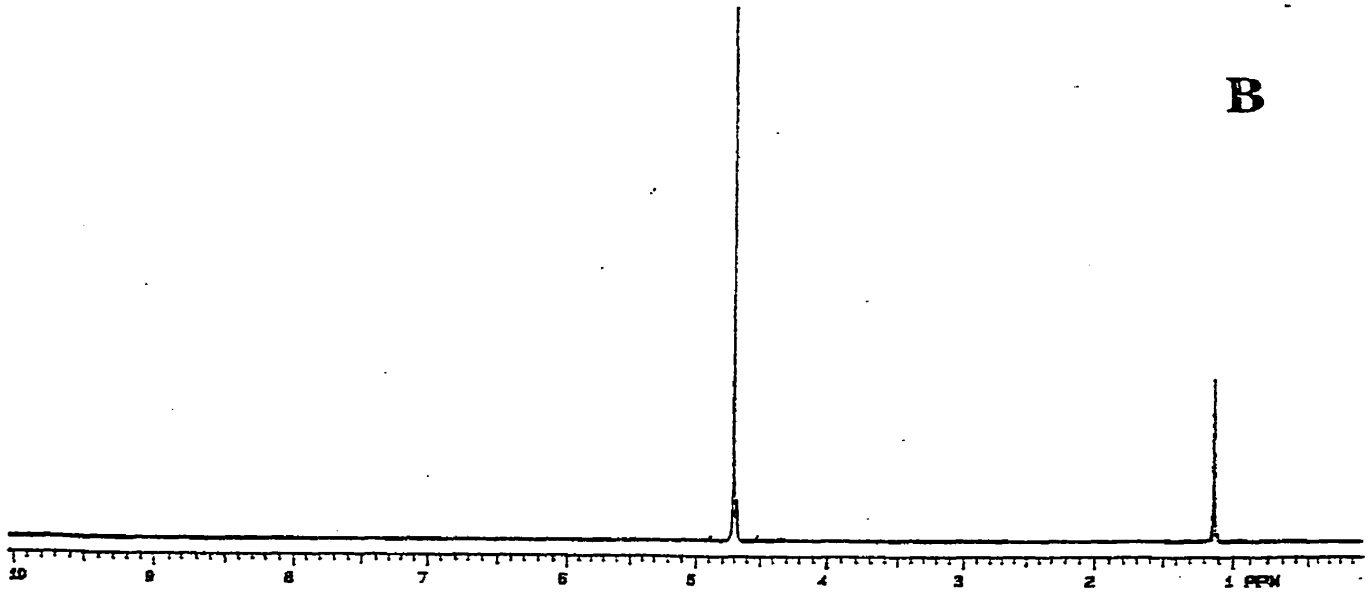

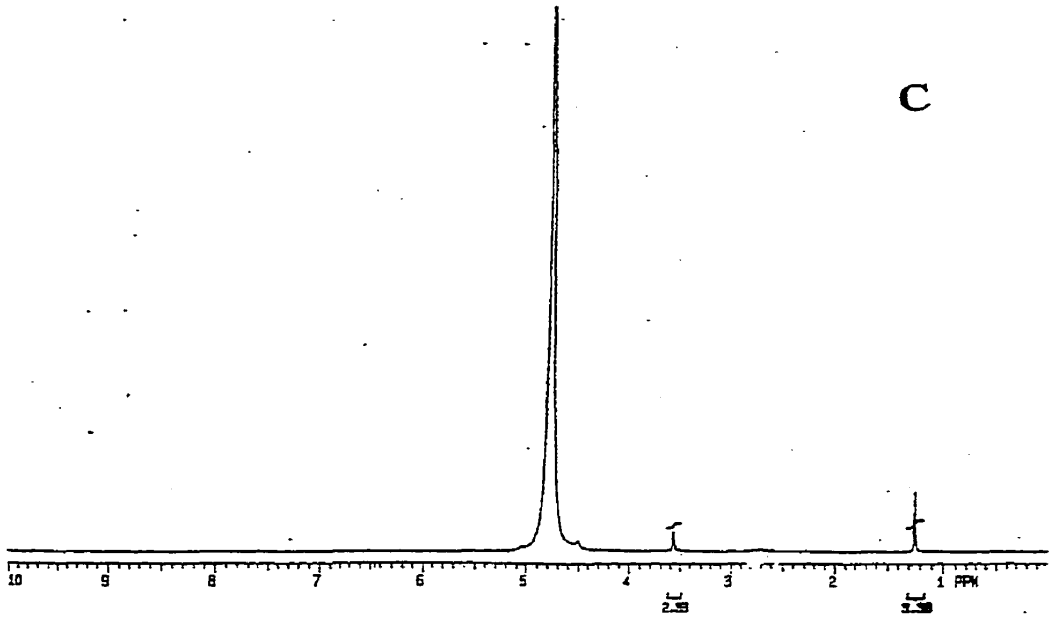

Figure 3.14 ^{1}H NMR titrations of equimolar solutions of $EuCl_3$, hbt•2HCl and *t*-butanol (10 mM) in D_2O. **A** 0 mM NaOD added. **B** 10 mM NaOD added. C 45 mM NaOD added.

^{1}H NMR titrations were also done for equimolar mixtures of $LnCl_3$, hbt•2HCl and *t*-butanol (10 mM each) using three other paramagnetic Ln^{3+} ions: Yb^{3+}, Pr^{3+} and Ho^{3+}. The ^{1}H NMR titrations yielded identical spectra to that observed in the case of $EuCl_3$ upon adding 0 mM, 10 mM and 45 mM NaOD. When an equimolar solution of hbt•2HCl and a diamagnetic lanthanide ion (La^{3+}, 10 mM) is titrated with 45 mM NaOD in a solution with *t*-BuOH (7.5 mM), a new broad singlet peak is observed with a chemical shift of δ= 3.65 ppm (Fig. 3.15) Since an approximately identical integration is observed for this broad singlet peak and the methylene peak of the free base hbt (δ= 3.52 ppm), the broad singlet peak likely is the methylene singlet of the hbt bound by two La^{3+} ions.

Similar bound and dissociated peaks are observed when diamagnetic Lu^{3+} is used instead of La^{3+}.

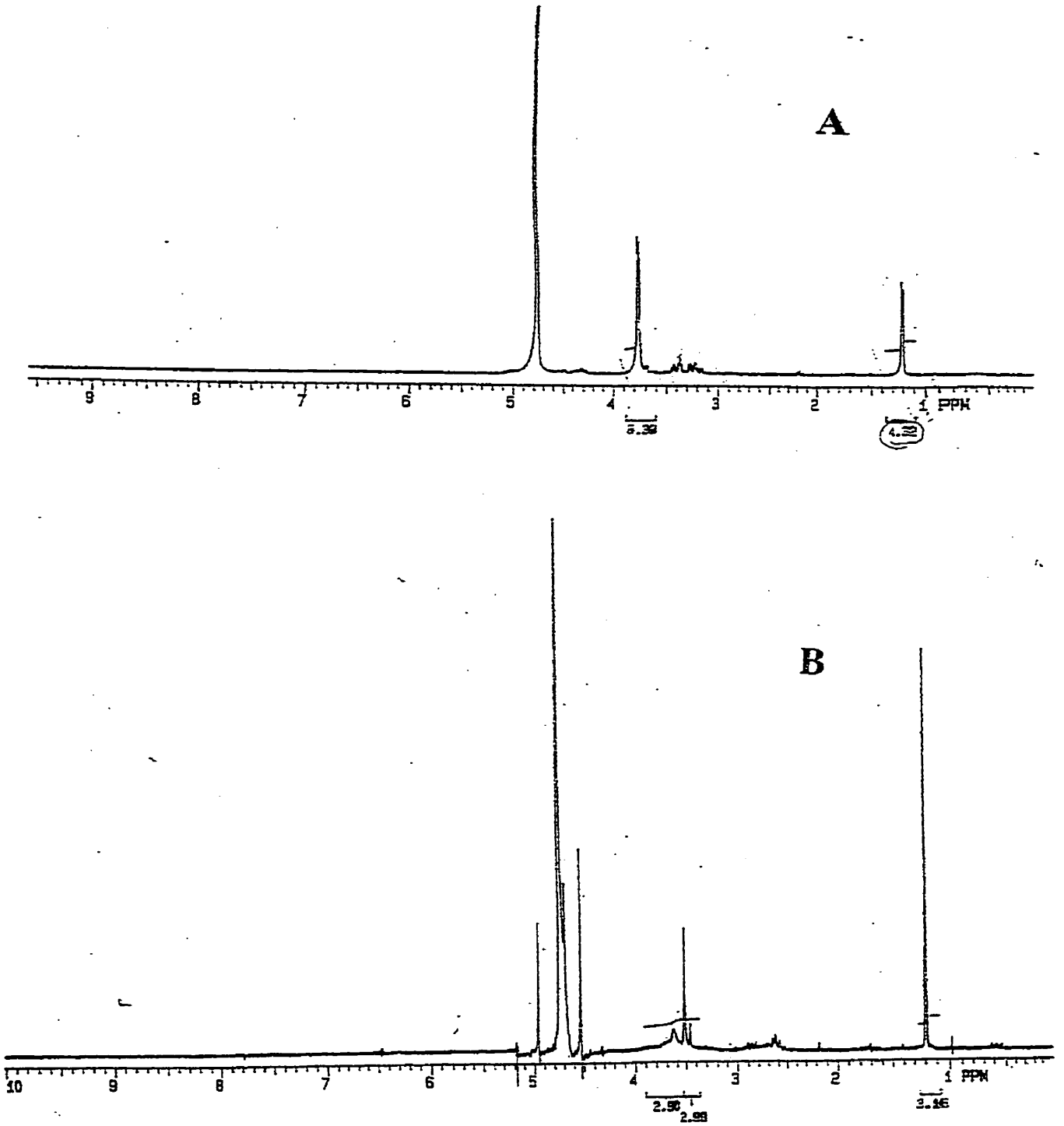

Figure 3.15 ^1H NMR titration with NaOD of equimolar solution of $LaCl_3$ and hbt•2HCl (10 mM) in the presence of a *t*-BuOH (7.5 mM) internal standard in D_2O. **A** 0 mM NaOD **B** 45 mM NaOD

Two X-ray crystal structures were obtained for Eu^{3+} complexes with hbt. A 2:2 Eu^{3+}:hbt structure was obtained initially from triclinic crystals that were prepared by slow cooling of a one-to-one mixture of $EuCl_3$ and free base hbt in an $EtOH/H_2O$ solvent mixture. The crystal structure shows that each Eu^{3+} ion is bound to one hbt molecule; additionally, the two Eu^{3+} ions are bridged by two alkoxide groups from the tris alcohol moieties of hbt (one alkoxide group from each hbt molecule) (Fig. 3.16). As stated previously, the ^1H NMR evidence also indicates that a 1:1 Eu^{3+}:hbt complex may form initially (above pKa_1 on titration curve (Fig. 3.10)) once the ligand binds to the europium metal (Fig. 3.14). While the author cautions the reader that solution state structures are often different from that observed in the solid state, this X-ray structure nevertheless gives valuable insights into the <u>possible</u> nature of the metal complex upon initial binding.

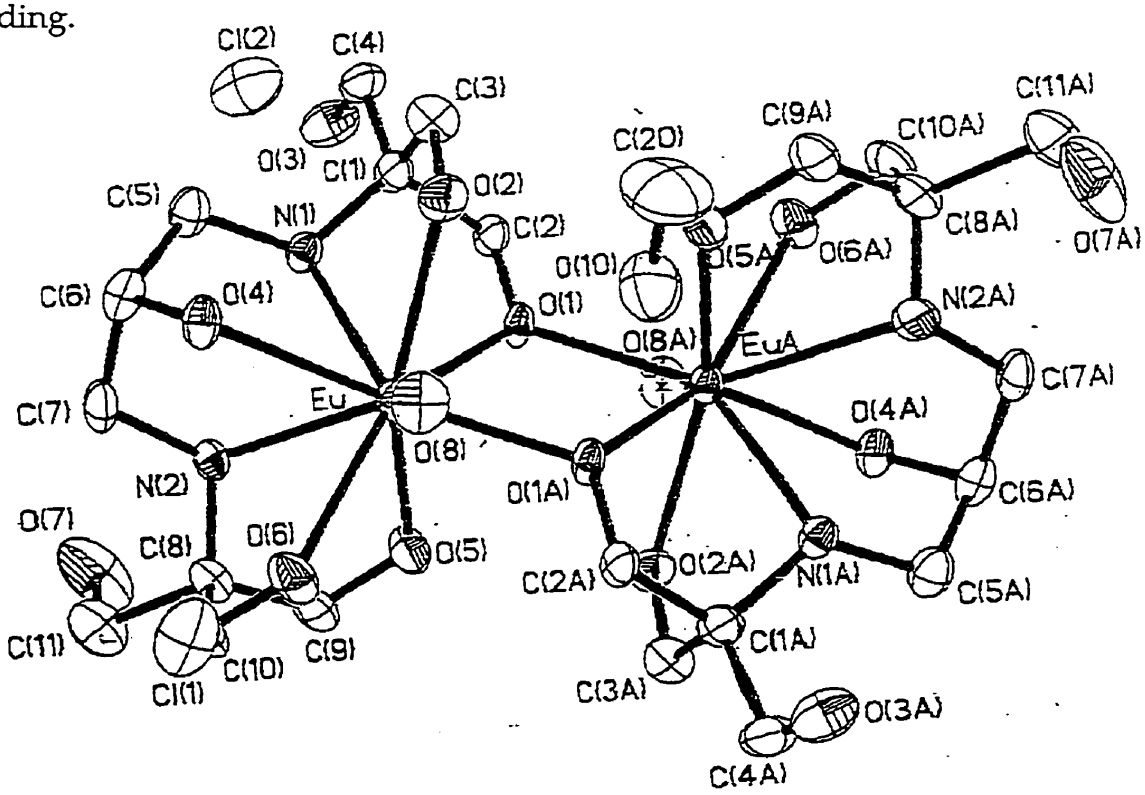

Figure 3.16 ORTEP Diagram from X-ray Crystal Structure of 2:2 Eu^{3+}:hbt complex.

Cubic crystals were also obtained by slow cooling of an aqueous mixture of the free base form of hbt, 2 equivalents of $EuCl_3$ and 5 equivalents of NaOH. The X-ray crystal structure obtained from this mixture reveals a dinuclear europium complex (2:1 Eu^{3+}:hbt, Figure 3.17**A**) which self-assembles to form a hexanuclear trimer (Fig. 3.17 **B**).

In the dinuclear complex crystal structure, each Eu^{3+} ion is octacoordinate with four coordinating groups from the alkoxide oxygens of the binding hbt, three groups from the solvent and one group from a metal-alkoxide oxygen from a neighbouring hbt molecule of the hexanuclear trimer. The three coordinating oxygen groups from the solvent are as follows: one solvent oxygen comes from a coordinating water molecule that binds each Eu^{3+} ion (Fig. 3.17 **A**, O5 and O4). A hydroxide bridge (O3) that links each metal to the other metal of the dinuclear complex is the second coordinating solvent-metal bond (which along with a secondary alkoxide (O4) form a four-membered ring diamond core). Finally, each metal ion is bound to two metal-coordinated oxides (O2 and O1) that are bridged by a proton. This proton may be acting as a low-barrier hydrogen bond since the distance between the oxides is only 2.48 Å.[26-27] Each metal-coordinated oxide is also bound to the metals of the neighbouring dinuclear complex of the hexanuclear trimer. Visually, one can picture the oxides as the centre of the hexanuclear trimer "triply-bladed paddle" (Fig. 3.17 **B**) with each dinuclear complex (Fig. 3.17 **A**) serving as one "blade" of the paddle (see Appendix 5).

The hexanuclear trimer contains 18 positive charges (6 Eu^{3+}), fifteen negative charges from the coordinated oxygens and three additional negative charges from the chloride counterions. The ratio of the components in the solution used to obtain the crystals of the hexanuclear trimer (1:2:5

hbt:$EuCl_3$:NaOH) is clear from the stoichiometry of the reaction: 3 hbt + 6 $EuCl_3$ + 15 NaOH = $Eu_6hbt_3Cl_3$ trimer + 15 NaCl.

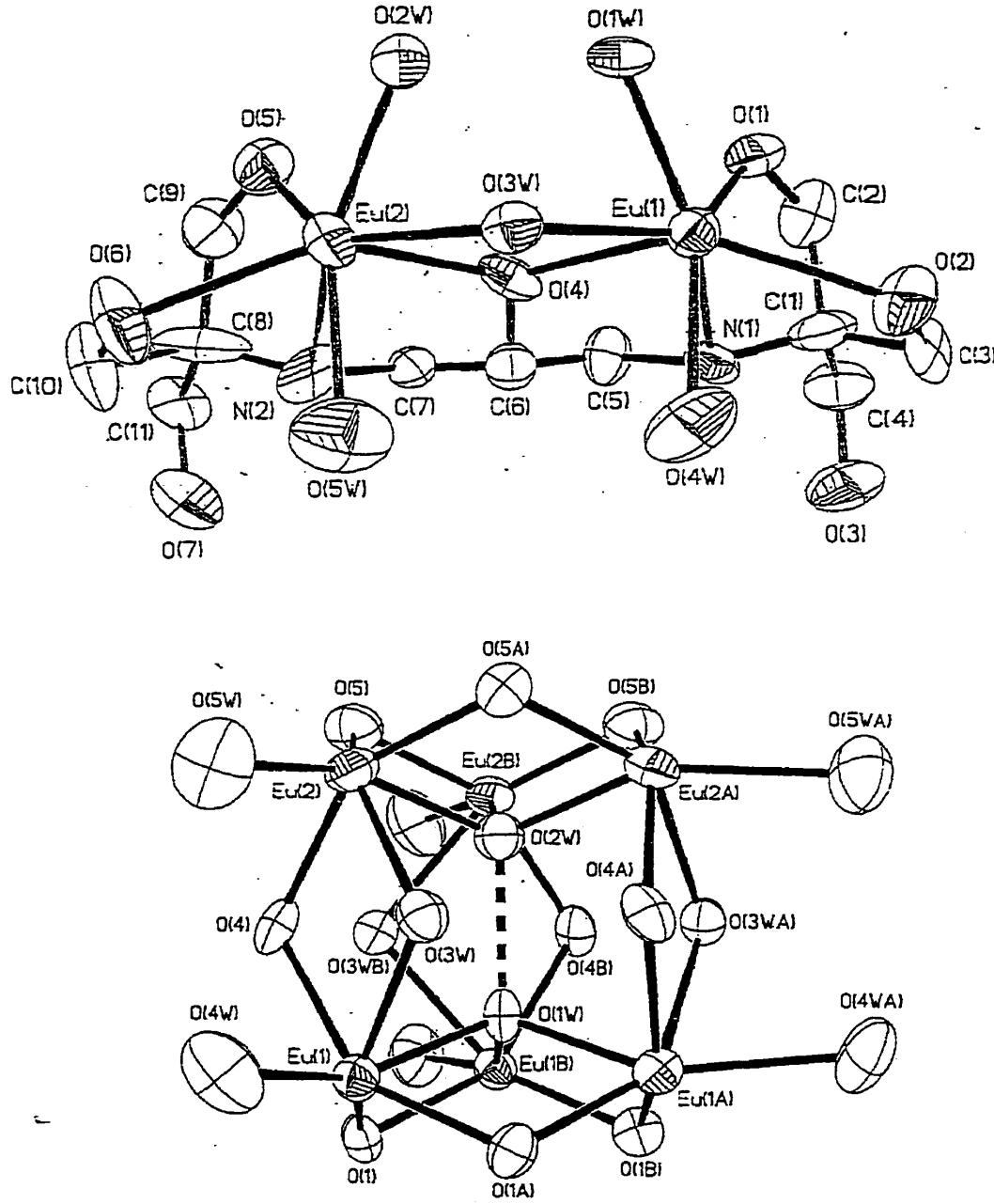

Figure 3.17 ORTEP diagram from the X-ray crystal structure of dinuclear complex **A** (top) and hexanuclear trimer **B** (bottom).

Since a 2:1 Eu^{3+}: hbt complex is formed in solution according to ^1H NMR data (Fig. 3.14) in the plateau region above the pKa_2 of the potentiometric titration (Fig. 3.10), it seems reasonable to propose that the dinuclear complex in the X-ray crystal structure (Fig. 3.17 **A**) is also formed in solution. (In the kinetics section of this chapter, it will also be seen that this 2:1 M:L complex is most reactive for hydrolyzing phosphates (Fig. 3.18).) The dinuclear complex shown in the X-ray crystal structure would make a good candidate catalyst for hydrolyzing phosphates for a number of reasons. First of all, the distance between the two Eu-Eu metals (3.98 Å) is very similar to that observed in enzyme phosphoesterases and other artificial simple metal complex phosphoesterases. Secondly, the four-membered-ring diamond core structure of Eu1, O3, Eu2 and O4 (Fig. 3.17 **A**) is also prominent in a number of enzyme phosphoesterases such as calcineurin-α, kidney bean purple acid phosphatase and protein phosphatase-1.[28-31] In enzyme as well as artificial metal phosphoesterases, the oxygens in the diamond core are possibly involved in the metal-nucleophile attack of the phosphate. Lastly, the two water molecules bound to each Eu^{3+} ion allow for the phosphate diester oxygens to bind both metals so as to give double Lewis acid activation for phosphate hydrolysis (see Fig. 2.1). As has been seen in a number of artificial metal complex phosphoesterases used in the past, double Lewis acid activation may act cooperatively with metal-nucleophile attack to give up to 10^{11}-fold rate acceleration for phosphate diester hydrolysis!

3.2.4 Kinetics of BNPP Hydrolysis Using Ln_2hbt

One of the difficulties in working with free Ln^{3+} ions is that their dimers or higher order aggregates form lanthanide-hydroxide gels at concentrations higher than 2 mM in water. This solubility problem is even more pronounced

when lanthanide dimers or higher order aggregates are dissolved in the presence of additional salts.

In the presence of half an equivalent of hbt however, several Ln^{3+} ions (Eu^{3+}, Ho^{3+}, Yb^{3+} and Pr^{3+}) were tested for solubility and were discovered to be soluble in water at concentrations as high as 100 mM!!! These considerably improved solubility properties allow for the kinetics of phosphate diester hydrolysis using Ln_2hbt to be observed at considerably higher concentrations than in the case of the free Ln^{3+} ions dimers or higher order aggregates.

In this chapter, the hydrolysis of bis-*p*-nitrophenyl phosphate (BNPP) by various lanthanide complexes is measured by observing the increase in *p*-nitrophenolate ion at λ=400 nm by UV-Vis spectrophotemtry. In the kinetics studies done with hbt, the pseudo-first-order rate constant observed is that for the release of a single equivalent of *p*-nitrophenolate ion as measured by UV-Vis absorbance.

A solution of 20 mM $EuCl_3$ and 10 mM hbt at pH 8.0 and 25°C was initially tested and a half-life of τ= 18 s for BNPP (50 μM) hydrolysis was observed. A solution of 20 mM $YbCl_3$ and 10 mM hbt at pH 7.0 and 25°C hydrolyzes BNPP with a half-life of approximately 6 s ($k_{obs} = 1.2 \times 10^{-1}$ s^{-1}). The latter rate is approximately 10 orders of magnitude faster than the estimated rate for BNPP hydrolysis in the absence of catalyst reported by Vance and Czarnik ($k_{obs}= 1.3 \times 10^{-11}$ s^{-1}).[32] This rate acceleration is comparable to that observed by micellar Th^{4+} and Ce^{4+}-promoted BNPP hydrolysis.[9-10]

Analysis of the product mixture in the case of Yb_2hbt and Eu_2hbt (10 mM)-promoted BNPP hydrolysis (after 10 half-lives are complete) by HPLC reveals quantitative production of the phosphate monoester NPP (*p*-nitrophenyl phosphate). Accumulation of NPP is expected since a $EuCl_3$ (10 mM) solution in the presence of 2 equivalents of hbt hydrolyzes NPP (4×10^{-4} s^{-1}, 25°C, pH 8.0)

approximately 100-fold slower than it hydrolyzes BNPP. ^{31}P NMR product analysis also revealed NPP formation (δ= -1.35 ppm) by a 2:1 Eu^{3+}:hbt solution (30 mM in hbt) after 5 half-lives of BNPP (1.5 mM) hydrolysis were complete. (A trace amount of BNPP (δ=-12.1ppm) was also present in the the ^{31}P NMR spectra.) The HPLC and ^{31}P NMR results therefore rule out the likelihood of metal-alkoxide attack of the phosphate diester since a hydrolysis rather than a transesterification product is observed.

If one presumes that the hexanuclear trimer shown in the X-ray structure (Fig. 3.16) is also formed in solution, there are two mechanistic possibilities for the phosphate diester hydrolysis. First, the phosphate may singly coordinate one metal while a metal-hydroxide acts as nucleophile. The other possibility is that the dinuclear Eu(III) complex might bind both phosphate oxygens to give double Lewis acid activation. This bridged phosphate is then attacked by a metal-oxide nucleophile, reminiscent of Wahnon's previously reported dinuclear substitutionally inert Co(III) complex which is proposed to invoke a metal-oxide attack of the phosphate centre for hydrolysis reactions.[33] The two mechanisms proposed above are kinetically indistinguishable for substitutionally labile metal complexes.

Although the results for the hydrolysis of BNPP using 20 mM $LnCl_3$ and 10 mM hbt are quite impressive, one cannot make a fair quantitative comparison between the free Ln^{3+} ion and the ligand-bound ion under these conditions since the Ln^{3+} ion in dimer or higher order aggregate form precipitates out as a lanthanide-hydroxide gel between pH 7 and 10 at such high concentrations. For this reason, kinetic comparisons are done instead using 2 mM $LnCl_3$ solutions, which were shown to be soluble in lanthanide ion dimer or higher order aggregate form by Hurst *et al.*[11]

The kinetics for Ln^{3+}-ion promoted BNPP hydrolysis in the absence of ligands and in the presence of one equivalent of "bis-tris" or two equivalents of hbt is compiled in the data table shown below (Table 3.1). Note that the rate of Ln^{3+} ion-promoted BNPP hydrolysis is slowed down by less than an order of magnitude in the presence of one equivalent of "bis-tris".

Metal	pH	k_{obs} (s^{-1}) (free salt)	k_{obs} (s^{-1}) (2:1 with hbt)	k_{obs} (s^{-1}) (1:1 with"bistris")
Eu	7.0	9.1×10^{-6}	1.3×10^{-5}	3.3×10^{-6}
Yb	7.0	3.9×10^{-6}	9.4×10^{-3}	2.5×10^{-6}
Eu	8.5	2.3×10^{-4}	8.5×10^{-3}	1.3×10^{-4}
Yb	8.5	1.5×10^{-4}	1.6×10^{-2}	3.9×10^{-5}

Table 3.1 Pseudo-first-order rate constants (k_{obs}, s^{-1}) for the hydrolysis of BNPP (50μM) with $LnCl_3$ (2mM) in HEPES or EPPS buffer (10mM) at 25°C in H_2O. The kinetic runs shown below were done in triplicate and were reproducible to within 10% error.

At each pH value with both Eu^{3+} and Yb^{3+} ions, when half an equivalent of hbt is bound to the Ln^{3+} ion, a rate acceleration is observed for BNPP hydrolysis over the free Ln^{3+} ion-promoted reaction. At pH 7.0, the rate for BNPP hydrolysis by Eu^{3+} ion in the presence of half an equivalent of hbt is only slightly greater than that reported for the free Eu^{3+} ion. However, at pH 8.5, the rate acceleration of hbt-bound over hbt-free Eu^{3+}-promoted hydrolysis has

increased to 37-fold. At pH 8.5, the rate acceleration of hbt-bound over hbt-free Yb^{3+} is approximately 100-fold. Most remarkably, a rate acceleration of 2300-fold is observed over the ligand-free rate when $YbCl_3$ is bound to half an equivalent of hbt at pH 7.0.

How can one rationalize the differences in reactivities using the different lanthanides at different pHs? To best understand the logic behind the rate accelerations in Table 3.1 above, the reader will wish to refer to the potentiometric titrations of $EuCl_3$ and $YbCl_3$ in the presence and absence of ligand (Fig. 3.10 and 3.12).

At pH 8.5, all four titrations are in the plateau region on the high pH end of the titration curves. In this region, the free Ln^{3+} ions are in dimer or higher order aggregate form and the Ln_2hbt complex has formed the 2:1 Ln^{3+}:hbt complex as was learned from the ^1H NMR titrations earlier in the chapter (Fig. 3.14). The kinetics data reveal that the Eu_2hbt complex is 36-fold faster than ligand-free Eu^{3+} dimer or higher order aggregate and the Yb_2hbt complex is 100-fold faster than the Yb^{3+} dimer or higher order aggregate.

At pH 7.0, the potentiometric titration of Yb^{3+} in the presence of half an equivalent of hbt shows that the solution at this pH is in the plateau region above the pKa_2 where the 2:1 Yb:hbt complex has formed. On the other hand, the free Yb^{3+} ion titration curve is at the lower end of the titration curve, which indicates that the Yb^{3+} ion is mostly in monomeric form at this pH. It is clear then that the unprecedented 2300-fold rate acceleration of hbt-bound YbCl3 over hbt-free $YbCl_3$ at pH 7.0 and 25°C is that of the 2:1 Yb:hbt complex over that of mostly monomeric Yb^{3+} ion.

The free Eu^{3+} ion potentiometric titration curve at pH 7.0 is below the pKa, indicating that Eu^{3+} is in mostly monomeric form. However, the potentiometric titration of Eu^{3+} in the presence of half an equivalent of hbt also

is below its pKa2, indicating that it is mostly in the form of the 1:1 Eu:hbt complex. Not suprisingly, the rate acceleration of the hbt-bound Eu^{3+} over hbt-free Eu^{3+} is negligeable and nowhere near as remarkable as in the case of Yb^{3+}.

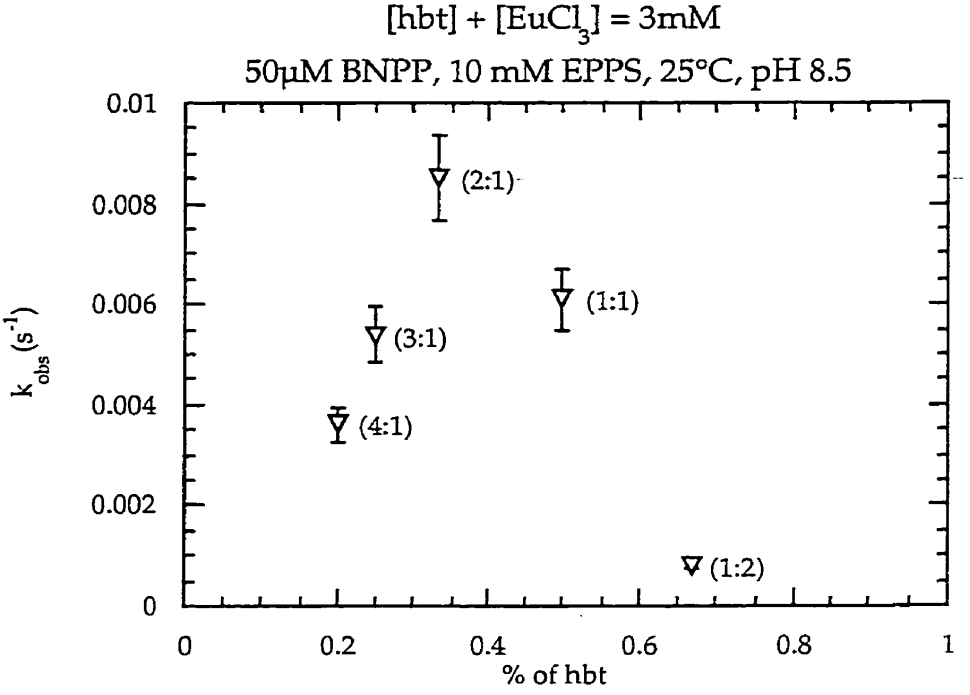

Figure 3.18 Variable metal-ligand ratio rate profile for Eu:hbt-promoted BNPP hydrolysis

A variable metal-ligand ratio rate profile was performed to confirm the nature of the Eu/hbt species hydrolyzing BNPP (Fig. 3.18). For this experiment, the total concentration of EuCl3 and hbt in the solution is 3 mM. As one would expect from the ^1H NMR spectra and the X-ray crystal structure data, maximal reactivity is observed for the 2:1 Eu:hbt mixture.

To learn more about the 2:1 Ln:hbt complexes that hydrolyze BNPP, pH rate profiles were effected. The pH rate profile curves (Fig. 3.19, data in Appendix 3.1) of EuCl3 and YbCl3 in the presence of half an equivalent of hbt

mimic the potentiometric titration curves (Figs. 3.10 and 3.12) above the pKa_2. Evidently, the 2:1 Ln:hbt species formed in the plateau region of the titration and pH rate profile is the maximally reactive species for hydrolyzing phosphates. The pH shift of the pKa_2 seen in the titration curves that is mimicked in the pH rate profile curves experimentally shows why the 2:1 Yb:hbt solution hydrolyzes phosphate esters rapidly at lower pH values than the 2:1 Eu:hbt solution. Note that the rate of hydrolysis in a 2:1 Ln:hbt solution of ionic strength I=0.1 M decreases the rate by approximately half versus that of solutions that are prepared in the absence of additional salts.

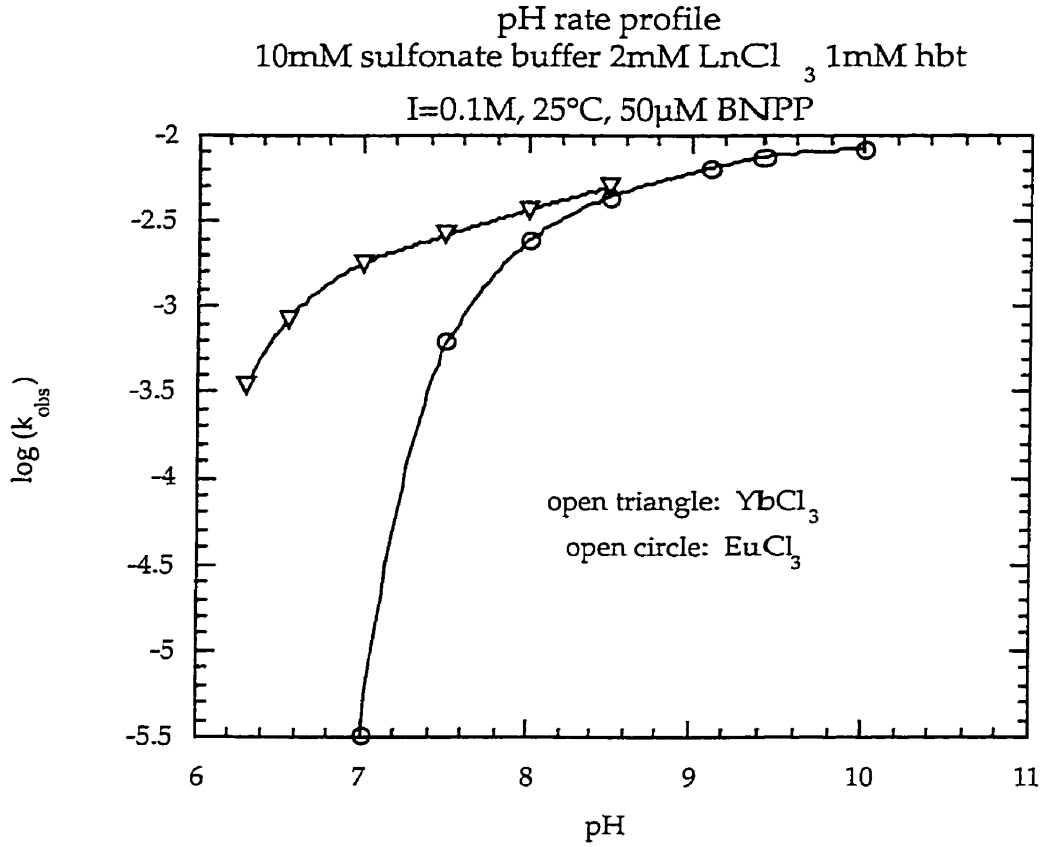

Figure 3.19 pH rate profile for $EuCl_3$ and $YbCl_3$-promoted phosphate diester hydrolysis in the presence of half an equivalent of hbt. The value k_{obs} is in units of reciprocal seconds.

3.2.5. Related Kinetics Studies

The unprecedented rate constants observed for Yb_2hbt-promoted BNPP hydrolysis beg the question: is Ln_2hbt also reactive for hydrolyzing other phosphate substrates? The answer to this question is YES, but the rate accelerations reported for BNPP hydrolysis are the most dramatic for any phosphate substrate observed to date using Ln_2hbt as a catalyst.

In Chapter 2, MPNP and HPNP hydrolysis and transesterification were observed to distinguish double Lewis acid activation from joint single Lewis acid activation/metal-nucleophile attack. The rates of Yb_2hbt-promoted MPNP and HPNP cleavage are compiled in Table 3.2. As in the case of Co(cyclen)-promoted cleavage, the rates of cleavage of the two substrates are very close to one another, The closeness in rates is not suprising since a metal-nucleophile attack is expected for the hydrolysis of the phosphates. However, it is surprising that Yb_2hbt-promoted MPNP hydrolysis is approximately 4-fold faster than HPNP transesterification. The slower rate of HPNP hydrolysis might be explained by a binding interaction of the hydroxypropyl group with the lanthanide groups of the metal complex.

	k_{obs} (s^{-1})
HPNP	$(1.7\pm0.1) \times 10^{-3}$
MPNP	$(8.0\pm0.4) \times 10^{-3}$

Table 3.2 2 mM $YbCl_3$, 1 mM hbt solution-promoted MPNP or HPNP (50 μM) hydrolysis in sulfonate buffer (10 mM) at pH 7.5 and 25°C in H_2O. Error is 5% from a triplicate of runs.

What are the resulting rates of hydrolysis when a phosphate with a poor leaving group is used instead of a *p*-nitrophenyl phosphate ester? In order to examine this question, the hydrolysis of the activated phosphate 2',3'-cAMP by

Yb_2hbt was monitored by HPLC and the results are compiled in Table 3.3. At pH 7.0 and 25°C, the Yb_2hbt- (1 mM) promoted hydrolysis of 2',3'-cAMP (k_{obs}= 9.4×10^{-3} s^{-1}) is between 4- to 5-fold faster than that of the ligand-free Yb^{3+} ion- (k_{obs}= 2.2×10^{-3} s^{-1}) promoted reaction. This rate acceleration is quite modest compared to the 2300-fold rate acceleration of BNPP under these conditions. It is particularly modest when one remembers that at pH 7.0 the Yb^{3+} ion is in mostly monomeric form while the hbt-bound Yb^{3+} ion is in 2:1 Yb:hbt dinuclear complex form. RNA hydrolysis using 2:1 Ln:hbt complexes is even less promising as initial studies indicate that Yb_2hbt-promoted ApA hydrolysis is slower than that of free Yb^{3+}-ion promoted hydrolysis at pH 7.0 and 25°C.

Certainly, the rate accelerations observed so far for phosphates with poor leaving groups pale in comparison with those for phosphates with good leaving groups. Nevertheless, it cannot be overemphasized that the hydrolysis of *p*-nitrophenyl phosphate esters with artificial metal phosphoesterases has more than an academic value in understanding the hydrolysis of phosphates with good leaving groups. For example, if a nucleotide residue of DNA is bound to a proton or a metal so as to make it a good leaving group, it will become an activated phosphate very much like BNPP or MPNP. As a result, this research has unquestionable potential application for the future development of artificial restriction enzymes. Additionally, the biologically important ATP and mRNA cap m^7GpppG have activated leaving groups.

	k_{obs} (s^{-1})
2 mM $YbCl_3$	$(2.2 \pm 0.2) \times 10^{-3}$
2 mM $YbCl_3$ 1 mM hbt	$(9.4 \pm 0.9) \times 10^{-3}$

Table 3.3 Pseudo-first-order rate constants for 2',3'-cAMP (50 μM) hydrolysis promoted by a 1 mM hbt, 2 mM $YbCl_3$ solution at pH 7.0, I=0.1 M and 25°C

In order to learn about the effect of structure on reactivity, a ligand closely related to hbt (2-hydroxypropyl-1,3-bis(diethanolamine) dihydrochloride salt (or hbd•2HCl)) was synthesized according to literature procedure (Fig. 3.20).[34] A potentiometric titration with sodium hydroxide was performed on the solution of hbd (1 mM) is dissolved in water. Two pKas are observed around which one equivalent of hydroxide is consumed for each pKa value (5.55 and 8.05) respectively.

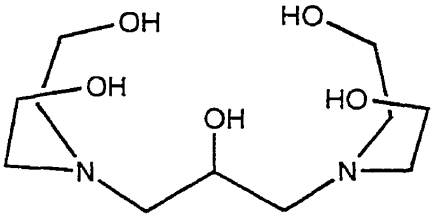

Figure 3.20 Ligand hbd was also tested for reactivity in the presence of two lanthanide ions.

The potentiometric titration of a solution of hbd (10 mM) in the presence of two equivalents $EuCl_3$ reveals that four equivalents of hydroxide per hbd are consumed around a pKa_1=6.6 followed by one equivalent of hydroxide consumed around a pKa_2=8.0 (Fig. 3.21). The 2:1 Eu:hbd solution was tested for phosphate diester hydrolysis in the plateau region above its pKa_2.

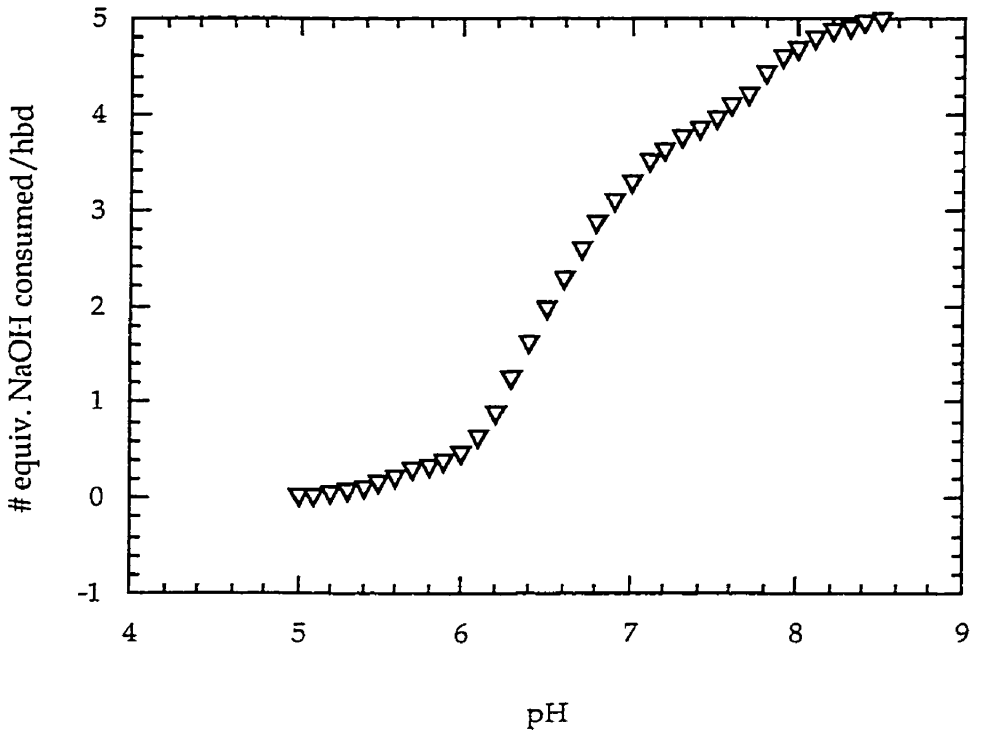

Figure 3.21 Potentiometric titration of an aqueous hbd (10 mM) solution in the presence of two equivalents $EuCl_3$ at 25°C.

When a 10 mM hbd aqueous solution is prepared in situ with two equivalents of $EuCl_3$, a half-life of approximately 6s (k_{obs}= 0.12 s^{-1}) for BNPP hydrolysis at 25°C and pH 8.0 is observed. A 10 mM hbd solution in the presence of two equivalents of $YbCl_3$ also hydrolyzes BNPP, with a half-life of *ca.* 4s (k_{obs}= 0.17 s^{-1}) at 25°C and pH 7.0. These rates are very close to the rate accelerations observed for the equivalent Ln_2hbt-promoted BNPP hydrolysis reactions.

However, when a lower concentration of hbd (1 mM) is dissolved in the presence of two equivalents of $EuCl_3$, the rate of Eu_2hbd-promoted BNPP hydrolysis at 25°C and pH 8.5 (k_{obs}= 7.8 x 10^{-4} s^{-1}) in 10 mM EPPS buffer is

approximately 10-fold slower than that observed for Eu_2hbt-promoted BNPP hydrolysis (k_{obs}= 8.5 x 10^{-3} s^{-1}) under identical conditions. Since the potentiometric titration graph for hbd at 1 mM in the presence of two equivalents of $EuCl_3$ also reaches a plateau at pH 8.5, this rate difference is most likely a result of the poorer binding of the hbd ligand to the Ln^{3+} ions. One can imagine that the binding properties of hbd and hbt to Ln^{3+} ions would be distinct since hbd has tertiary nitrogens that would not bind to metals as easily as the secondary nitrogens in the case of hbt.

3.4 EXPERIMENTAL

3.4.1 Chemicals

Hbt•2HCl and hbd•2HCl were synthesized according to literature procedure from epichlorohydrin and tris or diethanolamine.[34] Lanthanide chloride salts were purchased from Strem Chemicals. *tert*-Butanol, BNPP, 2',3'-cAMP, sulfonate buffers and internal standards were purchased from Sigma-Aldrich Canada. ApA was purchased from ICN Chemicals, Inc.

NMR Spectral Identification

^{31}P NMR Product Analysis. Trimethyl phosphate was used as an external reference. The Eu_2hbt/BNPP reaction mixture was prepared and quenched with an aqueous solution of $NH_4(H_2PO_4)$ (pH 5.5, 10-fold excess) after approximately 5 half-lives of BNPP hydrolysis were complete. BNPP (δ= -12.14 ppm), ammonium phosphate (δ= 0.0 ppm) and NPP (δ= -1.35 ppm) were compared with authentic samples.

Although the literature synthesis of hbt•2HCl and hbd•2HCl has been previously documented, there are no NMR structures reported for these compounds (the synthesis of hbt and hbd was reported in the 1940s, before NMR technology has blossomed the way it had in the decades since).

2-hydroxypropyl-1,3-bis(tris(hydroxymethyl)methylamine dihydrochloride salt. ^{1}H NMR (ppm): (in D_2O) δ 4.32 ppm (1H, mult.), 3.78 ppm (12 H, s), 3.3 ppm (4 H, mult.). **^{13}C NMR (ppm)**: (in D_2O with dioxane as internal reference) δ 69.8, 67.3, 61.4, 48.4.

2-hydroxypropyl-1,3-bis(diethanolamine) dihydrochloride salt. ^{1}H NMR (ppm): (in D_2O) δ 4.62 ppm (1H, mult.), 3.95 ppm (8H, t), 3.5 ppm (12H, mult.). **^{13}C NMR (ppm):** (in D_2O with dioxane as internal reference) δ 64.0, 59.7, 59.5, 58.6.

Potentiometric Titrations

Potentiometric titrations were done on the Radiometer Copenhagen RTS822 instrument at 25°C. A titration vessel jacket with thermostatted water (from RMS Lauda Thermostat) was used to maintain constant temperature throughout the course of the titration. All solutions to be titrated were prepared in 0.1M NaCl Milli Q water solutions to maintain approximately constant ionic strength throughout the titration. Lanthanide chloride solution concentrations were assigned by titrating with standardized NaOH. Standardized NaOH was purchased from Anachemia, Inc. and tested for accuracy versus a volumetrically prepared potassium acid phthalate solution before each titration day. The potassium acid phthalate standard was dried in an oven at 110°C for 2 hours and weighed carefully prior to preparing the solution.

UV/Vis Kinetics

All solutions for kinetics runs were degassed and carried out in Milli Q water. Temperature was maintained by the RMS Lauda thermostat. In general, pseudo-first-order rate constants for the hydrolysis of BNPP, MPNP and HPNP were obtained by observing 4-nitrophenolate increase at λ=400 nm. At pHs below 7.0, pseudo-first-order rate constants were obtained from 4-nitrophenol

increase observed at λ=316 nm. MPNP and HPNP runs were done simultaneously as in Chapter 2. Immediately prior to each run when a substrate other than BNPP was used, BNPP hydrolysis with the Ln_2hbt complex as catalyst was effected to determine that the quality of metal complex solution was adequate.

Ionic strength of I=0.1 M was achieved using NaCl as additional salt. The following biological sulfonate buffers were used for the kinetics depending on the pH region examined: MES, HEPES, TAPS, EPPS, PIPES and CHES.

HPLC Kinetics

Each run using Ln_2hbt as catalyst was quenched at various time intervals using ammonium phosphate monobasic at pH 5.5 as quenching agent. The quenched solutions were subsequently centrifuged for 2 minutes at 11,000 rpm in order to spin down any europium phosphate precipitate. The supernatant was then placed in an HPLC vial ready to run through the column. *p*-Nitrobenzenesulfonate sodium salt is used as the internal standard and has a retention time of 4.2 min. under all HPLC conditions below.

HPLC Conditions

The following conditions were used for all hydrolysis reactions below: the flow rate was set to 0.5 mL/min and the oven temperature was set at 40°C. The absorbance wavelength used is λ=254 nm with a reference wavelength of λ=450 nm. 25 μL of the supernatant are injected onto the C-18 reversed phase column.

In the case of BNPP hydrolysis, the supernatant is eluted for 5 minutes with 100% ammonium phosphate monobasic (0.2 M, pH 5.5). A 0-100% linear elution gradient of methanol/water (3:2) solution and $NH_4(H_2PO_4)$ follows over

the subsequent 20 minutes. The retention times and absorbances of hydrolysis products and substrates were compared with those of authentic samples: *p*-nitrophenyl phosphate (1.53 min.), *p*-nitrophenol (12.52 min.) and BNPP (20.20 min.).

In the case of 2′,3′-cAMP and ApA, the supernatant is eluted for 5 minutes with 100% ammonium phosphate monobasic (0.2M, pH 5.5). A 0-40% linear elution gradient of methanol/water (3:2) and $NH_4(H_2PO_4)$ follows over the subsequent 8 minutes. The retention times and absorbances of hydrolysis products and substrates were compared with those of authentic samples: 3′-AMP (3.8 min.), 2′,3′-cAMP (7.8 min.), 2′-AMP (8.3 min.) and ApA (11.4 min.).

X-Ray Crystal Structural Data

A big thanks to Brent Stranix, whose collaboration and expertise were necessary to obtain good crystal structures. The author is grateful to Young Seo Choi and Soon Jin Oh for following the procedure first done at McGill in order to make the crystals in Korea. The author is also thankful to Mr. Jungseok Heo for the X-ray crystallographic analysis. All structural data was collected in Korea with a Siemens SMART CCD diffractometer. Data has been deposited with the Cambridge Crstallographic Data Centre under CCDC 117436.

3.5 Chapter 3 References

1. Seo, J.S.; Sung, N-D; Hynes, R. C.; Chin, J. *Inorg. Chem.* **1996**, 35, 7472.

2. Linkletter, B; Chin, J. *Angew. Chem. Intl. Ed. Engl.* **1995** 34, 472-4.

3. Butcher, W.W.; Westheimer, F.H. *J. Am. Chem. Soc.* **1955** 77, 2420-4.

4. Eichhorn, G.L.; Butzow, J.J. *Biopolymers* **1965** 3, 79.

5. Rutherford, G.; Morgan, A.R. *Can. J. Biochem.* **1972** 50, 287-9.

6. Takasaki, B.K.; Chin, J. *J. Am. Chem. Soc.* **1993** 115, 9337-8.

7. Kamitani, J.; Sumaoka, J.; Asanuma, H.; Komiyama, M. *J. Chem. Soc, Perkin Trans. 2* **1998** 523-7.

8. Takasaki, B.K.; Chin, J. *J. Am. Chem. Soc.* **1994** 116, 1121-2.

9. Bracken, K.; Moss, R.A.; Ragunathan, K. *J. Am. Chem. Soc.* **1997** 119, 9323-4.

10. Moss, R.A.; Zhang, J.; Bracken, K. *Chem. Commun.* **1997**, 1639.

11. Hurst, P.; Takasaki, B.K.; Chin, J. *J. Am. Chem. Soc.* **1996**, 118, 9982-4.

12. Chin, K.O.A.; Morrow, J.R. *Inorg. Chem.* **1994**, 33, 5036-41.

13. Morrow, J.R.; Aures, K.; Epstein, D. *J. Chem. Soc., Chem. Commun.* **1995**, 2431.

14. Chappell, L.L.; Voss, D.A.; Horrocks, W.D.; Morrow, J.R. *Inorg. Chem.* **1998** 37, 3989-98.

15. Baker, B.F.; Khalili, H.; Wei, N.; Morrow, J.R. *J. Am. Chem. Soc.* **1997** 119, 8749-55.

16. Baker, B.F.; Lot, S.S.; Kringel, J.; Cheng-Flournoy, S.; Villiet, P.; Sasmor,H.; Siwkowski, A.; Chappell, L.L.; Morrow, J.R. *Nuc. Acids Res.* **1999** 27, 1547-51.

17. Rammo, J.; Hettich, R.; Roigk, A.; Schneider, H-J. *Chem. Commun.* **1996** 105-7.

18. Roigk, A.; Hettich, R.; Schneider, H-J. *Inorg. Chem.* **1998** 37, 751-6.

19. Ragunathan, K.; Schneider, H-J. *Angew. Chem. Intl. Ed. Engl.* **1996** 35, 1219-21.

20. Yashiro, M.; Ishibuko, A.; Komiyama, M. *J. Biochem.* **1996** 120, 1067-9.

21. Yatsimirsky, A.R.; Gómez-Taigle, P. *J. Chem. Soc, Dalton Trans.* **1998** 2957-9.

22. Oh, S.J.; Choi, Y-S.; Hwangbo, S.; Bae, S.C.; Ko, J.K.; Park, J.W. *Chem. Commun.* **1998** 2189-90.

23. Pfefferlé, J.-M.; Bünzli, G. *Helv. Chim. Acta* **1989** 72, 1487.

24. Cotton, F.A.; Wilkinson, G. Advanced Inorganic Chemistry: A Comprehensive Text 4th Ed., John Wiley & Sons: New York, 1980, pp. 981-2.

25. Dean, J.A. Lange's Handbook of Chemistry 14th Ed., McGraw-Hill, Inc.: New York, 1992, pp. 8.13-8.18.

26. Cleland, W.W.; Kreevoy, M.M. *Science* **1994** 264, 1887.

27. Hibbert, F.; Emsley, J. *Adv. Phys. Org. Chem.* **1990**, 26, 255.

28. Golberg, J.; Huang, H.-B.; Kwon, Y.-G.; Greenbard, P.; Nairn, A.C.; Kuriyan, J. *Nature* **1995** 376, 745.

29. Griffith, J.P.; Kim, J.L.; Kim, E.E.; Sintchak, M.D.; Thomson, J.A.; Fitzgibbon, M.J.; Fleming, M.A.; Caron, P.R.; Hsaio, K.; Navia, M.A. *Cell* **1995** 82, 507.

30. Kissinger, C.R.; Parge, H.E.; Kinighton, D.R.; Lewis, C.T.; Pelletier, L.A.; Tempczyk, A.; Kalish, V.J.; Tucker, K.D.; Showalter, R.E.; Moomaw, E.W.; Gastinel, L.N.; Habucka, N.; Chen, X.; Maldonado, F.; Barker, J.E.; Bacquet, R.; Villafranca, E. *Nature* **1995** 378, 641.

31. Sträter, N.; Klabunde, T.; Tucker, P.; Witzel, H.; Krebs, B. *Science* **1995** 268,1489.

32. Vance, D.H.; Czarnik, A.W. *J. Am. Chem. Soc.* **1993** 115, 12165.

33. Wahnon, D.; Lebuis, A.-M.; Chin, J. *Angew. Chem. Intl. Ed. Engl.* **1995** 35,2412.

34. Wotiz. J.; Pierce, J. *J. Am. Chem. Soc.* **1944** 66, 879-81.

Appendix 3.1

pH	2 mM YbCl3, 1mM hbt k_{obs} (s^{-1})	2 mM EuCl3, 1 mM hbt k_{obs} (s^{-1})
6.3	$(3.2\pm0.3) \times 10^{-4}$	----------
6.55	$(8.3\pm0.8) \times 10^{-4}$	----------
7.0	$(1.7\pm0.1) \times 10^{-3}$	$(3.3\pm0.3) \times 10^{-6}$
7.5	$(2.7\pm0.2) \times 10^{-3}$	$(6.5\pm0.6) \times 10^{-6}$
8.0	$(3.8\pm0.4) \times 10^{-3}$	$(2.2\pm0.2) \times 10^{-3}$
8.5	$(5.0\pm0.5) \times 10^{-3}$	$(4.3\pm0.5) \times 10^{-3}$
9.1	----------	$(6.4\pm0.3) \times 10^{-3}$
9.4	----------	$(7.5\pm0.3) \times 10^{-3}$
9.97	----------	$(8.2\pm0.4) \times 10^{-3}$

Table 3.4 Pseudo-first-order rate constants for the pH rate profile of LnCl3 (2 mM) in the presence of two equivalents of hbt with sulfonate buffer (10 mM), I=0.1M, 25°C. The error shown is within 10% based on a a triplicate of runs.

Chapter 4. Copper (ii) 6,6′-Diamino-2,2′-Bipyridine Complex Promoted Cleavage of Phosphate Diesters

4.1 Introduction

The metal complexes discussed in the previous chapters employ two metals to give enormous rate accelerations for the hydrolysis and transesterification reactions of phosphate diesters. In this chapter, however, a mononuclear metal complex is synthesized and tested for phosphate diester hydrolysis. Working with mononuclear complexes that hydrolyze phosphates is useful since mechanistic information can be gleaned more easily from a simpler one-metal complex. With the development of novel mononuclear metal complexes that employ different mechanisms to hydrolyze phosphate esters, hopefully novel dinuclear complexes similar to the mononuclear counterpart can be designed that will cleave phosphates even more rapidly than those reported to date.

As emphasized in previous chapters, working with phosphates with good leaving groups may have eventual application in the development of artificial restriction enzymes or for the hydrolysis of biologically important activated phosphates such as ATP, coenzyme A, NAD or NADP. Nevertheless, since nucleic acids have poor leaving groups, it is also extremely valuable to examine the hydrolysis of unactivated phosphates. In general, the mechanisms involved in unactivated phosphate hydrolysis are different from those involved for activated phosphates, with protonation or metal-binding of the leaving group as a likely necessary step for leaving group departure.

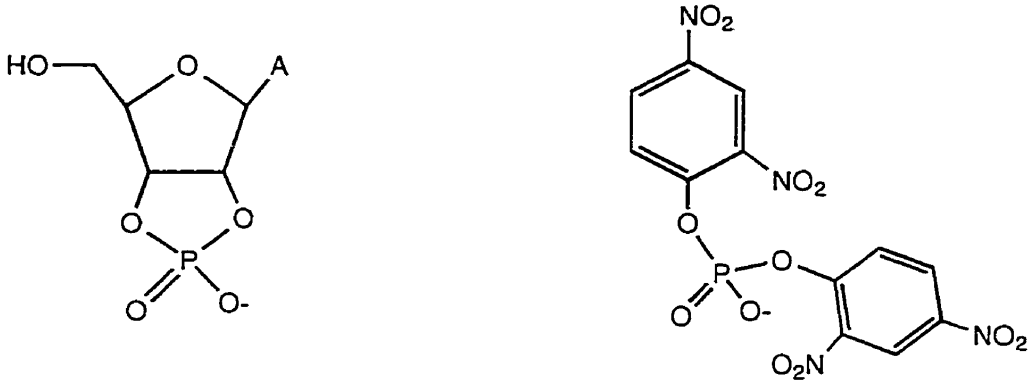

2'3'-cAMP BDNPP

Figure 4.1 Hydroxide-catalyzed second-order rate constants for BDNPP and 2′,3′-cAMP hydrolysis are very similar.

In this chapter, a metal complex-promoted hydrolysis of bis-2,4-dinitrophenyl phosphate (BDNPP) is compared with that of 2′,3′-cAMP (Figure 4.1). 2,4-dinitrophenolate is a particularly good leaving group (pKa=4) as a result of its two electron-withdrawing nitro groups that stabilize the dinitrophenolate ion. 2′,3′-cAMP on the other hand has a poor leaving group which has a pKa (pKa=13) comparable to that of ethylene glycol. Interestingly, however, the reported hydroxide-catalyzed rates for these two substrates are quite similar with 1.1 x 10^{-3} $M^{-1}s^{-1}$ second-order rate constant reported for 2′,3′-cAMP[1] and a 3.2 x 10^{-3} $M^{-1}s^{-1}$ rate constant for BDNPP.[2] It has been postulated that the fast rate for 2′,3′-cAMP hydrolysis arises from the five-membered-ring strain.

When a phosphate (or other substrate) is chelated to a metal in a bidentate fashion, it has been proposed that the rate of hydrolysis is approximately an order of magnitude faster than if it were bound in a unidentate manner. For example, in this laboratory Linkletter and Chin reported that Cu(neo) hydrolyzes ApA almost 3000 times faster than the background hydroxide-catalyzed rate.[3]

This 3000-fold rate acceleration is considerably faster than the approximately 2 orders of magnitude expected from single Lewis acid activation. (Crystal structures are available which show that a phosphate may chelate the copper complex.[4]) In the case of chelation however, two negative charges rather than one are quenched by the Lewis acid metal. Since two Lewis acid metals are not involved, chelation is not considered double Lewis acid activation. Instead since the negative charge from TWO Lewis bases are quenched by a single metal, chelation will be referred to as "quasi" double Lewis acid activation.

There were a number of important considerations involved in designing Cu(neo) as a catalyst for phosphate ester hydrolysis. Dimerization which would block potential phosphate-coordinating sites is not a problem as is the case for Cu(phen)-catalyzed ApA hydrolysis since the two methyl groups of the neocuproine ligand are believed to sterically repel the methyl groups of the second neocuproine moiety. Additionally, the methyl groups are postulated to provide the necessary steric bulk to allow for the ideal bond angle formation (approaching 76° for O-M-O bond angle)[5] for phosphate chelation of the metal centre. The relationship between better bond angles for phosphate chelation and improved hydrolysis rates has been shown.[6] Also, since the rate of Cu(neo)-promoted ApA hydrolysis is over 150-fold faster than 6,6'-dimethyl-2,2'-bipyridine copper (ii) (Cu(dmbp))-promoted hydrolysis, the rigidity of the phenanthroline ring is apparently advantageous.[4] Rotation of the bridging bond between the two pyridine rings of bipyridine (Figure 4.2) likely place the methyl groups in a less favorable position for prevention of dimerization and/or for the formation of the ideal bond angles for phosphate chelation.

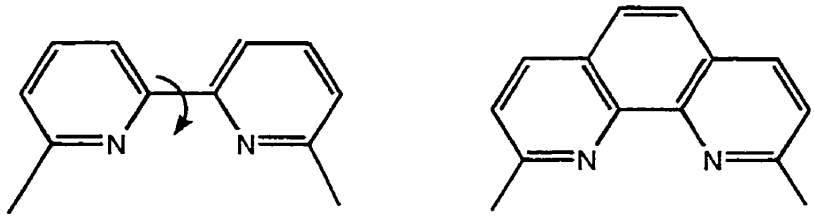

Figure 4.2 Neocuproine (at right) is a fused ring system where the methyl groups will be in the same plane. The dimethylbipyridine exhibits torsion between the two pyridine rings which would place the methyl groups in different planes.

In order to better understand the mechanisms involved in phosphate diester hydrolysis, one can make small changes in the structure of known simple artificial metal phosphoesterases and observe the effect of these changes on the reactivity. In his PhD thesis, Mark Wall recently reported that a 2,9-diamino-1,10-diaminophenanthroline copper (ii) complex (Cu(dap)) hydrolyzes 2′,3′-cAMP 850-fold faster than Cu(neo).[7] Restated: by simply changing the methyl groups to amino groups, almost three orders of magnitude rate acceleration is observed.

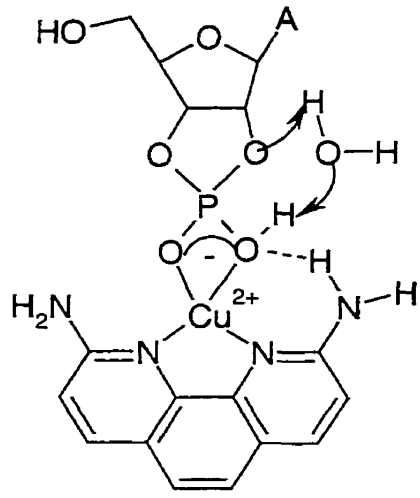

Figure 4.3 Hydrogen bonding mechanism is proposed to allow a proton switching mechanism to take place that accelerates the rate of 2′,3′-cAMP hydrolysis.

In his thesis, Wall examines multiple possible mechanisms for the role of the amino group in the rate acceleration observed for 2′,3′-cAMP hydrolysis. Nucleophilic catalysis by the amino group is neatly ruled since the phosphoramidate intermediate (not observed in HPLC trace for 2′,3′-cAMP hydrolysis) is not hydrolyzed to any appreciable extent under the same experimental conditions as used for 2',3'-cAMP hydrolysis. Intramolecular general base catalyzed deprotonation of the metal-bound OH is ruled out because the basicity of the amino group is too weak (the reported pKa for the conjugate acid 2-aminopyridinium is -7.6).[22] Instead, an intramolecular hydrogen bonding mechanism is proposed where proton switching by a water molecule is involved in the protonation of the leaving group. (Figure 4.3) As a result of this deprotonation/protonation step, Wall postulates that the intramolecular hydrogen bonding is considerably more important for

phosphates with poor leaving groups than for phosphates with good leaving groups.[7]

Shiraishi *et. al.* have previously reported that 6,6′-diamino-2,2′-bipyridine (dabp) forms a one-to-one complex with Cu^{2+} ion. In this paper, Shiraishi[8] reported the stability constant (log K_b) at 25°C for the 1:1 Cu^{2+}:dabp complex (log K_b= 6.7). This value represents a significant improvement in stability over the 1:1 Cu^{2+}: 6,6'-dimethyl-2,2'bipyridine[9] Cu(dmbp) complex (log K_b= 4.9), but a decrease in stability versus Cu^{2+}:2,2'-bipyridine (Cu(bp)).[10] The decrease in stability of the Cu(dmbp) versus Cu(bp) is believed to result from the steric repulsion of the methyl groups. In the case of Cu(dabp) however, the electron-donating properties of the amino groups increase the overall basicity of the ligand versus Cu(dmbp) and almost one hundred fold improvement in binding results. The stability constant for Cu(dabp) is not as large however as that reported for Cu(dap) (log K_b =8.0).[7]

In the results and discussion section of this chapter, a study of the hydrolyses of BDNPP and 2′,3′-cAMP using Cu(dabp) is reported. Additionally, HPNP, MPNP and HP*m*NP hydrolysis reactions using Cu(dabp) catalyst is reported to examine the mode of activation of the metal for these phosphate diesters.

4.2 Results and Discussion

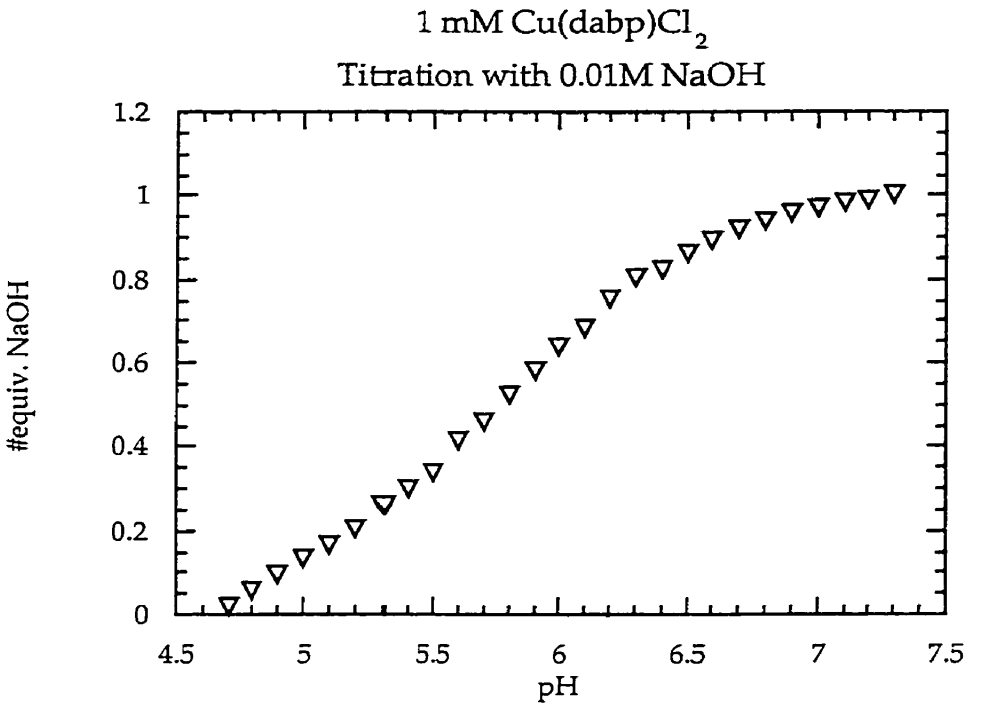

Figure 4.4 Potentiometric titration of Cu(dabp)Cl_2 with 0.01N NaOH

6,6'-diamino-2,2'-bipyridine (dabp) and a slight excess of copper (ii) chloride were mixed together in acetone/methanol to make the Cu(dabp)Cl_2 complex. Cu(dabp)Cl_2 was dissolved in water and titrated potentiometrically using sodium hydroxide to reveal one equivalent of hydroxide consumed and a pKa= 5.7 at 25°C (Figure 4.4). This pKa is 1.3 pKa units less than the pK_a of Cu(dmbp)Cl_2 (pKa=7.0 at 25°C). This difference may be explained by a proposed intramolecular hydrogen bonding effect whereby the amino group hydrogen bonds to the metal-bound water, which allows a base to abstract a hydrogen from the aquo group more readily (Figure 4.5). Cu(dap) in comparison has a pKa of 5.5 versus the pKa= 7.0 of Cu(neo), a difference of 1.5 pKa units. The modestly greater shift of Cu(dap) vs. Cu(neo) as compared to Cu(dabp) vs. Cu(dmbp) is possibly a result of the greater rigidity of the

phenanthroline ring which allows the hydrogen bonding distance to the metal-bound water to be more ideal than in the case of Cu(dabp). However, since the pKa difference is slight between the Cu(dap) and Cu(dabp) complexes, definitive conclusions cannot be made about the differences between the two pKas.

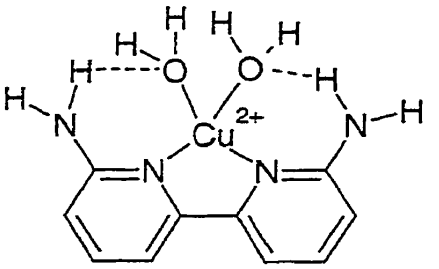

Figure 4.5 Cartoon showing the effect of intramolecular hydrogen bonding on the pKa of Cu(dabp)$(OH_2)_2$.

If it is true that a hydrogen bond donor (such as the amino group of dabp or dap) acts to lower the pKa of the metal-bound water, it is logical that a hydrogen bond acceptor would increase the pKa of the metal-bound water. To test this hypothesis, 2,2'-bi-1,8-naphthyridine (binp) was synthesized and the pKa of both the ligand and the copper-bound binaphthyridine were determined spectrophotometrically. An increase in pKa versus Cu(dmbp) would be expected since one of the naphthyridine nitrogens can accept the proton from the metal-bound water (see Fig. 4.7).

For the ligand, the isosbestic point was found at λ=336 nm and the change in molar absorptivity coefficient versus pH measured at λ=358 nm, where maximal change was observed. The pKa for 2,2'-bi-1,8-naphthyridine (binp) was determined to be 3.7 (Figure 4.6.1). Similarly, an isosbestic point for Cu(binp) was found (λ= 348 nm) and the change in molar absorptivity coefficient was measured at λ=372 nm (Appendix 4.1). At higher concentrations, it is believed that dimerization of Cu(binp) occurs, so it was necessary to go to lower concentrations values in order to determine the pKa of the monomer. At

concentration values lower than 30μM Cu(binp), the pKa was determined to be 7.7 (Figure 4.6.2).

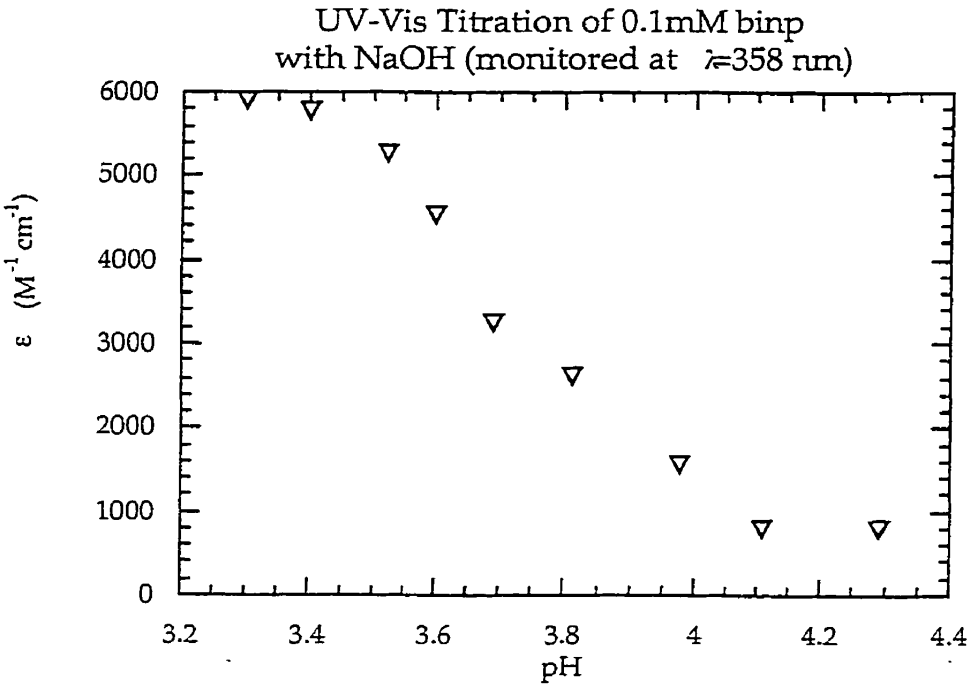

Figure 4.6.1 Spectrometric titration of 2,2'-bi-1,8-naphthyridine at 25°C.

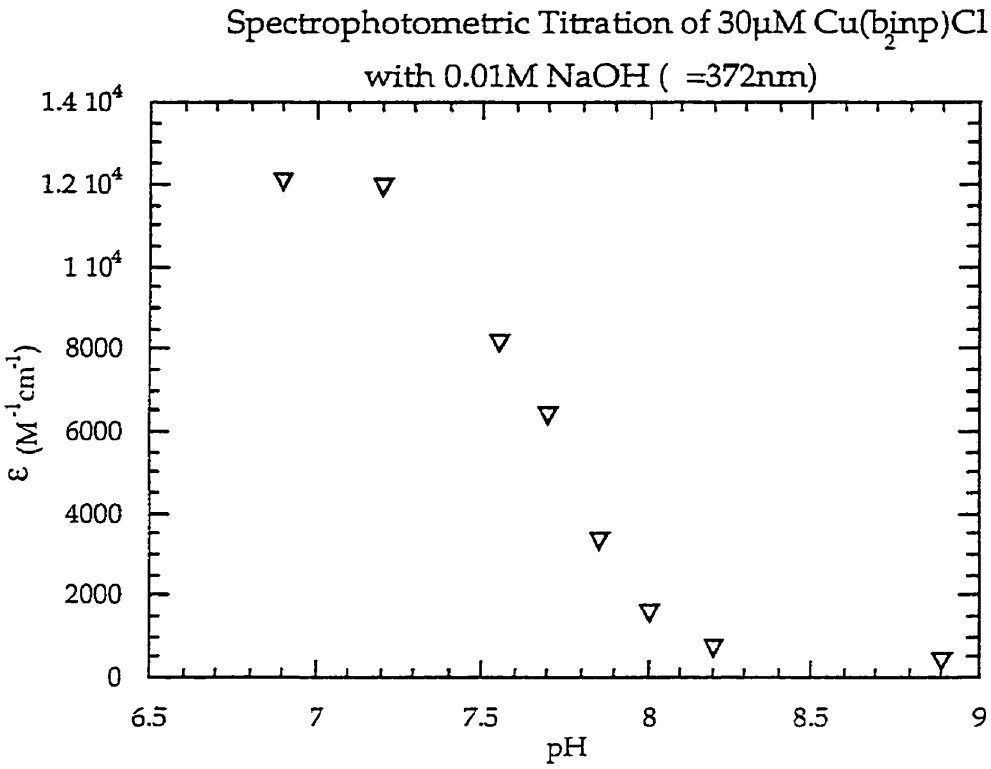

Figure 4.6.2 Spectrophotometric titrations of Cu(binp)Cl_2 at 25°C.

The pKa value for Cu(binp) is 0.7 pKa units higher than Cu(dmbp) which indicates that hydrogen bond acceptance of a metal-bound aquo group is indeed possible and supports the hydrogen bond donation hypothesis for the lowering of the pKa in the case of Cu(dabp) (Fig. 4.7).

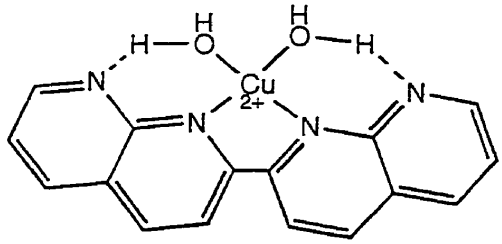

Figure 4.7 Cartoon of Cu(binp) showing how the hydrogen-bond acceptor would increase the pKa of the metal complex.

The lower pKa of Cu(dabp) versus Cu(dmbp) is similar to the difference in the pKa of Cu(dap) versus Cu(neo). This similarity begs the question: is a similar rate acceleration on phosphate diester hydrolysis observed using Cu(dabp) as is observed for Cu(dap)-promoted hydrolysis? Initially, BDNPP hydrolysis was tested to see what effect Cu(dabp) has on phosphates with good leaving groups.

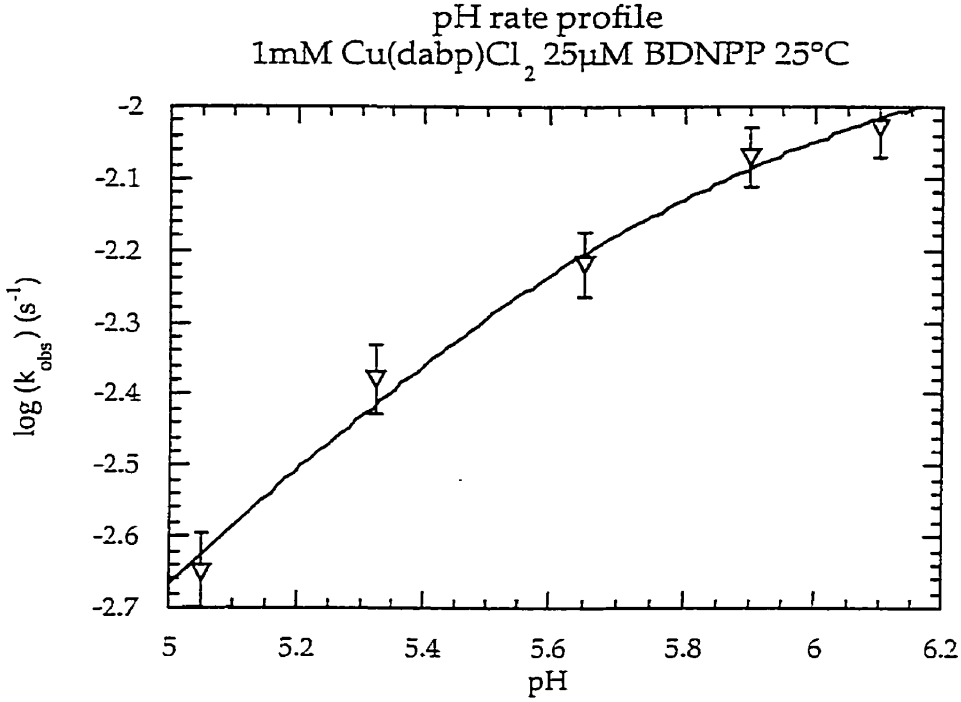

Figure 4.7 pH rate profile for Cu(dabp)-promoted BDNPP hydrolysis. Data is fit to equation 4.1 to yield $k=(1.4\pm0.1) \times 10^{1}\ M^{-1}s^{-1}$; $K_a= (1.9 \pm 0.2) \times 10^{-6}\ M^{-1}$. The kinetically-determined pKa agrees nicely with the potentiometrically determined pKa. The goodness-of-fit R= 0.995.

In order to glean information about Cu(dabp)-promoted BDNPP hydrolysis, a pH rate profile was carried out. Pseudo-first-order rate constants were obtained for BDNPP hydrolysis for each pH value shown in Fig. 4.7 and were fit to the equation: $[X]_t= [A]_o(1-e^{-kt})$ by monitoring 2,4-dinitrophenolate increase. As in the case of Cu(dap)-promoted BDNPP hydrolysis, only one

equivalent of 2,4-dinitrophenolate is produced from Cu(dabp)-promoted BDNPP hydrolysis. The data from the pH rate profile was fit to the following equation:

$$k_{obs} = \frac{kKa[M]_t}{[H^+] + Ka} \qquad \textbf{(Equation 4.1)}$$

where k is the second-order rate constant for BDNPP hydrolysis, Ka is the acid dissociation constant for the metal-bound water and $[M]_t$ is the total concentration of Cu(dabp) catalyst (Equation 4.1 is derived in Appendix 4.2).

metal complex	k ($M^{-1}s^{-1}$)	relative rate
Cu(dap)[7]	2.3×10^1	7.2×10^3
Cu(dabp)	1.4×10^1	4.4×10^3
Cu(neo)[4]	1.6×10^0	5.0×10^2
OH^-[2]	3.2×10^{-3}	1

Table 4.1 The second-order rate constants for the hydrolysis of BDNPP at 25°C using several copper (ii) complexes.

The pH rate profile graph (Fig. 4.7) indicates that the aquo-hydroxy form of Cu(dabp) is the active form of the metal catalyst for the hydrolysis of BDNPP as is the case in Cu(dap)-promoted[7] and many other metal complex-promoted phosphate diester hydrolysis reactions.[11-13] The second-order-rate constant obtained from this graph represents a 4800-fold increase for Cu(dabp)-promoted BDNPP hydrolysis over the background hydroxide-catalyzed rate (3.2×10^{-3} $M^{-1}s^{-1}$). The rate constant is also approximately 9 times faster than the reported

Cu(neo)-promoted hydrolysis rate but is only 60% of the reported rate of Cu(dap)-promoted hydrolysis (Table 4.1).

The faster Cu(dap) rate over Cu(dabp) rate may result from a more ideal hydrogen bonding distance to the phosphate oxygen due to the rigidity of the fused aromatic rings. Although the difference between the two rates is modest, the effect of the postulated hydrogen bonding on the rate of hydrolysis rate for phosphates with good leaving groups is expected to be relatively modest since only a 10-fold difference between Cu(dap)- and Cu(neo)-promoted BDNPP hydrolysis is observed. However, considering that the difference between the Cu(dabp)- and Cu(dap)-promoted rates is small, one should be cautious before jumping to any mechanistic conclusions. For example, one might also conclude that the rate difference results from a less ideal bond angle for phosphate chelation for Cu(dabp) because of the twisting of the bridging bond between the two pyridine rings. The proposed mechanism for Cu(dabp)-promoted BDNPP hydrolysis is identical to that proposed for Cu(dap)-promoted hydrolysis[7] and is shown below (Fig. 4.8).

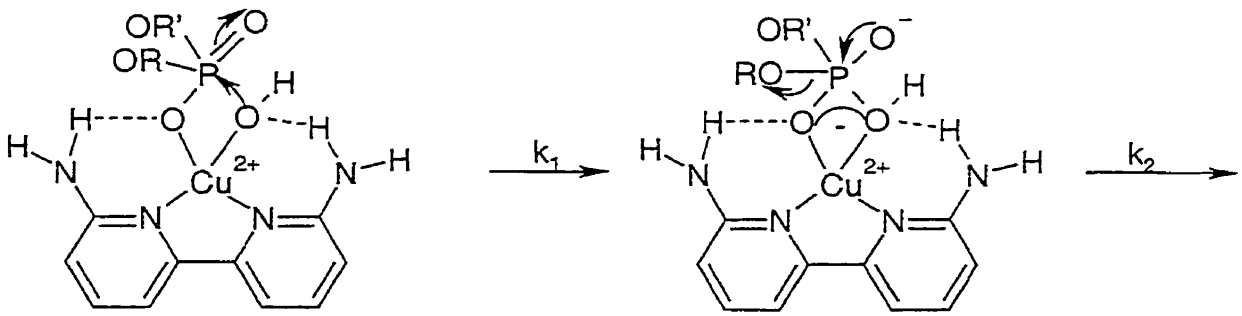

Figure 4.8 Proposed mechanism for Cu(dabp)-promoted BDNPP hydrolysis and other phosphate diesters with good leaving groups.

So what effect does Cu(dabp)Cl_2 have on the hydrolysis reaction of phosphate substrates with poor leaving groups? To examine this question, the

hydrolysis of 2′,3′-cAMP using Cu(dabp) was observed. The pH rate profile for 2′,3′-cAMP hydrolysis shown below (Figure 4.9) was obtained from HPLC measurements of the pseudo-first-order decreases of the substrate (2′,3′-cAMP) and the concomitant increases of the hydrolysis products (2′-AMP and 3′-AMP) (Figure 4.10 and Appendix 4.3). As in the case of Cu(dabp)Cl_2-promoted BDNPP hydrolysis, the data is fit to equation 4.1.

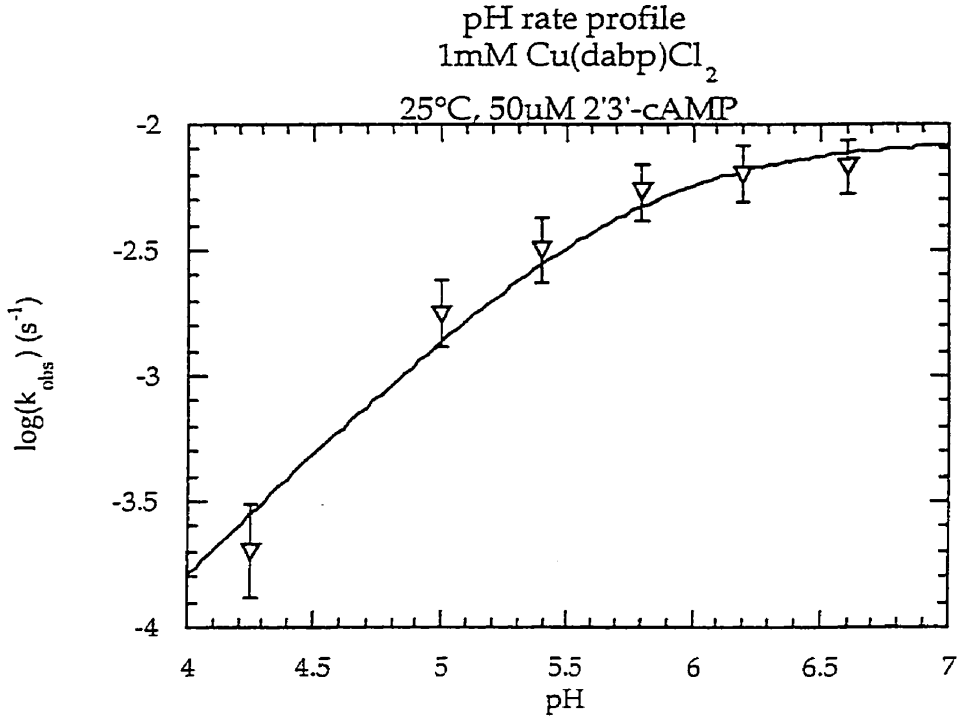

Figure 4.9 pH rate profile for Cu(dabp)Cl_2-promoted 2′,3′-cAMP hydrolysis. Data is fit to equation 4.1 to yield a second-order rate constant k= (8.7 ± 0.9) x 10^0 $M^{-1}s^{-1}$ and a Ka= (1.9 ± 0.3) x 10^{-6} s^{-1}. Goodness-of-fit R value: R= 0.99.

The second-order rate constant reported for Cu(dabp)-promoted 2',3'-cAMP hydrolysis is approximately 8000 times faster than the background hydroxide-catalyzed rate. This rate is also approximately 25-fold faster than the rate of a recently reported dinuclear Cu(II) complex-promoted hydrolysis of the cyclic phosphate.[14]

Cu(dabp) hydrolysis is 120 times faster than Cu(neo)-promoted 2′,3′-cAMP hydrolysis but is approximately four times slower than Cu(dap)-promoted hydrolysis (Table 4.2). The relative importance of the Cu(dabp)-promoted 2′,3′-cAMP cleavage reaction supports the proposed intramolecular hydrogen bonding/proton switching mechanism shown in Figure 4.3. As one would expect from this mechanism, the postulated hydrogen bond donation for phosphates with poor leaving groups would be more important than in the case of those with good leaving groups. And indeed, the difference between Cu(dabp) and Cu(neo)-promoted BDNPP hydrolysis is only 9-fold, while the difference in

catalyst	k ($M^{-1}s^{-1}$)
OH^{-1}	1.1×10^{-3}
Cu(neo)[4]	6.6×10^{-2}
Cu(dabp)	8.7×10^{0}
Cu(dap)[7]	3.8×10^{1}

Table 4.2 Comparison of second-order rate constants for catalyzed hydrolysis of 2′,3′-cAMP at 25°C.

the hydrolysis rates between these two metal complexes is 120-fold in the case of 2',3'-cAMP hydrolysis. Additionally, if one assumes that the hydrogen bonding distance is not as ideal for Cu(dabp) as for Cu(dap) based on Cu(dabp)'s higher pKa value (5.73 vs. 5.5), it is not unreasonable to suggest that the change in difference between Cu(dap)- versus Cu(dabp)-promoted phosphate hydrolysis rates from 1.6-fold in the case of BDNPP hydrolysis to 4.4-fold in the case of 2',3'-cAMP hydrolysis may result from the differing hydrogen bonding properties of the two complexes. However, since the rate differences between the two

complexes are modest, one cannot make any definitive conclusions in that regard.

Interestingly, the hydrolysis products exhibited a 6:1 preference for 3′-AMP over 2′-AMP. Cu(dap)-promoted 2′,3′-cAMP hydrolysis exhibited a similar product preference (16:1 3′-AMP: 2′-AMP). Although 3′-nucleotide monophosphates are 2 kJ/mol more stable than their 2′ analogues, a ratio of only 1.4-2.6 to 1 would be expected given this thermodynamic difference.[15] Presently, it is not clear what causes the regiospecificity. There has been speculation that the preference may be a result of π stacking between the pyridine or phenanthroline ring and the base since no hydrolysis product preference is observed in the case of Co(cyclen)-promoted 2′,3′-cAMP hydrolysis. Additionally, Massoud *et. al.* have shown that the phenanthroline ring of copper phenanthroline complexes may stack with adenine base. [16-17]

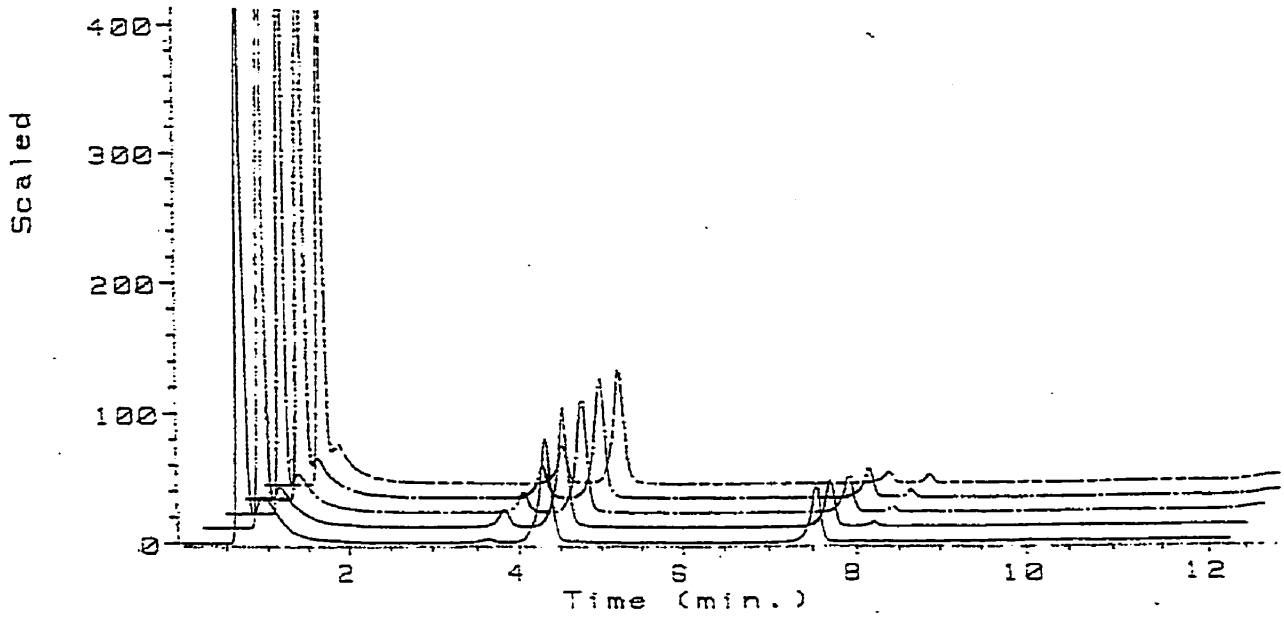

Figure 4.10 Sample HPLC trace of 2′,3′-cAMP hydrolysis with Cu(dabp). The retention times of the peaks are as follows: 3′-AMP (3.5 min.), 2′3′-cAMP (7.5 min.) and 2′-AMP (8.0 min.).

In Chapter 2, a series of experiments were done using Cu_2bbmp as metal catalyst to distinguish double Lewis acid activation as the mode of activation for HPNP hydrolysis from joint single Lewis acid activation/metal-nucleophile attack and joint single Lewis acid activation/leaving group activation. Here a similar study using Cu(dabp) as catalyst is effected using the same cast of chemicals: HPNP, MPNP and HP*m*NP. While there are not two metals in the case of Cu(dabp), these experiments serve to further illustrate the utility of using different substrates to rule out various modes of activation.

substrate	rate (s^{-1})	relative rates
HPNP	$(6.6\pm0.3) \times 10^{-4}$	1
MPNP	$(3.3\pm0.2) \times 10^{-5}$	0.05
HP*m*NP	$(8.7\pm0.4) \times 10^{-5}$	0.13

Table 4.3 Cu(dabp)-promoted hydrolysis of various *p*-nitrophenyl phosphate esters. Conditions: 1mM Cu(dabp)Cl_2, 50μM substrate, 25°C, pH 6.6.

The observed rate of Cu(dabp)-promoted HPNP cleavage is approximately 20-fold faster than the metal complex-promoted MPNP hydrolysis (Table 4.3). This rate difference indicates that unlike in the case of Co(cyclen), single Lewis acid activation/metal-nucleophile attack is NOT the mode of activation for phosphate diester cleavage since one would expect the rates of MPNP and HPNP cleavage to be the same in this case. Cu(dabp)-promoted HP*m*NP transesterification is between 7- and 8-fold slower than the corresponding HPNP cleavage (Figure 4.11). These observed rates place the difference between HPNP and HP*m*NP transesterification rates about where would one would expect from the linear free energy profile for metal complexes

that exhibit double Lewis acid activation (Figure 2.7). Therefore, it is reasonable to propose that the phosphate ester is chelated to the metal ("quasi" double Lewis acid activation) when the transesterification reaction takes place.

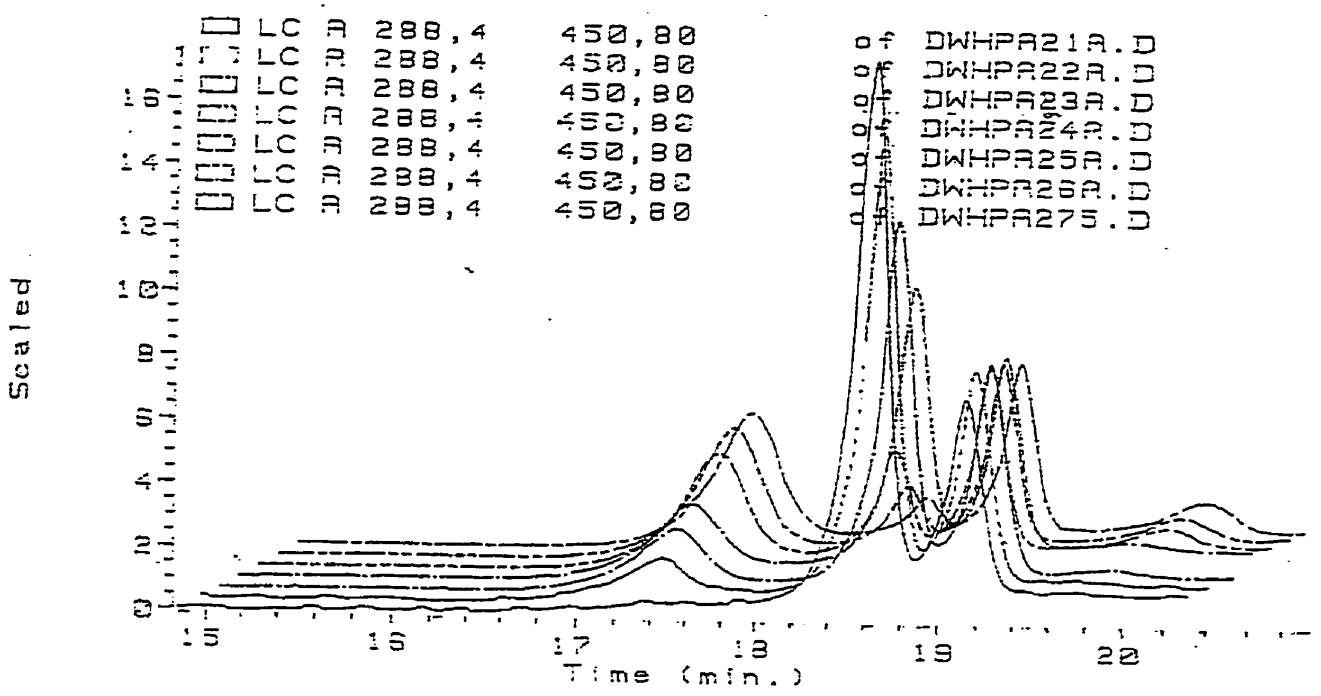

Figure 4.11 HPLC trace of the simultaneous HPNP and HP*m*NP hydrolysis reactions with Cu(dabp). Reaction conditions are as shown in Table 4.3. The retention times of the identified peaks are as follows: *p*-nitrophenol (17.4 min.); HPNP (18.5 min.); HP*m*NP (19.0 min.); *m*-nitrophenol (20.0 min.).

4.3 Experimental

4.3.1 Chemicals

6,6′-diamino-2,2′-bipyridine[18-19] and 2,2′-bi-1,8-naphthyridine[20-21] were synthesized by literature procedures and confirmed by ^1H NMR spectrometry and melting point determination. BDNPP was provided by Philip Hurst who synthesized the phosphate diester according to literature procedure.[2] 2′,3′-cAMP was purchased from Sigma-Aldrich. $CuCl_2$ was purchased from Les Laboratoires MAT, Inc.

Synthesis

Preparation of copper (ii) 6,6′-diamino-2,2′-bipyridine chloride. A solution of 6,6′-diamino-2,2′-bipyridine (30 mg, 0.16mmol) was completely dissolved in acetone (0.5 mL) and added dropwise to a stirring methanolic solution (0.5 mL) of anhydrous $CuCl_2$ (25mg, 0.19 mmol). A dark green precipitate formed immediately which was collected by suction filtration. The green powder was washed first with cold methanol and subsequently with anhydrous ethyl ether. The powder was dried under vacuum overnight and weighed (48 mg, 0.15 mmol, 94%). Elemental analysis calculated for $C_{10}H_{10}N_4CuCl_2$: C, 37.4; H 3.14; N 17.4; Cu 19.82. Found: C, 37.04; H 3.29; N 17.03; Cu 19.36.

Preparation of copper (ii) 2,2′-bi-1,8-naphthyridine chloride. A solution of 2,2′-bi-1,8-naphthyridine (30 mg, 0.18 mmol) was dissolved in ethanol and added dropwise with stirring to a solution of anhydrous $CuCl_2$ (28 mg, 0.21 mmol) dissolved in ethanol. A green precipitate formed which was collected by suction filtration and subsequently washed with cold ethanol and anhydrous ethyl ether. The powder was dried under vacuum overnight and weighed (47 mg, 0.16

mmol, 89%). Elemental analysis calculated for $C_{16}H_{10}N_4CuCl_2$: C, 48.93; H 2.57; N 14.27. Found: C, 48.72; H 2.61; N 14.15.

4.3.2 Kinetics

UV-Vis Spectrophotometer

All solutions were prepared volumetrically as always. BDNPP hydrolysis was monitored by observing 2,4-dinitrophenolate production at λ=400 nm. HPNP and MPNP comparative hydrolyses were done as in the experimental section of chapter 2. Data for pseudo-first-order increases and pH rate profiles were fit to curves using Kaleidgraph 3.0.1 iterative least-squares fitting procedure. The method of initial rates is used for Cu(dabp)-promoted MPNP hydrolysis.

HPLC Conditions

Simultaneous HPNP and HP*m*NP hydrolysis (so that both substrates and their hydrolysis products may be observed) was measured using the following conditions (conditions in Chapter 2 do not separate all 4 substrates): 2.1 x 100 mm 5µm ODS Hypersil C-18 column was used which was maintained at 40°C with a micro-oven. Absorbance was monitored at λ= 288.4 nm with a reference wavelength of λ= 450.8 nm. The column was initially eluted with 100% 10mM potassium phosphate solution at pH 6.0 (sol'n A) for 5 minutes. A linear gradient for the next two minutes occurred which brought the eluting solvent to a mixture of 75% sol'n A and a 25% 90/10 sol'n A/MeOH mixture (sol'n B). A second linear gradient followed over the next ten minutes whereby the elution mixture was brought to a 10% sol'n A/ 90% sol'n B mixture. For the subsequent and last three minutes of the elution profile, the eluent ratio (10%A/90%B mixture) was maintained.

HPNP and HP*m*NP transesterification substrates and products were compared with authentic samples which were run previously using the above conditions. The observed retention times were as follows: *p*-nitrophenol (17.4 min.); HPNP (18.5 min.); HP*m*NP (19.0 min.); *m*-nitrophenol (20.0 min.). Integrations were compared versus a *p*-nitrobenzene sulfonic acid internal standard.

2′,3′-cAMP hydrolysis was monitored using the same column and temperature as above. Absorbance was monitored at λ=254 nm with a reference wavelength of λ=450 nm. Elution with ammonium phosphate buffer (0.2M, pH 5.5) for 5 min. was succeeded by a linear gradient of 0 to 40% 60/40 methanol/water over the following 8 minutes.

2′,3′-cAMP hydrolysis substrates and products were compared with authentic samples. The observed retention times were as follows: 3′-AMP (3.5 min.), 2′,3′-cAMP (7.5 min.); 2′-AMP (8.0 min.).

4.3.3 Potentiometric Titrations

Potentiometric titrations were done according to the protocol discussed in the experimental section in Chapter 3.

4.4 Chapter 4 References

1. Abrash, H.L.; Cheung, C.; Davis, J. *Biochem.* **1967** 6, 1298-1303.

2. Bunton, C.A.; Farber, S.J. *J. Org. Chem.* **1969** 34, 767-772.

3. Linkletter, B.; Chin, J. *Angew. Chem. Intl. Ed. Engl.* **1995** 34, 472-4.

4. Linkletter, B., Ph.D. thesis, McGill University, 1995.

5. Anderson, B.; Milburn, R.M.; Harrowfield, J.M.; Robertson, G.B.; Sargeson, A.M. *J. Am. Chem. Soc.* **1977** 99, 2652-9.

6. Connolly, J.A.; Banaszcyk, M.; Hynes, R.C.; Chin, J. *Inorg. Chem.* **1994** 33, 665-9.

7. Wall, M., Ph.D. thesis, McGill University, 1997.

8. Kishi, N.; Araki, K.; Shiraishi, S. *Bull. Chem. Soc. Jpn.* **1984** 57, 2121-6.

9. James, B.R.; Williams, R.J. *J. Chem. Soc.* **1961** 2007-2019.

10. Perrin, D. Stability Constant of Metal Ion Complexes Part B, Ed. 1, Pergamon Press: Oxford, 1979.

11. Chin, J.; Banaszcyk, M.; Jubian, V.; Zou, X. *J. Am. Chem. Soc*, **1989** 111, 186-90.

12. Norman, P.R.; Cornelius, R.D. *J. Am. Chem. Soc.* **1982** 104, 2356-61.

13. Kim, J.H.; Chin, J. *J. Am. Chem. Soc.* **1992** 114, 9792-5.

14. Liu, S.; Luo, Z.; Hamilton, A.D. *Angew. Chem. Intl. Ed. Engl.* **1997** 36,2678.

15. Oivanen, M.; Lönnberg, H. *Trends in Organic Chemistry* **1991** 2, 183-98.

16. Massoud, S.; Tribolet, R.; Sigel, H. *Eur. J. Biochem.* **1990** 187, 387-93.

17. Massoud, S.; Sigel, H. *Eur. J. Biochem.* **1989** 179, 451-8.

18. Schneider, J.; Kelly, J.W., *J. Am. Chem. Soc.* **1995** 2533-46.

19. Rillema, D.P. *Synthetic Communications* **1990** 20, 1233-9.

20. Thummel, R. *J. Org. Chem.* **1984** 49, 2208-12.

21. Caluwe, P.; Majewicz, T. *J. Org. Chem.* **1974** 39, 151

22. Jencks, W.P.; Regenstein, J. Handbook of Biochemistry Chemical Rubber Company: Cleveland, OH, 1970.

Chapter 4 Appendix

Appendix 4.1 Sample spectrometric titration runs of binp and Cu(binp) showing isosbestic point and change in spectrum versus pH.

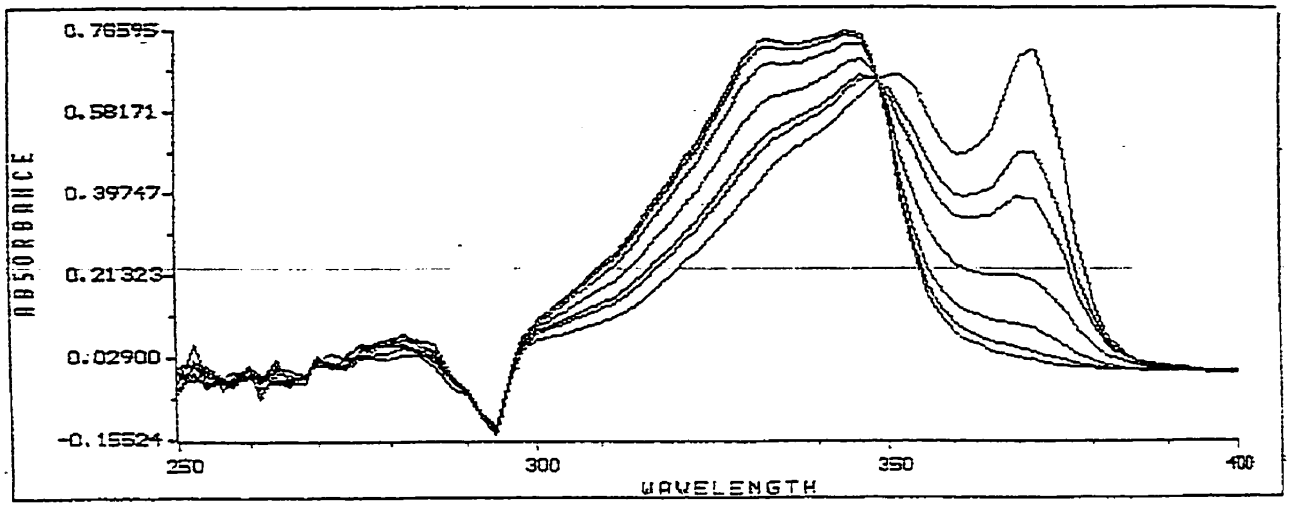

Appendix 4.1.1 A 60μM $Cu(binp)Cl_2$ is titrated with NaOH to give the following spectrometric profile. The isosbestic point is observed at λ=348 nm. The change of absorbance with pH is observed at λ=372 nm; at this wavelength, the absorptivity coefficient decreased with increasing pH.

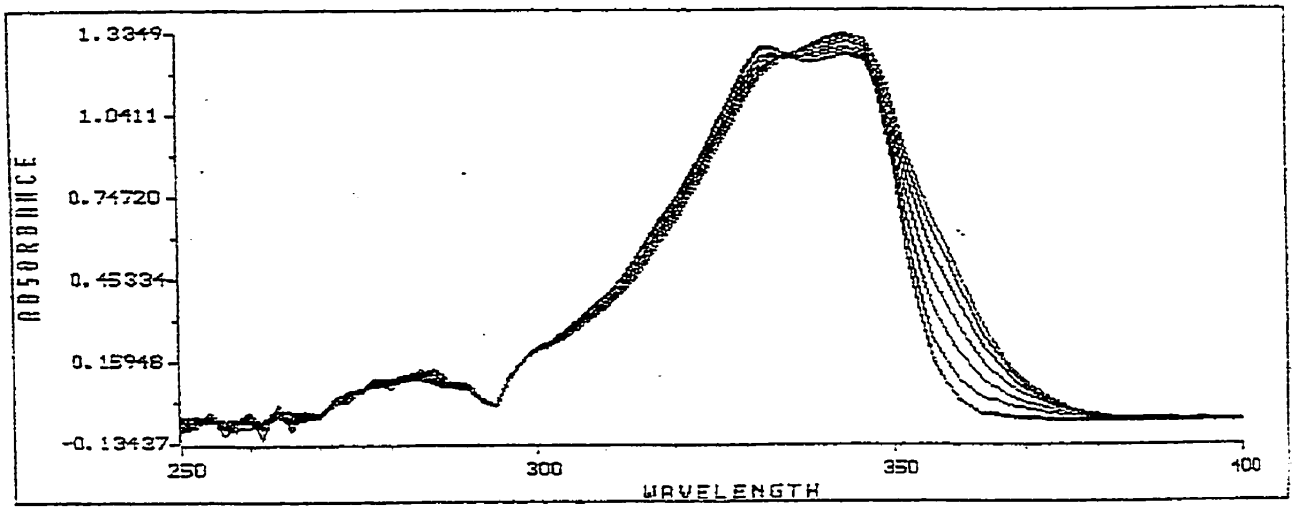

Appendix 4.1.2 A 0.1 mM binp solution is titrated with NaOH to give the following spectrometric profile. The isosbestic point is observed at λ=336 nm. The change of absorbance with pH is observed at λ=358 nm; at this wavelength, the absorptivity coefficient decreased with increasing pH.

Appendix 4.2 Derivation of equation for pH rate profile

Below is a derivation of equation 4.1.

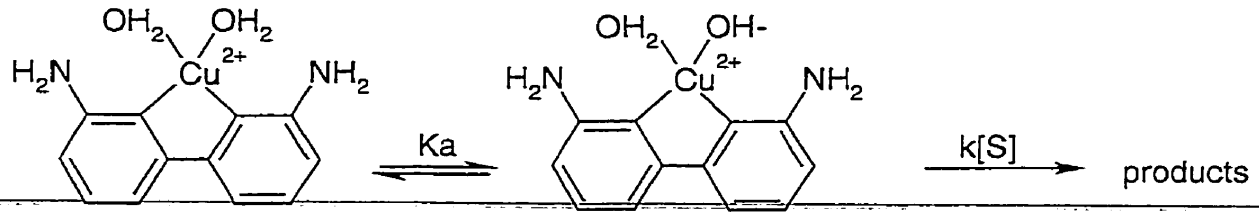

S is an abbreviation for substrate, which in this chapter is either 2′,3′-cAMP or BDNPP.

1. $Ka = [Cu(dabp)(OH)(OH_2)]\,[H^+]/[Cu(dabp)(OH_2)_2]$ **(Eqn. 4.2)**

2. $rate = k\,[Cu(dabp)(OH)(OH_2]\,[S]$ **(Eqn 4.3)**

3. This rate under pseudo-first-order conditions may be expressed as:

$$rate = k[Cu(dabp)(OH)(OH_2)]$$ **(Eqn. 4.4)**

4. $[M]_t$ is the total concentration of the metal complex and is expressed as:

$$[M]_t = [Cu(dabp)(OH)(OH_2)] + [Cu(dabp)(OH_2)_2]$$ **(Eqn. 4.5)**

5. Plugging equation 4.2 into equation 4.5 yields:

$$[M]_t = [Cu(dabp)(OH)(OH_2)]\,(1 + [H^+]/K_a)$$ **(Eqn. 4.6)**

6. Plugging equation 4.6 into equation 4.4 yields:

$$k_{obs} = \frac{kKa[M]_t}{[H^+] + Ka}$$ **(Equation 4.1)**

Appendix 4.3 2′,3′-cAMP hydrolysis

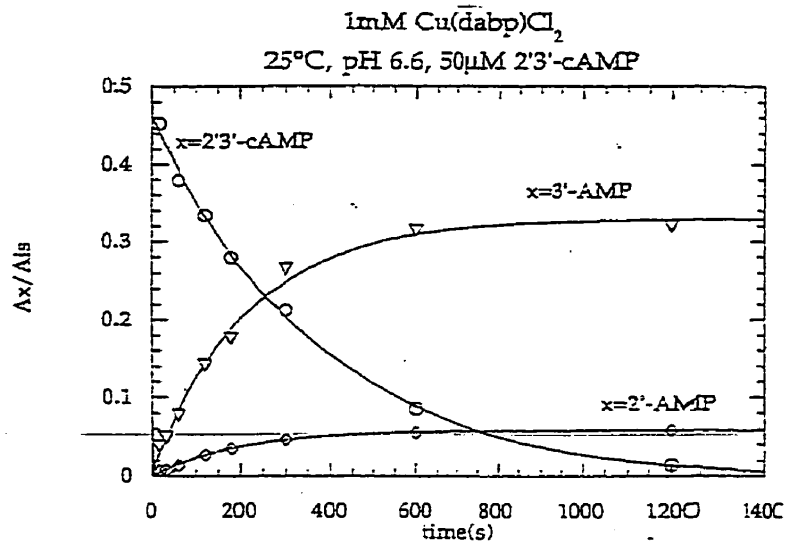

Figure 4.12 Sample run of 2′,3′-cAMP using Cu(dabp) as catalyst

Appendix 4.4 pH rate profile data

pH	k_{obs} (s^{-1})
4.25	$(2.0\pm0.2) \times 10^{-4}$
5.0	$(1.9\pm0.2) \times 10^{-3}$
5.4	$(3.5\pm0.2) \times 10^{-3}$
5.8	$(5.6\pm0.3) \times 10^{-3}$
6.2	$(6.2\pm0.3) \times 10^{-3}$
6.6	$(6.5\pm0.3) \times 10^{-3}$

Figure 4.13 Pseudo-first-order rate constants of pH rate profile for $Cu(dabp)Cl_2$ - (1 mM) promoted 2′,3′-cAMP (50 µM) hydrolysis at 25°C. Error shown is the standard deviation of a triplicate of runs.

Contributions to Knowledge

1. The dinuclear metal complex Cu2bbmp cleaves HPNP almost 100-fold faster than it hydrolyzes MPNP. As a result, joint single Lewis acid activation/metal-nucleophile attack is ruled out as a potential mode of activation for the two metal-promoted phosphate diester hydrolysis.

2. A dinuclear lanthanide complex Ln2hbt is prepared which is considerably more soluble in water than the free lanthanide ion or higher order aggregate. At pH 7.0 and 25°C, Yb2hbt (10 mM) hydrolyzes BNPP in water with a half-life of 6 s. This rate is 10 orders of magnitude faster than the uncatalyzed reaction, which is one of the fastest rate accelerations for BNPP hydrolysis reported to date.

3. Yb2hbt (2 mM) hydrolyzes BNPP 2300 times faster than the free Yb^{3+} ion (2 mM) in water at pH 7.0 and 25°C. This is an unprecedented rate acceleration for ligand-bound Ln^{3+}-promoted phosphate diester hydrolysis over ligand-free Ln^{3+}-promoted hydrolysis.

4. An X-ray crystal structure for Eu2hbt is reported. To the author's knowledge, this is the first X-ray crystal structure reported for a dinuclear lanthanide complex that is active for hydrolyzing phosphate diesters.

5. A mononuclear copper complex, Cu(dabp) is reported here which hydrolyzes the activated phosphate 2',3'-cAMP 8000 times faster than the background rate. This rate acceleration makes Cu(dabp) one of the fastest metal complexes for hydrolyzing 2',3'-cAMP ever reported. The difference in pKa between Cu(binp)

and Cu(dabp) supports the intramolecular hydrogen bonding mechanism proposed for Cu(dabp)-assisted 2′,3′-cAMP hydrolysis.

Publications Resulting from This Research

Wall, M; Linkletter, B.; Williams, D.; Lebuis, A.-M.; Hynes, R.C.; Chin, J. "Rapid Hydrolysis of 2′,3′-cAMP with a Cu(II) Complex: Effect of Intramolecular Hydrogen Bonding on the Basicity and Reactivity of a Metal-Bound Hydroxide" *J. Am. Chem. Soc.* **1999** 121, 4710-1.

Appendix 5. Crystal Structure Data from Hbt Complexes

Appendix 5.2 2:2 Eu:hbt Complex

Table 1. Crystal data and structure refinement for 1.

Identification code	xc67
Empirical formula	$C_{12}H_{17}Cl_2EuN_2O_9$
Formula weight	556.14
Temperature	296(2) K
Wavelength	0.71073 Å
Crystal system	Triclinic
Space group	$P\bar{1}$
Unit cell dimensions	a = 8.777(2) Å alpha = 107.74(2)° b = 10.203(3) Å beta = 110.35(3)° c = 12.252(4) Å gamma = 90.55(2)°
Volume, Z	979.4(4) $Å^3$, 2
Density (calculated)	1.886 Mg/m^3
Absorption coefficient	3.520 mm^{-1}
F(000)	544
Crystal size	0.2 x 0.3 x 0.3 mm
θ range for data collection	1.86 to 24.22°
Limiting indices	$-10 \le h \le 9$, $-11 \le k \le 10$, $-8 \le l \le 14$
Reflections collected	3999
Independent reflections	2938 (R_{int} = 0.0345)
Absorption correction	Semi-empirical from psi scans
Refinement method	Full-matrix least-squares on F^2
Data / restraints / parameters	2938 / 0 / 229
Goodness-of-fit on F^2	1.143
Final R indices [I>2σ(I)]	R1 = 0.0510, wR2 = 0.1566
R indices (all data)	R1 = 0.0541, wR2 = 0.1599
Largest diff. peak and hole	1.667 and -2.853 $eÅ^{-3}$

Table 2. Atomic coordinates [x 10^4] and equivalent isotropic displacement parameters [$Å^2$ x 10^3] for 1. U(eq) is defined as one third of the trace of the orthogonalized U_{ij} tensor.

	x	y	z	U(eq)
Eu	19(1)	196(1)	1597(1)	20(1)
Cl(1)	-4178(3)	1715(3)	3482(3)	49(1)
Cl(2)	-1505(4)	-3763(3)	2267(3)	45(1)
N(1)	2579(9)	-966(7)	2409(7)	23(2)
N(2)	2085(10)	1668(8)	3740(7)	29(2)
O(1)	1446(7)	-451(7)	276(5)	24(1)
O(2)	-422(8)	-2431(7)	717(6)	32(2)
O(3)	5520(9)	-2078(8)	2110(8)	44(2)
O(4)	-54(7)	-669(7)	3278(5)	27(1)
O(5)	1221(9)	2501(7)	1811(6)	33(2)
O(6)	-1143(9)	2079(7)	2798(6)	37(2)
O(7)	4469(10)	4010(11)	5479(9)	75(3)
O(8)	-2851(8)	-592(7)	1149(6)	33(2)
C(1)	2568(13)	-2090(10)	1324(8)	30(2)
C(2)	2671(13)	-1317(10)	443(9)	26(2)
C(3)	1046(11)	-3096(10)	758(9)	29(2)
C(4)	4000(13)	-2938(10)	1571(9)	34(2)
C(5)	2645(13)	-1366(11)	3492(9)	30(2)
C(6)	1642(12)	-507(10)	4158(9)	29(2)
C(7)	2153(12)	1042(10)	4686(8)	31(2)
C(8)	1694(11)	3113(9)	3953(8)	24(2)
C(9)	1949(14)	3562(10)	2969(9)	36(2)
C(10)	-78(13)	3148(11)	3881(9)	38(3)
C(11)	2809(8)	4157(6)	5313(6)	42(3)
O(10)	-4095(8)	-2385(6)	-1179(6)	52(2)
C(20)	-4873(8)	-3633(6)	-1453(6)	69(4)

Table 3. Bond lengths [Å] and angles [°] for 1.

Eu-O(1)#1	2.320(5)	Eu-O(1)	2.334(6)
Eu-O(8)	2.452(6)	Eu-O(5)	2.469(7)
Eu-O(6)	2.507(6)	Eu-O(4)	2.510(6)
Eu-O(2)	2.535(7)	Eu-N(1)	2.582(7)
Eu-N(2)	2.596(8)	Eu-Eu#1	3.8310(14)
N(1)-C(1)	1.471(11)	N(1)-C(5)	1.497(11)
N(2)-C(7)	1.477(11)	N(2)-C(8)	1.483(11)
O(1)-C(2)	1.398(10)	O(1)-Eu#1	2.320(5)
O(2)-C(3)	1.455(11)	O(3)-C(4)	1.413(14)
O(4)-C(6)	1.479(11)	O(5)-C(9)	1.426(12)
O(6)-C(10)	1.440(12)	O(7)-C(11)	1.415(11)
C(1)-C(3)	1.487(14)	C(1)-C(4)	1.529(12)
C(1)-C(2)	1.551(12)	C(5)-C(6)	1.516(13)
C(6)-C(7)	1.510(14)	C(8)-C(9)	1.505(14)
C(8)-C(10)	1.528(14)	C(8)-C(11)	1.631(11)
O(10)-C(20)	1.33		

O(1)#1-Eu-O(1)	69.2(2)	O(1)#1-Eu-O(8)	74.6(2)
O(1)-Eu-O(8)	126.8(2)	O(1)#1-Eu-O(5)	77.1(2)
O(1)-Eu-O(5)	79.8(2)	O(8)-Eu-O(5)	128.1(2)
O(1)#1-Eu-O(6)	95.1(2)	O(1)-Eu-O(6)	148.1(2)
O(8)-Eu-O(6)	70.7(2)	O(5)-Eu-O(6)	69.5(2)
O(1)#1-Eu-O(4)	146.8(2)	O(1)-Eu-O(4)	130.9(2)
O(8)-Eu-O(4)	72.4(2)	O(5)-Eu-O(4)	127.3(2)
O(6)-Eu-O(4)	77.2(2)	O(1)#1-Eu-O(2)	93.1(2)
O(1)-Eu-O(2)	72.4(2)	O(8)-Eu-O(2)	72.0(2)
O(5)-Eu-O(2)	152.2(2)	O(6)-Eu-O(2)	138.0(2)
O(4)-Eu-O(2)	73.7(2)	O(1)#1-Eu-N(1)	134.5(2)
O(1)-Eu-N(1)	66.1(2)	O(8)-Eu-N(1)	128.2(2)
O(5)-Eu-N(1)	102.6(2)	O(6)-Eu-N(1)	128.0(2)
O(4)-Eu-N(1)	68.1(2)	O(2)-Eu-N(1)	85.8(2)
O(1)#1-Eu-N(2)	139.2(2)	O(1)-Eu-N(2)	108.2(2)
O(8)-Eu-N(2)	124.7(2)	O(5)-Eu-N(2)	62.8(2)
O(6)-Eu-N(2)	65.3(2)	O(4)-Eu-N(2)	66.7(2)
O(2)-Eu-N(2)	125.8(2)	N(1)-Eu-N(2)	65.9(2)
O(1)#1-Eu-Eu#1	34.71(14)	O(1)-Eu-Eu#1	34.47(13)
O(8)-Eu-Eu#1	101.8(2)	O(5)-Eu-Eu#1	75.9(2)
O(6)-Eu-Eu#1	124.8(2)	O(4)-Eu-Eu#1	154.9(2)
O(2)-Eu-Eu#1	81.3(2)	N(1)-Eu-Eu#1	100.2(2)
N(2)-Eu-Eu#1	130.4(2)	C(1)-N(1)-C(5)	116.8(7)
C(1)-N(1)-Eu	104.3(5)	C(5)-N(1)-Eu	112.9(5)
C(7)-N(2)-C(8)	117.1(7)	C(7)-N(2)-Eu	112.1(6)
C(8)-N(2)-Eu	106.7(5)	C(2)-O(1)-Eu#1	123.4(5)
C(2)-O(1)-Eu	122.1(5)	Eu#1-O(1)-Eu	110.8(2)
C(3)-O(2)-Eu	115.8(5)	C(6)-O(4)-Eu	108.3(5)
C(9)-O(5)-Eu	122.2(6)	C(10)-O(6)-Eu	120.6(5)
N(1)-C(1)-C(3)	112.2(8)	N(1)-C(1)-C(4)	114.3(8)
C(3)-C(1)-C(4)	106.4(8)	N(1)-C(1)-C(2)	103.5(7)
C(3)-C(1)-C(2)	110.6(8)	C(4)-C(1)-C(2)	109.8(8)
O(1)-C(2)-C(1)	110.9(7)	O(2)-C(3)-C(1)	113.1(7)
O(3)-C(4)-C(1)	111.2(8)	N(1)-C(5)-C(6)	111.4(7)
O(4)-C(6)-C(7)	104.3(7)	O(4)-C(6)-C(5)	108.4(8)
C(7)-C(6)-C(5)	116.9(8)	N(2)-C(7)-C(6)	112.4(8)
N(2)-C(8)-C(9)	106.2(7)	N(2)-C(8)-C(10)	109.4(8)
C(9)-C(8)-C(10)	111.5(8)	N(2)-C(8)-C(11)	112.8(7)
C(9)-C(8)-C(11)	111.5(7)	C(10)-C(8)-C(11)	105.6(7)
O(5)-C(9)-C(8)	110.3(8)	O(6)-C(10)-C(8)	109.9(7)
O(7)-C(11)-C(8)	107.3(6)		

Symmetry transformations used to generate equivalent atoms:

#1 -x,-y,-z

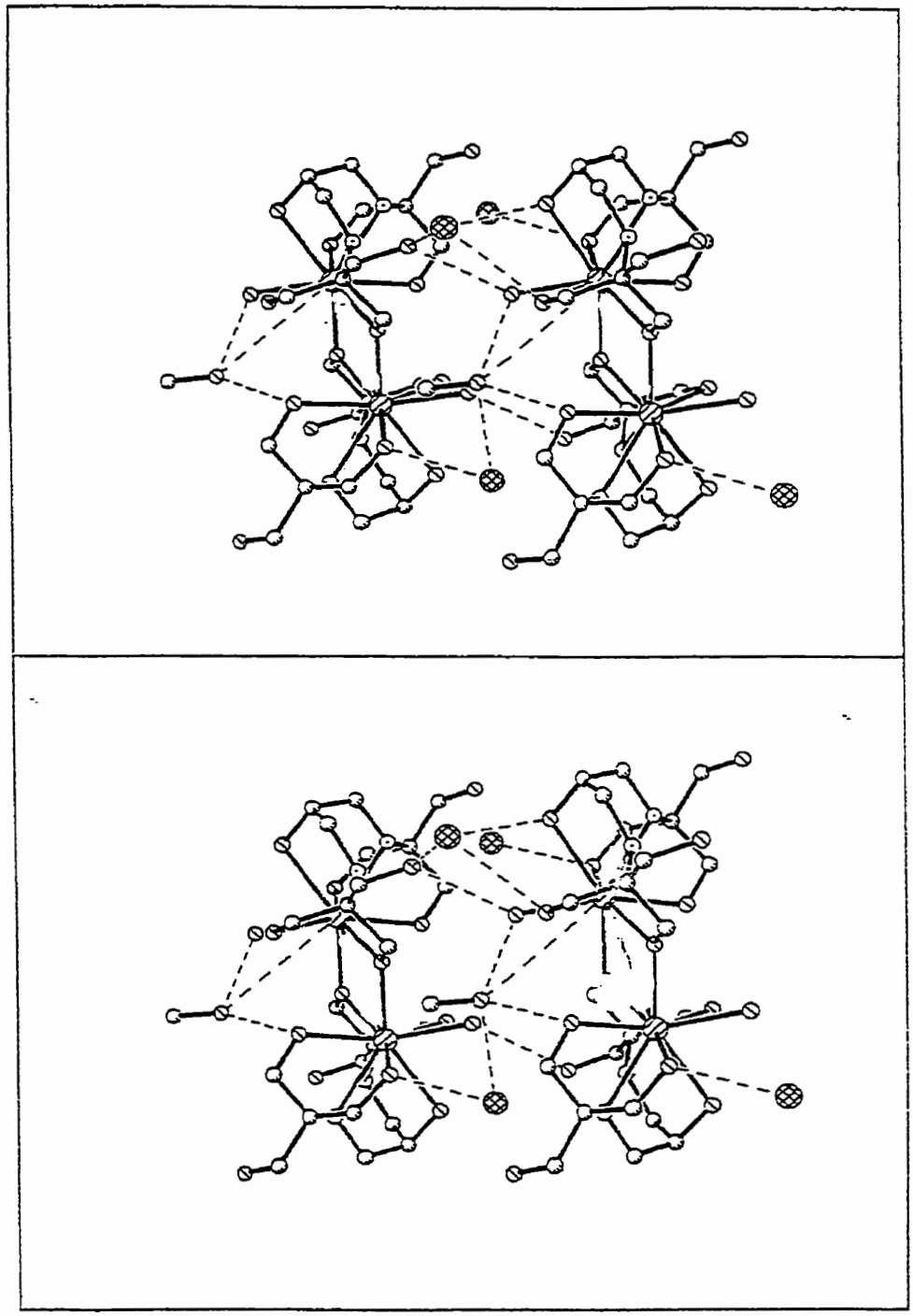

Table 4. Anisotropic displacement parameters [$Å^2 \times 10^3$] for 1.
The anisotropic displacement factor exponent takes the form:
$-2\pi^2 [(ha^*)^2 U_{11} + ... + 2hka^*b^* U_{12}]$

	U11	U22	U33	U23	U13	U12
Eu	20(1)	28(1)	15(1)	8(1)	9(1)	6(1)
Cl(1)	33(2)	75(2)	48(2)	32(2)	15(1)	8(1)
Cl(2)	44(2)	47(2)	66(2)	31(2)	34(2)	13(1)
N(1)	23(4)	29(4)	23(4)	12(3)	11(3)	-6(3)
N(2)	40(5)	53(4)	22(4)	10(4)	19(4)	14(4)
O(1)	23(3)	43(4)	15(3)	13(3)	12(3)	17(3)
O(2)	30(4)	38(4)	32(4)	14(3)	13(3)	13(3)
O(3)	34(4)	46(4)	60(5)	27(4)	18(4)	14(4)
O(4)	20(4)	41(4)	20(3)	12(3)	8(3)	1(3)
O(5)	40(4)	31(4)	23(3)	3(3)	12(3)	-1(3)
O(6)	30(4)	45(4)	32(4)	3(3)	16(3)	12(3)
O(7)	31(5)	90(7)	58(6)	-23(5)	3(4)	-4(5)
O(8)	17(3)	48(4)	25(4)	14(3)	11(3)	-2(3)
C(1)	41(6)	35(5)	25(5)	14(4)	23(5)	19(5)
C(2)	32(6)	34(5)	21(5)	13(4)	17(4)	11(4)
C(3)	19(5)	34(5)	34(5)	8(4)	12(4)	3(4)
C(4)	45(7)	33(5)	34(5)	17(5)	20(5)	19(5)
C(5)	27(5)	44(6)	26(5)	16(5)	13(4)	10(5)
C(6)	24(5)	43(6)	25(5)	18(5)	8(4)	5(4)
C(7)	33(6)	49(6)	18(5)	13(5)	13(4)	12(5)
C(8)	15(5)	25(5)	24(5)	-1(4)	6(4)	-5(4)
C(9)	43(7)	35(5)	34(6)	6(5)	23(5)	12(5)
C(10)	46(7)	39(6)	26(5)	-2(4)	20(5)	11(5)
C(11)	31(6)	40(6)	40(6)	-2(5)	9(5)	-10(5)
O(10)	50(5)	56(5)	42(5)	12(4)	11(4)	-4(4)
C(20)	81(11)	41(7)	80(10)	12(7)	30(9)	-11(7)

Table 5. Hydrogen coordinates (x 10^4) and isotropic displacement parameters ($Å^2$ x 10^3) for 1.

	x	y	z	U(eq)
H(2A)	3726(13)	-773(10)	772(9)	31
H(2B)	2553(13)	-1982(10)	-332(9)	31
H(3A)	935(11)	-3630(10)	-60(9)	35
H(3B)	1144(11)	-3724(10)	1212(9)	35
H(4A)	3920(13)	-3425(10)	2107(9)	41
H(4B)	3942(13)	-3614(10)	816(9)	41
H(5A)	3763(13)	-1236(11)	4042(9)	36
H(5B)	2232(13)	-2331(11)	3226(9)	36
H(6)	1630(12)	-849(10)	4799(9)	35
H(7A)	1447(12)	1465(10)	5098(8)	38
H(7B)	3251(12)	1230(10)	5279(8)	38
H(9A)	1468(14)	4397(10)	2940(9)	43
H(9B)	3101(14)	3754(10)	3153(9)	43
H(10A)	-166(13)	3007(11)	4592(9)	45
H(10B)	-403(13)	4039(11)	3862(9)	45
H(11A)	2619(8)	5098(6)	5380(6)	50
H(11B)	2537(8)	3919(6)	5924(6)	50

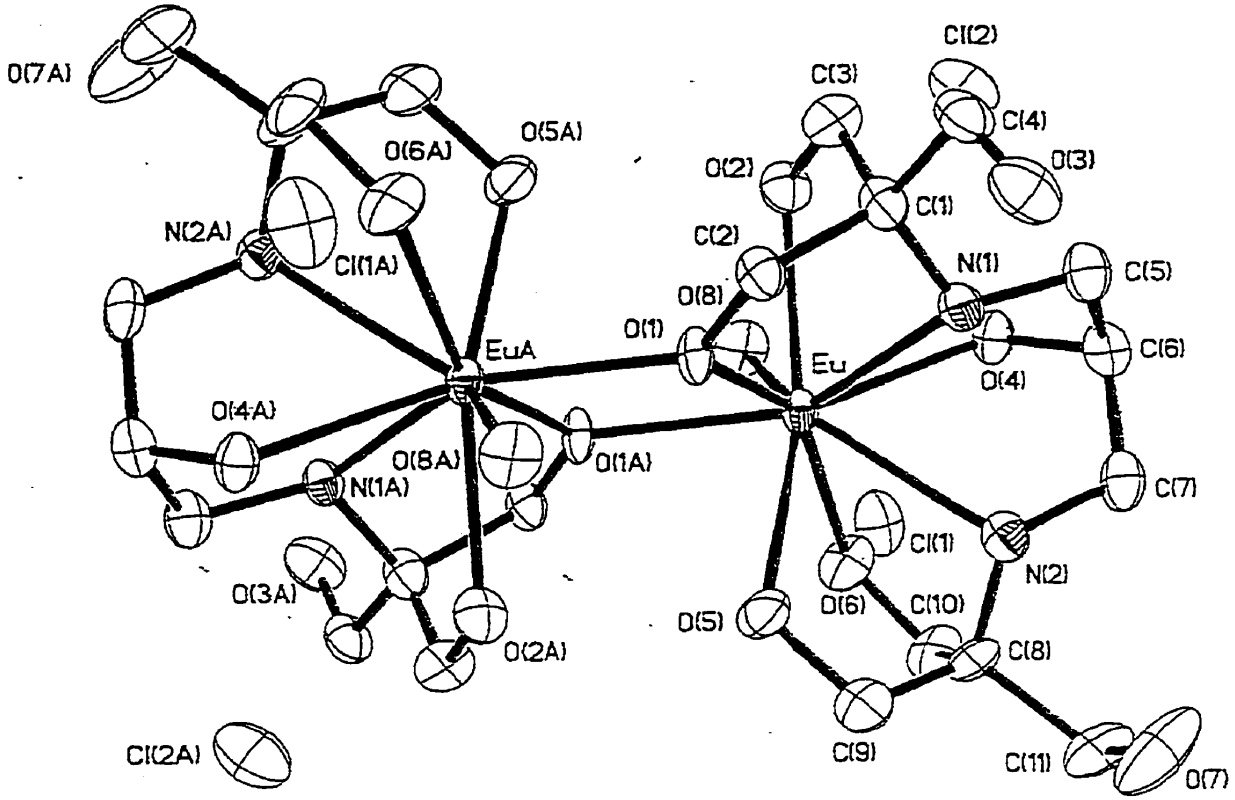
O(7A)
O(6A)
O(5A)
N(2A)
Cl(1A)
EuA
O(4A)
O(8A)
N(1A)
O(1A)
O(3A)
O(2A)
Cl(2A)
O(1)
Eu
Cl(2)
C(3)
C(4)
O(3)
O(2)
C(1)
C(2)
N(1)
C(5)
O(8)
C(6)
O(4)
C(7)
Cl(1)
N(2)
O(6)
C(10)
O(5)
C(8)
C(9)
C(11)
O(7)

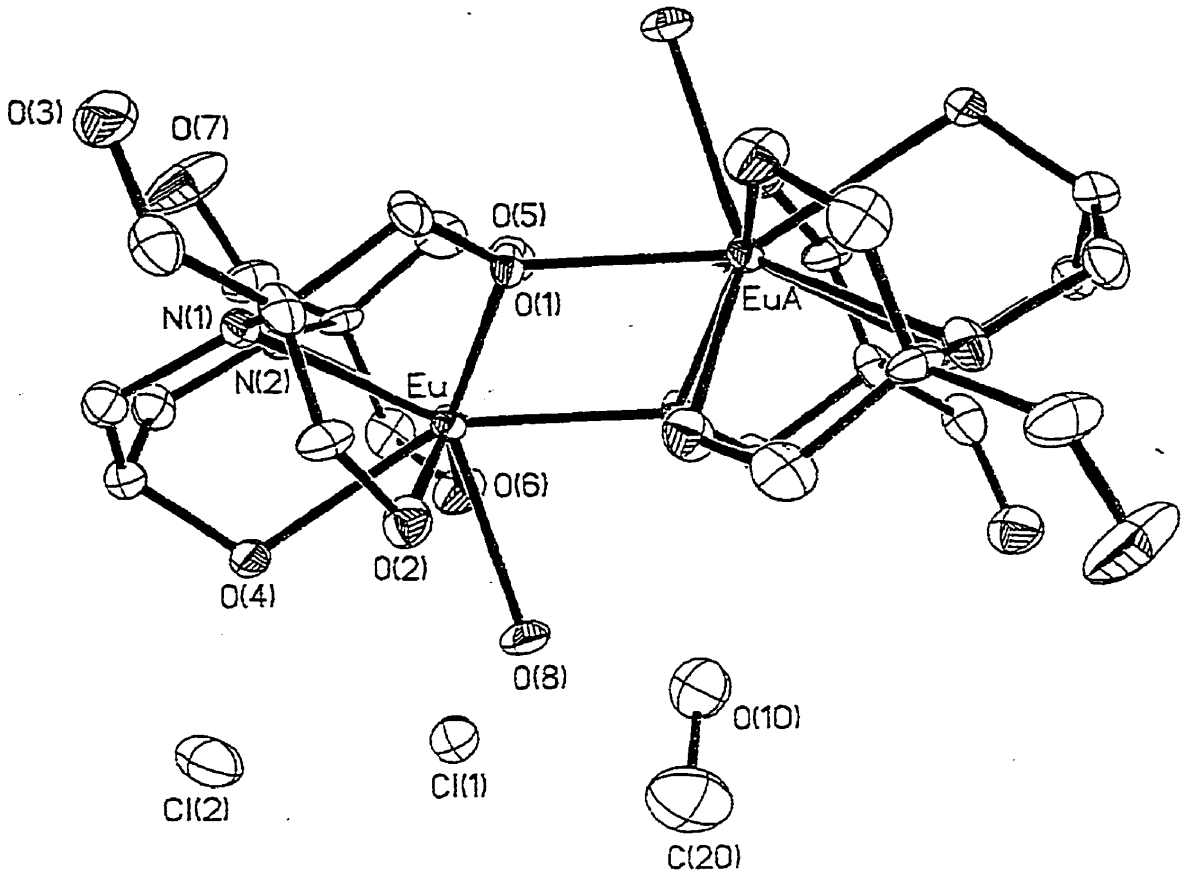
O(3)
O(7)
O(5)
O(1)
EuA
N(1)
N(2)
Eu
O(6)
O(2)
O(4)
O(8)
O(10)
Cl(1)
Cl(2)
C(20)

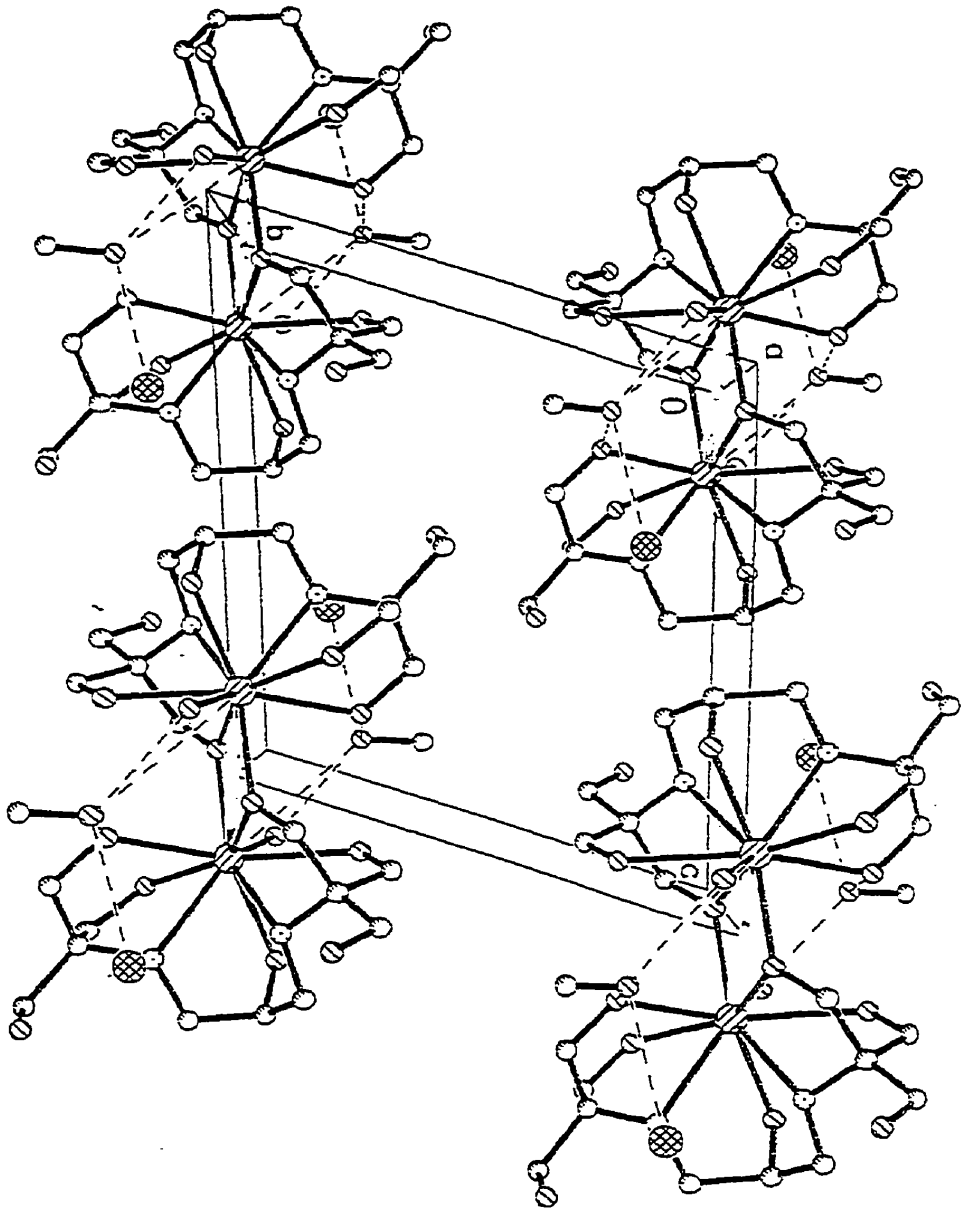

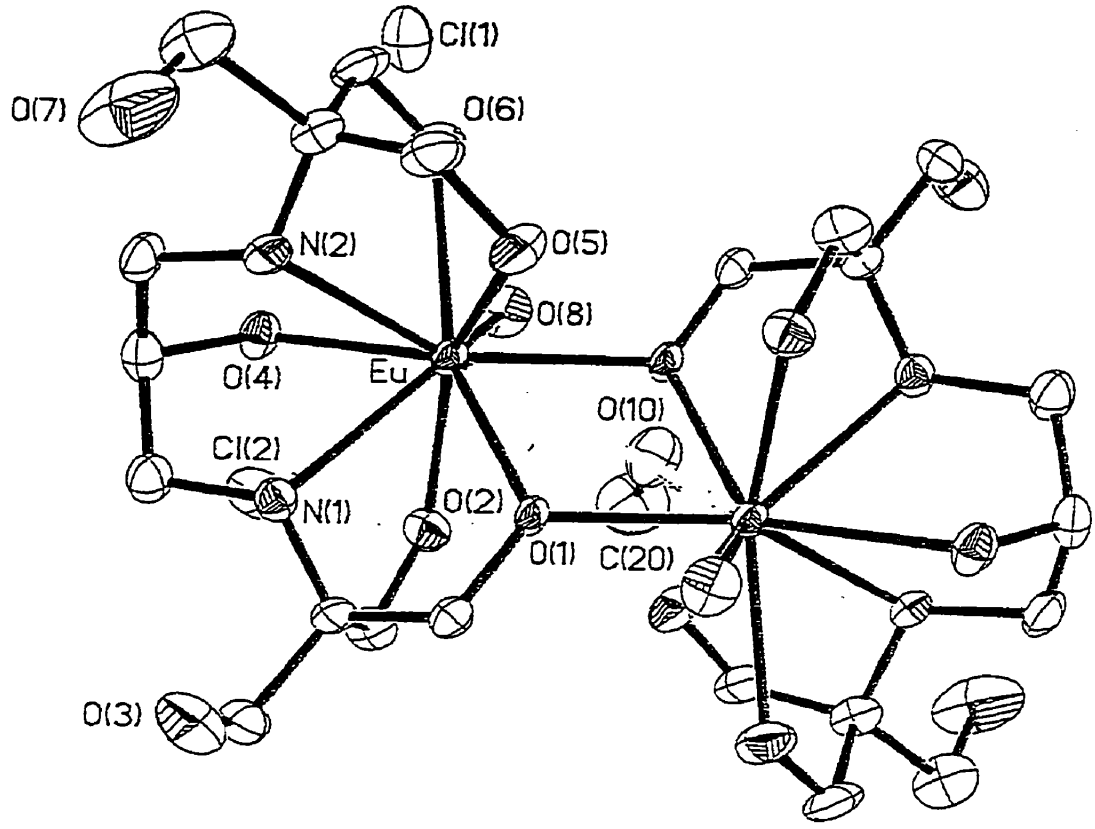
Cl(1)
O(7)
O(6)
N(2)
O(5)
O(8)
O(4)
Eu
O(10)
Cl(2)
N(1)
O(2)
O(1)
C(20)
O(3)

Appendix 5.2 2:1 Eu:hbt Complex

Table 1. Crystal data and structure refinement for xc111.

Identification code	bind
Empirical formula	$C_{11}H_{26}ClEu_2N_2O_{10}$
Formula weight	687.72
Temperature	295(2) K
Wavelength	0.71073 Å
Crystal system	Cubic
Space group	$I\bar{4}3d$
Unit cell dimensions	a = 31.4063(3) Å alpha = 90° b = 31.4063(3) Å beta = 90° c = 31.4063(3) Å gamma = 90°
Volume, Z	30977.8(5) $Å^3$, 48
Density (calculated)	1.770 Mg/m^3
Absorption coefficient	4.956 mm^{-1}
F(000)	15888
Crystal size	0.50 x 0.50 x 0.40 mm
θ range for data collection	1.83 to 25.31°
Limiting indices	$-36 \le h \le 29$, $-37 \le k \le 30$, $-28 \le l \le 36$
Reflections collected	63088
Independent reflections	4488 (R_{int} = 0.1276)
Completeness to θ = 25.31°	96.0 %
Absorption correction	SADABS
Max. and min. transmission	0.2418 and 0.1907
Refinement method	Full-matrix least-squares on F^2
Data / restraints / parameters	4488 / 0 / 264
Goodness-of-fit on F^2	1.226
Final R indices [I>2σ(I)]	R1 = 0.0593, wR2 = 0.1437
R indices (all data)	R1 = 0.0691, wR2 = 0.1560
Absolute structure parameter	-0.03(4)
Largest diff. peak and hole	1.520 and -0.840 $eÅ^{-3}$

Table 2. Atomic coordinates [x 10^4] and equivalent isotropic displacement parameters [$Å^2$ x 10^3] for xc111. U(eq) is defined as one third of the trace of the orthogonalized U_{ij} tensor.

	x	y	z	U(eq)
Eu(1)	3000(1)	1320(1)	8917(1)	36(1)
Eu(2)	2268(1)	2055(1)	8185(1)	42(1)
Cl(1)	1740(2)	891(2)	9617(2)	91(2)
O(1)	3314(3)	777(3)	8548(3)	44(3)
O(2)	3197(4)	799(4)	9445(4)	56(3)
O(3)	2345(5)	-172(5)	9225(5)	74(4)
O(4)	2454(3)	1364(3)	8404(3)	36(2)
O(5)	2259(3)	1830(4)	7483(4)	53(3)
O(6)	1626(5)	2360(5)	7877(5)	78(4)
O(7)	857(5)	1304(6)	7741(5)	85(5)
N(1)	2556(4)	648(4)	8906(4)	41(3)
N(2)	1677(4)	1522(5)	8034(4)	48(4)
C(1)	2871(5)	320(5)	8974(6)	45(4)
C(2)	3214(5)	350(5)	8622(5)	44(4)
C(3)	3033(6)	382(5)	9401(5)	50(4)
C(4)	2677(6)	-126(5)	8950(6)	51(4)
C(5)	2310(6)	640(5)	8512(5)	47(4)
C(6)	2128(5)	1072(5)	8439(5)	43(4)
C(7)	1850(5)	1097(6)	8065(6)	50(4)
C(8)	1523(6)	1660(7)	7618(6)	57(5)
C(9)	1889(6)	1678(7)	7315(6)	58(5)
C(10)	1336(7)	2095(6)	7676(7)	68(6)
C(11)	1183(5)	1363(7)	7437(7)	66(6)
O(1W)	3389(3)	1611(3)	8389(3)	35(4)
O(2W)	2941(3)	2059(3)	7941(3)	41(4)
O(3W)	2740(3)	2089(3)	8845(3)	36(2)
O(4W)	2487(5)	1459(4)	9487(4)	67(4)
O(5W)	1795(5)	2134(7)	8807(5)	94(6)
O(6W)	2283(4)	2393(4)	9601(5)	67(6)
O(7W)	1712(13)	473(14)	7030(14)	230(30)
O(8W)	2500	-550(15)	10000	240(30)
O(9W)	670(40)	1460(50)	8990(50)	1400(200)

Table 3. Bond lengths [Å] and angles [°] for xc111.

Eu(1)-O(1W)	2.250(6)	Eu(1)-O(1)#1	2.280(11)
Eu(1)-O(1)	2.288(11)	Eu(1)-O(4)	2.355(10)
Eu(1)-O(2)	2.412(11)	Eu(1)-O(4W)	2.448(13)
Eu(1)-N(1)	2.530(13)	Eu(1)-O(3W)	2.559(10)
Eu(1)-C(1)	3.173(15)	Eu(1)-C(2)	3.257(16)
Eu(1)-C(6)	3.220(17)	Eu(1)-Eu(1)#1	3.6596(13)
Eu(1)-Eu(1)#2	3.6596(13)	Eu(1)-Eu(2)	3.9844(10)
Eu(2)-O(2W)	2.248(6)	Eu(2)-O(5)#1	2.259(11)
Eu(2)-O(5)	2.316(12)	Eu(2)-O(4)	2.350(10)
Eu(2)-O(6)	2.435(14)	Eu(2)-O(5W)	2.466(15)
Eu(2)-N(2)	2.545(14)	Eu(2)-O(3W)	2.548(10)
Eu(2)-C(8)	3.194(18)	Eu(2)-C(9)	3.208(18)
Eu(2)-C(6)	3.218(17)	Eu(2)-Eu(2)#1	3.6577(15)
Eu(2)-Eu(2)#2	3.6577(15)	O(1)-C(2)	1.40(2)
O(1)-Eu(1)#2	2.280(11)	O(2)-C(3)	1.414(19)
O(3)-C(4)	1.38(2)	O(4)-C(6)	1.380(19)
O(5)-C(9)	1.36(2)	O(5)-Eu(2)#2	2.259(11)
O(6)-C(10)	1.38(2)	O(7)-C(11)	1.42(3)
N(1)-C(1)	1.45(2)	N(1)-C(5)	1.458(19)
N(2)-C(7)	1.44(2)	N(2)-C(8)	1.46(2)
C(1)-C(3)	1.45(2)	C(1)-C(4)	1.53(2)
C(1)-C(2)	1.55(2)	C(5)-C(6)	1.49(2)
C(6)-C(7)	1.46(2)	C(8)-C(10)	1.50(3)
C(8)-C(11)	1.53(3)	C(8)-C(9)	1.50(3)
O(1W)-Eu(1)#1	2.251(6)	O(1W)-Eu(1)#2	2.251(6)
O(1W)-O(2W)	2.45(2)	O(2W)-Eu(2)#1	2.244(6)
O(2W)-Eu(2)#2	2.245(6)	O(4W)-O(5W)	3.71(2)

O(1W)-Eu(1)-O(1)#1	72.4(4)	O(1W)-Eu(1)-O(1)	72.2(3)
O(1)#1-Eu(1)-O(1)	105.3(5)	O(1W)-Eu(1)-O(4)	82.5(4)
O(1)#1-Eu(1)-O(4)	143.9(4)	O(1)-Eu(1)-O(4)	90.6(4)
O(1W)-Eu(1)-O(2)	129.9(5)	O(1)#1-Eu(1)-O(2)	81.9(4)
O(1)-Eu(1)-O(2)	74.4(4)	O(4)-Eu(1)-O(2)	134.1(4)
O(1W)-Eu(1)-O(4W)	145.5(4)	O(1)#1-Eu(1)-O(4W)	95.6(4)
O(1)-Eu(1)-O(4W)	141.9(4)	O(4)-Eu(1)-O(4W)	90.6(4)
O(2)-Eu(1)-O(4W)	77.6(5)	O(1W)-Eu(1)-N(1)	128.9(3)
O(1)#1-Eu(1)-N(1)	147.2(4)	O(1)-Eu(1)-N(1)	67.0(4)
O(4)-Eu(1)-N(1)	68.8(4)	O(2)-Eu(1)-N(1)	65.4(4)
O(4W)-Eu(1)-N(1)	78.2(4)	O(1W)-Eu(1)-O(3W)	74.2(4)
O(1)#1-Eu(1)-O(3W)	78.7(3)	O(1)-Eu(1)-O(3W)	142.9(4)
O(4)-Eu(1)-O(3W)	69.7(3)	O(2)-Eu(1)-O(3W)	141.5(4)
O(4W)-Eu(1)-O(3W)	71.7(4)	N(1)-Eu(1)-O(3W)	127.6(4)
O(1W)-Eu(1)-C(1)	120.8(4)	O(1)#1-Eu(1)-C(1)	124.8(4)
O(1)-Eu(1)-C(1)	49.0(4)	O(4)-Eu(1)-C(1)	90.2(4)
O(2)-Eu(1)-C(1)	47.3(4)	O(4W)-Eu(1)-C(1)	92.9(4)
N(1)-Eu(1)-C(1)	26.4(4)	O(3W)-Eu(1)-C(1)	153.9(4)
O(1W)-Eu(1)-C(2)	93.3(4)	O(1)#1-Eu(1)-C(2)	115.8(4)
O(1)-Eu(1)-C(2)	21.3(4)	O(4)-Eu(1)-C(2)	90.6(4)
O(2)-Eu(1)-C(2)	60.5(4)	O(4W)-Eu(1)-C(2)	120.7(4)
N(1)-Eu(1)-C(2)	47.9(4)	O(3W)-Eu(1)-C(2)	157.5(4)
C(1)-Eu(1)-C(2)	27.8(4)	O(1W)-Eu(1)-C(6)	102.6(4)
O(1)#1-Eu(1)-C(6)	163.8(4)	O(1)-Eu(1)-C(6)	87.1(4)
O(4)-Eu(1)-C(6)	22.5(4)	O(2)-Eu(1)-C(6)	111.9(4)
O(4W)-Eu(1)-C(6)	79.9(4)	N(1)-Eu(1)-C(6)	47.3(4)
O(3W)-Eu(1)-C(6)	85.2(4)	C(1)-Eu(1)-C(6)	71.2(4)

C(2)-Eu(1)-C(6)	79.4(4)	O(1W)-Eu(1)-Eu(1)#1	35.6(2)
O(1)#1-Eu(1)-Eu(1)#1	36.8(3)	O(1)-Eu(1)-Eu(1)#1	89.6(3)
O(4)-Eu(1)-Eu(1)#1	113.6(2)	O(2)-Eu(1)-Eu(1)#1	109.6(3)
O(4W)-Eu(1)-Eu(1)#1	124.2(3)	N(1)-Eu(1)-Eu(1)#1	156.5(3)
O(3W)-Eu(1)-Eu(1)#1	71.5(2)	C(1)-Eu(1)-Eu(1)#1	133.6(3)
C(2)-Eu(1)-Eu(1)#1	109.0(3)	C(6)-Eu(1)-Eu(1)#1	135.7(3)
O(1W)-Eu(1)-Eu(1)#2	35.6(2)	O(1)#1-Eu(1)-Eu(1)#2	89.7(3)
O(1)-Eu(1)-Eu(1)#2	36.7(3)	O(4)-Eu(1)-Eu(1)#2	84.2(2)
O(2)-Eu(1)-Eu(1)#2	104.7(3)	O(4W)-Eu(1)-Eu(1)#2	174.5(3)
N(1)-Eu(1)-Eu(1)#2	98.1(3)	O(3W)-Eu(1)-Eu(1)#2	108.0(2)
C(1)-Eu(1)-Eu(1)#2	85.3(3)	C(2)-Eu(1)-Eu(1)#2	57.7(3)
C(6)-Eu(1)-Eu(1)#2	94.6(3)	Eu(1)#1-Eu(1)-Eu(1)#2	60.0
O(1W)-Eu(1)-Eu(2)	69.8(4)	O(1)#1-Eu(1)-Eu(2)	112.8(3)
O(1)-Eu(1)-Eu(2)	112.9(3)	O(4)-Eu(1)-Eu(2)	32.1(2)
O(2)-Eu(1)-Eu(2)	159.6(3)	O(4W)-Eu(1)-Eu(2)	86.5(3)
N(1)-Eu(1)-Eu(2)	99.0(3)	O(3W)-Eu(1)-Eu(2)	38.6(2)
C(1)-Eu(1)-Eu(2)	122.2(3)	C(2)-Eu(1)-Eu(2)	119.8(3)
C(6)-Eu(1)-Eu(2)	51.7(3)	Eu(1)#1-Eu(1)-Eu(2)	89.931(16)
Eu(1)#2-Eu(1)-Eu(2)	90.038(16)	O(2W)-Eu(2)-O(5)#1	72.9(4)
O(2W)-Eu(2)-O(5)	71.8(3)	O(5)#1-Eu(2)-O(5)	106.0(6)
O(2W)-Eu(2)-O(4)	82.8(4)	O(5)#1-Eu(2)-O(4)	144.4(4)
O(5)-Eu(2)-O(4)	90.0(4)	O(2W)-Eu(2)-O(6)	129.7(6)
O(5)#1-Eu(2)-O(6)	82.2(5)	O(5)-Eu(2)-O(6)	74.4(5)
O(4)-Eu(2)-O(6)	133.3(4)	O(2W)-Eu(2)-O(5W)	146.8(4)
O(5)#1-Eu(2)-O(5W)	95.8(6)	O(5)-Eu(2)-O(5W)	140.9(5)
O(4)-Eu(2)-O(5W)	90.6(5)	O(6)-Eu(2)-O(5W)	77.0(6)
O(2W)-Eu(2)-N(2)	128.8(3)	O(5)#1-Eu(2)-N(2)	147.3(4)
O(5)-Eu(2)-N(2)	67.1(4)	O(4)-Eu(2)-N(2)	68.2(4)
O(6)-Eu(2)-N(2)	65.1(5)	O(5W)-Eu(2)-N(2)	77.0(5)
O(2W)-Eu(2)-O(3W)	74.5(4)	O(5)#1-Eu(2)-O(3W)	78.7(4)
O(5)-Eu(2)-O(3W)	142.6(4)	O(4)-Eu(2)-O(3W)	69.9(3)
O(6)-Eu(2)-O(3W)	142.0(4)	O(5W)-Eu(2)-O(3W)	72.7(4)
N(2)-Eu(2)-O(3W)	127.1(4)	O(2W)-Eu(2)-C(8)	120.0(4)
O(5)#1-Eu(2)-C(8)	125.3(5)	O(5)-Eu(2)-C(8)	48.7(4)
O(4)-Eu(2)-C(8)	89.3(4)	O(6)-Eu(2)-C(8)	47.4(5)
O(5W)-Eu(2)-C(8)	92.2(5)	N(2)-Eu(2)-C(8)	26.5(5)
O(3W)-Eu(2)-C(8)	153.6(4)	O(2W)-Eu(2)-C(9)	93.4(4)
O(5)#1-Eu(2)-C(9)	116.4(5)	O(5)-Eu(2)-C(9)	21.7(4)
O(4)-Eu(2)-C(9)	90.1(5)	O(6)-Eu(2)-C(9)	59.9(5)
O(5W)-Eu(2)-C(9)	119.2(5)	N(2)-Eu(2)-C(9)	47.7(5)
O(3W)-Eu(2)-C(9)	157.5(4)	C(8)-Eu(2)-C(9)	27.0(5)
O(2W)-Eu(2)-C(6)	102.8(4)	O(5)#1-Eu(2)-C(6)	164.0(4)
O(5)-Eu(2)-C(6)	86.6(4)	O(4)-Eu(2)-C(6)	22.5(4)
O(6)-Eu(2)-C(6)	111.2(5)	O(5W)-Eu(2)-C(6)	79.5(6)
N(2)-Eu(2)-C(6)	46.8(4)	O(3W)-Eu(2)-C(6)	85.4(4)
C(8)-Eu(2)-C(6)	70.4(5)	C(9)-Eu(2)-C(6)	78.8(5)
O(2W)-Eu(2)-Eu(2)#1	35.4(2)	O(5)#1-Eu(2)-Eu(2)#1	37.5(3)
O(5)-Eu(2)-Eu(2)#1	89.5(3)	O(4)-Eu(2)-Eu(2)#1	113.7(2)
O(6)-Eu(2)-Eu(2)#1	110.0(4)	O(5W)-Eu(2)-Eu(2)#1	125.4(4)
N(2)-Eu(2)-Eu(2)#1	156.7(3)	O(3W)-Eu(2)-Eu(2)#1	71.7(2)
C(8)-Eu(2)-Eu(2)#1	133.5(4)	C(9)-Eu(2)-Eu(2)#1	109.3(3)
C(6)-Eu(2)-Eu(2)#1	135.8(3)	O(2W)-Eu(2)-Eu(2)#2	35.5(2)
O(5)#1-Eu(2)-Eu(2)#2	90.4(3)	O(5)-Eu(2)-Eu(2)#2	36.4(3)
O(4)-Eu(2)-Eu(2)#2	84.0(2)	O(6)-Eu(2)-Eu(2)#2	104.5(4)
O(5W)-Eu(2)-Eu(2)#2	173.8(5)	N(2)-Eu(2)-Eu(2)#2	98.1(3)
O(3W)-Eu(2)-Eu(2)#2	108.1(2)	C(8)-Eu(2)-Eu(2)#2	84.6(3)
C(9)-Eu(2)-Eu(2)#2	57.9(3)	C(6)-Eu(2)-Eu(2)#2	94.4(3)
Eu(2)#1-Eu(2)-Eu(2)#2	60.0	O(2W)-Eu(2)-Eu(1)	70.2(4)
O(5)#1-Eu(2)-Eu(1)	113.1(3)	O(5)-Eu(2)-Eu(1)	112.3(3)

O(4)-Eu(2)-Eu(1)	32.2(2)	O(6)-Eu(2)-Eu(1)	159.2(4)
O(5W)-Eu(2)-Eu(1)	87.1(4)	N(2)-Eu(2)-Eu(1)	98.5(3)
O(3W)-Eu(2)-Eu(1)	38.8(2)	C(8)-Eu(2)-Eu(1)	121.3(4)
C(9)-Eu(2)-Eu(1)	119.5(4)	C(6)-Eu(2)-Eu(1)	51.8(3)
Eu(2)#1-Eu(2)-Eu(1)	90.070(16)	Eu(2)#2-Eu(2)-Eu(1)	89.962(16)
C(2)-O(1)-Eu(1)#2	130.1(9)	C(2)-O(1)-Eu(1)	122.3(9)
Eu(1)#2-O(1)-Eu(1)	106.5(4)	C(3)-O(2)-Eu(1)	118.0(9)
C(6)-O(4)-Eu(2)	116.8(9)	C(6)-O(4)-Eu(1)	116.7(9)
Eu(2)-O(4)-Eu(1)	115.8(4)	C(9)-O(5)-Eu(2)#2	133.6(11)
C(9)-O(5)-Eu(2)	119.2(10)	Eu(2)#2-O(5)-Eu(2)	106.1(4)
C(10)-O(6)-Eu(2)	119.4(11)	C(1)-N(1)-C(5)	118.3(13)
C(1)-N(1)-Eu(1)	102.4(9)	C(5)-N(1)-Eu(1)	108.6(9)
C(7)-N(2)-C(8)	117.4(14)	C(7)-N(2)-Eu(2)	108.7(9)
C(8)-N(2)-Eu(2)	102.4(11)	C(3)-C(1)-N(1)	106.3(15)
C(3)-C(1)-C(4)	107.8(14)	N(1)-C(1)-C(4)	111.9(13)
C(3)-C(1)-C(2)	114.3(14)	N(1)-C(1)-C(2)	109.2(13)
C(4)-C(1)-C(2)	107.4(14)	C(3)-C(1)-Eu(1)	82.8(9)
N(1)-C(1)-Eu(1)	51.1(7)	C(4)-C(1)-Eu(1)	162.7(12)
C(2)-C(1)-Eu(1)	79.1(8)	O(1)-C(2)-C(1)	109.5(13)
O(1)-C(2)-Eu(1)	36.4(7)	C(1)-C(2)-Eu(1)	73.1(8)
O(2)-C(3)-C(1)	110.0(13)	O(3)-C(4)-C(1)	111.5(14)
N(1)-C(5)-C(6)	108.5(13)	O(4)-C(6)-C(7)	110.2(14)
O(4)-C(6)-C(5)	109.4(13)	C(7)-C(6)-C(5)	113.8(14)
O(4)-C(6)-Eu(2)	40.7(7)	C(7)-C(6)-Eu(2)	80.3(10)
C(5)-C(6)-Eu(2)	149.2(11)	O(4)-C(6)-Eu(1)	40.8(7)
C(7)-C(6)-Eu(1)	150.2(12)	C(5)-C(6)-Eu(1)	79.7(9)
Eu(2)-C(6)-Eu(1)	76.5(4)	N(2)-C(7)-C(6)	109.2(13)
N(2)-C(8)-C(10)	106.9(16)	N(2)-C(8)-C(11)	112.6(17)
C(10)-C(8)-C(11)	109.2(15)	N(2)-C(8)-C(9)	109.0(14)
C(10)-C(8)-C(9)	110.1(19)	C(11)-C(8)-C(9)	109.0(16)
N(2)-C(8)-Eu(2)	51.1(9)	C(10)-C(8)-Eu(2)	82.2(10)
C(11)-C(8)-Eu(2)	163.2(14)	C(9)-C(8)-Eu(2)	77.0(10)
O(5)-C(9)-C(8)	115.0(15)	O(5)-C(9)-Eu(2)	39.1(7)
C(8)-C(9)-Eu(2)	76.0(10)	O(6)-C(10)-C(8)	110.2(15)
O(7)-C(11)-C(8)	109.5(18)	Eu(1)#1-O(1W)-Eu(1)#2	108.8(4)
Eu(1)#1-O(1W)-Eu(1)	108.8(4)	Eu(1)#2-O(1W)-Eu(1)	108.8(4)
Eu(1)#1-O(1W)-O(2W)	110.1(4)	Eu(1)#2-O(1W)-O(2W)	110.1(4)
Eu(1)-O(1W)-O(2W)	110.2(4)	Eu(2)#1-O(2W)-Eu(2)#2	109.1(4)
Eu(2)#1-O(2W)-Eu(2)	109.0(4)	Eu(2)#2-O(2W)-Eu(2)	109.0(4)
Eu(2)#1-O(2W)-O(1W)	109.9(4)	Eu(2)#2-O(2W)-O(1W)	109.9(4)
Eu(2)-O(2W)-O(1W)	109.8(4)	Eu(2)-O(3W)-Eu(1)	102.5(3)
Eu(1)-O(4W)-O(5W)	93.7(4)	Eu(2)-O(5W)-O(4W)	92.6(5)

Symmetry transformations used to generate equivalent atoms:

#1 z-1/2,-x+1/2,-y+1 #2 -y+1/2,-z+1,x+1/2

Table 4. Anisotropic displacement parameters [$Å^2 \times 10^3$] for xc111.
The anisotropic displacement factor exponent takes the form:
$-2\pi^2 [(ha^*)^2 U_{11} + ... + 2hka^*b^* U_{12}]$

	U11	U22	U33	U23	U13	U12
Eu(1)	37(1)	37(1)	34(1)	2(1)	-1(1)	-3(1)
Eu(2)	32(1)	46(1)	48(1)	0(1)	-6(1)	5(1)
Cl(1)	128(6)	85(4)	60(3)	-8(3)	24(3)	-31(4)
O(1)	47(6)	44(6)	40(6)	3(5)	2(5)	-2(5)
O(2)	75(9)	48(7)	46(7)	13(5)	-10(6)	-5(6)
O(3)	67(9)	79(10)	77(10)	17(8)	22(7)	-19(7)
O(4)	34(5)	38(6)	38(6)	2(4)	-1(4)	-1(4)
O(5)	36(6)	79(9)	44(6)	9(6)	-4(5)	-2(6)
O(6)	58(9)	66(9)	109(13)	-1(8)	-22(8)	12(7)
O(7)	51(9)	109(13)	95(12)	-2(10)	-5(8)	1(8)
N(1)	51(8)	33(7)	37(7)	1(5)	-3(6)	1(6)
N(2)	36(7)	68(10)	45(8)	-9(7)	-12(6)	5(6)
C(1)	44(9)	34(8)	58(10)	13(7)	-2(7)	-13(7)
C(2)	47(9)	42(9)	42(9)	0(7)	-5(7)	-3(7)
C(3)	60(11)	54(10)	37(9)	4(7)	-9(8)	-16(8)
C(4)	56(11)	33(9)	65(12)	-8(8)	1(9)	-10(7)
C(5)	56(10)	52(10)	31(8)	-7(7)	-8(7)	-8(8)
C(6)	39(9)	48(9)	43(9)	-2(7)	9(7)	6(7)
C(7)	32(8)	58(11)	51(11)	-13(9)	-5(7)	-3(7)
C(8)	41(10)	74(13)	57(12)	-7(9)	-12(8)	9(9)
C(9)	43(10)	89(14)	41(10)	10(9)	-12(8)	0(9)
C(10)	57(12)	67(13)	81(14)	-2(10)	-43(11)	9(9)
C(11)	19(8)	96(16)	84(15)	10(12)	-24(9)	-1(9)
O(1W)	35(4)	35(4)	35(4)	-4(4)	4(4)	-4(4)
O(2W)	41(4)	41(4)	41(4)	6(4)	-6(4)	6(4)
O(3W)	33(5)	36(6)	39(6)	-4(4)	5(4)	-3(4)
O(4W)	86(10)	64(8)	50(8)	3(6)	16(7)	-6(7)
O(5W)	60(9)	151(17)	71(10)	-33(10)	2(7)	9(10)
O(6W)	58(9)	58(9)	83(11)	-44(7)	17(7)	-2(6)

Table 5. Hydrogen coordinates (x 10^4) and isotropic displacement parameters ($Å^2$ x 10^3) for xc111.

	x	y	z	U(eq)
H(1)	2364	652	9144	49
H(2)	1455	1556	8241	59
H(2A)	3465	198	8708	53
H(2B)	3109	222	8364	53
H(3A)	2808	337	9603	61
H(3B)	3254	178	9458	61
H(4A)	2575	-177	8667	62
H(4B)	2893	-333	9012	62
H(5A)	2085	434	8525	56
H(5B)	2490	561	8278	56
H(7A)	2009	1031	7813	60
H(7B)	1623	894	8091	60
H(9A)	1940	1397	7207	69
H(9B)	1811	1855	7078	69
H(10A)	1262	2212	7404	82
H(10B)	1081	2076	7844	82
H(11A)	1066	1484	7181	79
H(11B)	1309	1094	7366	79

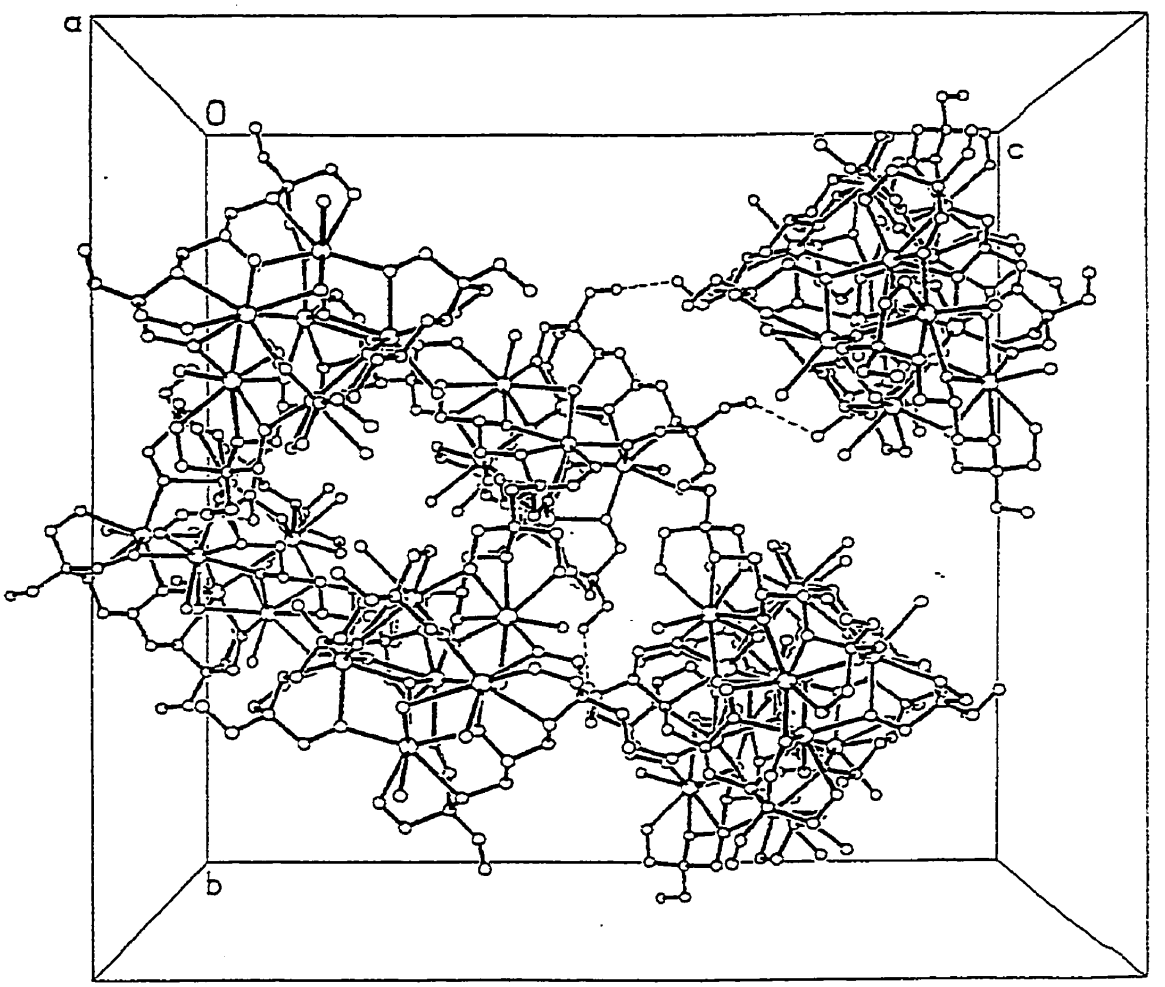
a
O
c
b